Northumbria University
NEWCASTLE

# Visible Light Optical Camera Communication for Electroencephalography Applications

Geetika Aggarwal

A thesis submitted in partial fulfilment of the requirements of the University of Northumbria at Newcastle for the degree of

**Doctor of Philosophy**

Research undertaken in the Faculty of Engineering and Environment

21 January 2020

# Abstract

Due to the cable-free deployment and flexibility of wireless communications, the data transmission in the applications of home and healthcare has shown a trend of moving wired communications to wireless communications. One typical example is electroencephalography (EEG). Evolution in the radio frequency (RF) technology has made it is possible to transmit the EEG data without data cable bundles. However, presently, the RF-based wireless technology used in EEG suffers from electromagnetic interference and might also have adverse effects on the health of patient and other medical equipment used in hospitals or homes. This puts some limits in RF-based EEG solutions, which is particularly true in RF restricted zones like Intensive Care Units (ICUs). As a recently developed optical wireless communication (OWC) technology, visible light communication (VLC) using light-emitting diodes (LEDs) for both simultaneous illumination and data communication has shown its advantages of free from electromagnetic interference, potential huge unlicensed bandwidth and enhanced data privacy due to the line transmission of light. The most recent development of VLC is the optical camera communication (OCC), which is an extension of VLC IEEE standard 802.15.7, also referred to as visible light optical camera communication (VL-OCC). Different from the conventional VLC where traditional photodiodes are used to detect and receive the data, VL-OCC uses the imaging camera as the photodetector to receive the data in the form of visible light signals. The data rate requirement of EEG is dependent on the application; hence this thesis investigates a low cost, organic LED (OLED)-driven VL-OCC wireless data transmission system for EEG applications.

The proposed VL-OCC system consists of an organic LED (OLED) screen acting as the transmitter and a camera working as the receiver. In the proposed system, the

OLED's screen is partitioned into several blocks. In this thesis, a model and hardware testbed of the proposed system is developed and the key parameters, such as communication distance, the partition of the OLED screen and the size of partition block, OLED flashing rates and angle deviation, are investigated to evaluate the performance of the proposed VL-OCC for EEG. The thesis showed that the proposed system can achieve a data rate of 2 $kbps$ at a bit error rate (BER) of 3.8 $\times 10^{-3}$. The comparison results of partition blocks of OLED screen illustrate that pixel size 16-by-16 gives better BER performance in comparison to 8-by-8-pixel OLED screen, however, data bits transmitted are reduced due to the increase in pixel size. The thesis also deals with the experiments of angle deviation using the 16-by-16pixel OLED screen and Thorlabs camera. The data rate achieved is 2 $kbps$ at a BER of 2.3 $\times 10^{-3}$ and the link distance achieved was 30cm with angle deviation, while 50 cm link distance was achieved without angle deviation. The results illustrate that the distortions in the bits received per frame increased with increase in distance thus resulting in poor BER performance at farther distances and larger angle deviation. Furthermore, this thesis also investigated the pixel size 32, of OLED screen in context to BER and link distance. The experiments were performed in LOS deploying OOK-NRZ modulation scheme using 32-by-32-pixel OLED screen as transmitter and three different cameras of 18 megapixels (MP) MP, 8MP and 5 MP respectively as the receiver. The results depict that digital single-lens reflex (DSLR) camera of 18 MP outperforms smartphone camera J3 Samsung Galaxy of 5 MP and Thorlabs camera of 8 MP as DSLR camera is capable to transmit error-free bit rate of 2.8 $kbps$at 30 fps up to 5.5m due to increase in resolution.

# Declaration

I declare that the work contained in this thesis has not been submitted for any other award and that it is all my own work at Northumbria University. I also confirm that this work fully acknowledges opinions, ideas and contributions from the work of others. Any ethical clearance for the research presented in this thesis has been approved. Approval has been sought and granted by the Faculty Ethics Committee / University Ethics Committee / external committee.

**I declare that the word count of this Thesis is 32, 580**

Name: Geetika Aggarwal

Signature:

Date: 21 January 2020

# Acknowledgements

First, my sincere apologies in case I have unintentionally missed someone. Second, I would like to express my sincere thanks to my principal supervisor Dr Xuewu Dai for his continuous support, motivation, guidance and encouragement throughout my study at Northumbria University.

Third, I am grateful to my second supervisor Dr Richard Binns for his help, guidance and support throughout the PhD journey.

Fourth, I extend my special thanks to my third supervisor from Sheffield Hallam University, Prof. Reza Saatchi for valuable discussions and useful feedback.

Fifth, I extend my gratitude to Prof. Zabih (Fary) Ghaseemlooy for giving me an opportunity to pursue a PhD at Northumbria University.

Sixth, I thank Prof. Krishna Busawon, for providing the necessary guidance at times during the PhD study.

Seventh, I will always be grateful to graduate school especially, Stuart Hutchinson and Catherine Heron for their continuous support and guidance in context to university rules and regulations. They have been my emotional support during the tenure of 4 years of study, providing help whenever needed.

Eighth, I extend my gratitude to all my students (MSc and undergraduate whom I have met during a teaching in the past two years) for appreciation, kind support and nominating me for the awards.

Ninth, I extend my thanks to the academic societies IEEE and IET, and their branches at university for trusting me and giving me the responsibility of leadership, which enhanced my skills.

Tenth, I will always be grateful to the marketing team specifically, telecentre at Northumbria University for offering me part-time work as a student and then gave me the responsibility of leadership as a supervisor which greatly enhanced both my confidence and communication skills.

Last but not least, I extend my gratitude to my Dad for his unending support and encouragement despite his health issues in the last four years. Also, I am grateful and express my gratitude towards my sister too for her continuous motivation during the 4 years of the time of my PhD study ABROAD as a self – funded PhD student.

# Dedication

Without the unending support of Dad and my sister, the journey of studying ABROAD would not have been possible, being a self-funded student. I dedicate everything that I have achieved and this thesis to my Dad (Mr Virinder Aggarwal), Sister (Miss Anupam Aggarwal) and Mom (Late. Mrs Veena Aggarwal).

# Glossary of Acronyms

| | |
|---|---|
| ADC | Analogue to digital converter |
| APD | Avalanche photodiode |
| ASCII | American standard code for information interchange |
| ASK | Amplitude shift keying |
| AWGN | Additive white gaussian noise |
| BCI | Brain-computer interface |
| BER | Bit error rate |
| CCD | Charged coupled device |
| CDMA | Code division multiple access |
| CMOS | Complementary metal-oxide semiconductor |
| CSK | Code shift keying |
| DIP | Digital image processing |
| DSLR | Digital single-lens reflex camera |
| EEG | Electroencephalography |
| EMI | Electromagnetic interference |
| FSO | Free space optics |
| fps | Frames per second |
| FOV | Field of view |
| GaAs | Gallium arsenide |
| GaN | Gallium nitride |
| HSI | Hue saturation intensity |
| HSV | Hue saturation value |
| ICU | Intensive care unit |
| IM/DD | Intensity modulation direct detection |

| | |
|---|---|
| IS | Image sensor |
| ISI | Intersymbol interferences |
| LAN | Local area network |
| LCD | Liquid crystal displays |
| LED | Light-emitting diode |
| Li-Fi | Light fidelity |
| LOS | Line of sight |
| MIMO | Multiple-input-multiple-output |
| MP | Megapixel |
| NFC | Near field communication |
| NIR | Near-infrared |
| NRZ | Non-return-to-zero |
| OCC | Optical camera communication |
| OFDM | Orthogonal frequency division multiplexing |
| OIoT | Optical internet of things |
| OLED | Organic light-emitting diode |
| OOK-NRZ | On-off keying non-return to zero |
| OWC | Optical wireless communication |
| PAM | Pulse amplitude modulation |
| PCB | Printed circuit board |
| PD | Photodiode |
| PIN | Positive-intrinsic-negative |
| PPM | Pulse position modulation |
| PWM | Pulse width modulation |
| QR | Quick response |
| RGB | Red-green-blue |
| RF | Radiofrequency |

| | |
|---|---|
| RS | Rolling shutter |
| RZ | Return to zero |
| Rx | Receiver |
| Si | Silicon |
| SM | Spatial modulation |
| TH | Time hopping |
| TIA | Transimpedance amplifier |
| Tx | Transmitter |
| UFSOOK | Undersampled frequency shift on-off keying |
| UPSOOK | Undersampled phase shift on-off keying |
| UV | Ultraviolet |
| V2V | Vehicle-to-vehicle |
| VLC | Visible light communication |
| VL-OCC | Visible light optical camera communication |
| VoIP | Voice over IP |
| WLED | White light-emitting diode |
| WDM | Wavelength division multiplexing |
| 5G | Fifth generation |

# Glossary of Symbols

| | |
|---|---|
| $D$ | Size of the block in terms of pixel |
| $R_1$ | Number of rows per frame |
| $C_1$ | Number of columns per frame |
| $b_n$ | Transmitted bits from Microcontroller before S/P |
| $s^{(t)}$ | Dimensional signal transmitted after S/P |
| $y^{(t)}$ | Received dimensional signal |
| $v^{(t)}$ | Noise realization which is known by white noise |
| $x^{(t)}$ | The signal at the optical channel |
| q | Electron charge |
| N | Total number of bits transmitted. |
| $R_b$ | Data rate |
| q | Electron charge |
| $\Re$ | The responsivity of the photodetector |
| $\otimes$ | Convolution operator |
| $h(t)$ | Impulse response of the optical channel |
| $\eta B$ | Efficiency of bandwidth |
| $Tb$ | Bit duration |
| $\delta()$ | Dirac delta function |
| $\eta P$ | Power efficiency |
| $\gamma$ | Duty cycle |

# Table of Contents

# List of Tables

# List of Figures

# Chapter 1 Introduction

## 1.1 Background

Over recent decades, there has been an ever-increasing utilization of Internet, multimedia, cloud-based services, and the Internet of things, over wireless links. High demand for communication connection leading to congestion in radio frequencies (RF) has created the need for a supplementary, license-free method of transmitting data. Recently, LED-based visible light communication (VLC) systems using solid-state light-emitting diodes have gained a lot of research interest since visible light spectrum (380nm- 780nm) is freely available and does not fall under any spectrum regulations [1, 2]. Furthermore, LED-based VLC coexists with the present illumination system in our homes, offices and other indoor facilities in the form of light-emitting diodes (LEDs). LED lights are energy-efficient, and they can save up to 85% and 60% energy compared to the incandescent and fluorescent lights respectively while providing the same brightness and illumination levels. With the increase in the efficiency of low-cost solid-state devices such as LEDs, it is estimated that LEDs will completely take over the existing illuminating sources. Unlike traditional illumination source, LEDs can be used for data transmission for a wide range of practical wireless applications including indoor navigation, security systems, automation and control of appliances, data transmission, local area networks, healthcare and industrial monitoring that require low or high data-rate short-range communication systems [3, 4].

In the past few years, the demand for monitoring systems for various purposes in different fields has increased dramatically. To increase the efficiency of the workforce, wireless monitoring systems implemented to achieve better monitoring performance

with low cost, high reliability, and convenience [5]. Among the wireless monitoring systems, the indoor-environment monitoring system such as for EEG applications in healthcare is highly demanded due to brain monitoring in analysing several diseases like epilepsy, mental disorder and many more [6-8]. Most of the researches on indoor environment monitoring systems have used a radio frequency (RF) wireless communication medium or a wired communication technique. However, long-term usage of RF communication for wireless data transmission may deteriorate human health and cause adverse biological effects in the human body. In addition, RF technology generates electromagnetic interference (EMI), which not only jeopardize the performance of the medical instruments in the hospital but also cause malfunction of medical devices implanted in patients [9, 11]. Therefore, visible light communication (VLC) technology is one of the wireless communication methods, which can act as a substitute for the existing RF communication methods. The EMI-free and hazardless properties of VLC not only make VLC a better long-term wireless communication technique for indoor environments but also support the possibility of implementing wireless communication in RF-sensitive areas such as Intensive care units in hospitals [12, 13]. The pervasive use of cameras has led to not only a diverse set of camera-based sensing applications but also to novel opportunities to use cameras to communicate information [14]. The conventional VLC systems deploy photodiodes as receivers, requiring hardware, infrastructure modifications in addition to a smaller field of view (FOV), but the use of cameras reduce the infrastructure cost due to inbuilt filters, and a wider FOV coverage gives the ability to scale a larger area. The wider FOV and the movement of camera rotation, without any additional adjustments to maintain the line-of-sight (LOS), allows the patient to be anywhere within the room and FOV. In conventional VLC systems, PD is the receiver which requires hardware modification

due to filters and amplifiers; however, with the receiver being the camera the cost of implementation is considerably reduced due to inbuilt filters and focusing properties, reducing the unwanted noise [14-16]. The combination of the visible light source and camera receiver section is also termed as Visible Light Optical Camera Communication (VL-OCC).

This chapter presents the aims and objectives as well as outlining the contributions in context to the VL-OCC system for EEG applications. Additionally, presented is the thesis structure. A list of publications including peer-reviewed journals and referred conferences generated during the PhD study and the awards won are also mentioned in this chapter.

## 1.2 Problem Statement

Epilepsy is the second most prevalent brain disorder first being a stroke. In the UK, there are 0.6 million cases of epilepsy and about 60 million worldwide out of which 75% of cases have been reported in developing countries. People with epilepsy have high risks of personal injuries, such as premature and sudden unexpected death, and the impact of epilepsy extends to unemployment, depression and anxiety. Monitoring the human brain function has a great potential in helping us to understand how it operates and ultimately be able to detect early signs of disease and thus assist with diagnosing and monitoring brain-related disorders [17]. Electroencephalography (EEG), discovered by Hans Berger in 1924 is a procedure to record the electrical activity of the brain to diagnose diseases such as epilepsy, brain death, comma etc. EEG uses sensors placed on the head. The sensors can tell when the electrical activity from the brain increases or decreases and when displayed on a screen, it looks like a series of

waves known as brainwaves. The brain waves are categorised as shown in Table 1.1 [18].

Table 1.1. EEG Brainwave categorisation [18].

| **Brain wave** | **Frequency (Hz)** | **Occurrence** |
|---|---|---|
| Delta | 0.5-4 | During sleep |
| Theta | 4-7.5 | Unconscious like meditation |
| Alpha | 8-13 | Relaxation state |
| Beta | 14-26 | While working |
| Gamma | Above 26 | Deep thinking |

For instance, if the EEG signal received or measured from brain scalp is of the frequency range between 8Hz to 13Hz then the patient is said to be in relaxation state referring to Table 1.1. Similarly, following the brain wave categorization, brain diseases are analysed by doctors stating the health condition of the patient.

The conventional EEG recording techniques are deployed using several scalp electrodes, which involves long preparation time and are tedious [19, 20]. However, the advancement in RF-based wireless technology has led to the wearable EEG headsets Nuerosky, Imec, emotive etc, which are used for brain monitoring for specific applications like sleep disorders, cognitive analysis and many more depending upon the specific applications and the number of channels required for brain monitoring [21]. In recent years, due to the advancement in wireless technology the quality of healthcare has significantly increased at hospitals and healthcare environments. However, the priority

for the wireless technology to be preferred or used in healthcare applications or hospitals is not to have electromagnetic interference (EMI) because EMI might affect the health of the patient and the medical equipment in use thus posing a serious health hazard specifically in RF restrictive areas like ICUs [14]. Furthermore, the RF-based technology such as Bluetooth and ZigBee used in many EEG machines for data communication suffer from lack of frequency spectrum, eavesdropping, EMI and multipath fading [22, 23]. It has been stated that diverse usage of RF devices in hospitals especially in RF sensitive areas such as Intensive Care Units (ICUs), could result in adverse effects on both patient's health and medical devices due to electromagnetic interference [12, 13]. In order to overcome the above-illustrated problems by current RF-based wireless wearable EEG systems, the proposed EEG systems must be EMI free, low cost, wireless unlike the traditional systems which are tedious, wired, have EMI and provide discomfort to patients [12]. In view of shortcomings of EEG products based on RF technology, VLC is the promising solution due to low-cost, secure, no eavesdropping and free from EMI. VLC has been extensively used in areas such as vehicle to vehicle communication, Li-FI, underwater applications, military applications [23, 24] but the research work of VLC for EEG in healthcare has just begun over the past few years.

### 1.2.1 Data transmission in EEG applications

The authors in [25] presented a VLC system based on time hopping (T/H) using LED/PD pair for Electrocardiogram (ECG). The advantage of the system being that it could be used in RF restricted areas and in an emergency due to security and free from EMI. In [26] authors proposed a simple VLC based indoor monitoring system deploying the OOK modulation scheme. The LED/PD pair was used for the transmission and reception of data through sensors thus providing an efficient

communication system free from EMI and safe to both humans and medical equipment. In [27] authors demonstrated a dust monitoring system using VLC deploying wavelength division multiplexing (WDM) through RGB LEDs. The incoming light signals were differentiated using a colour sensor and then received and processed by a microcontroller thus enabling the medical team to monitor the indoor air -quality and improve the environmental conditions of hospitals. The authors in [28] proposed a VLC system for EEG signal transmission using three RGB LEDs as transmitter and three photodiodes as the receiver. In [29] the authors proposed a VLC based LabVIEW system for single-channel EEG transmission using LED/PD pair. Experiments performed in LOS with OOK-NRZ modulation resulted in improvement in SNR to 12.29 dB at 1m. The authors in [30] proposed a VLC system for ECG, which is non-invasive process to record the electrical activity of heart deploying LED/PD pair using time hopping (TH)scheme. The authors in [31] presented a low data rate static patient monitoring system in hospitals based on VLC using OOK modulation scheme deploying LED/PD pair. The proposed system was EMI free in comparison to RF protocols. As, VLC systems, use LED and PD as transmitter and receiver respectively, hence the authors in [32] proposed a medical portable device to download and access the healthcare information connected to the optical sensor using high brightness LED (HB-LED) and a high-speed photodetector.

### 1.2.2 Recent advances in VLC

The low-cost VLC system, free from EMI is best suited in healthcare especially in ICU's due to wellbeing of clinical staff and patients [33-36]. Wearable EEGs can monitor brain-computer interfaces, fatigue, and emotional and mental states, but the RF wireless radiation posed long-term risks to the patient's brain. The Pukyong

National University, South Korea team avoided this hazard by integrating VLC into a wearable EEG device equipped with electrodes to gather brain activity data and a microcontroller as an analogue data filter and analogue-to-digital converter. The researchers considered this to be an alternative to Bluetooth technology due to VLC being safe for human wellbeing [37]. Scientists and Researchers at National Taiwan University have developed a violet laser diode as an alternative to the LEDs typically used in VLC systems for indoor lighting. The researchers refined the chemistry and adjusted the phosphor thickness of their violet laser's diffuser plats to achieve a data rate capacity as high as 12 gigabits per second at distances over seven meters. If greater volumes of data could be transmitted by VLC systems, it would also make the technology more attractive to health care providers [36]. Scientists and Researchers at Kyoto, Japan have built up a VLC framework that utilizes a camcorder and an occasion timing encoding method to screen numerous pulses. The LED on the wearable heart screen flashes a sign comparing to every heartbeat that is caught by the camera. The encoding highlight records and breaks down the heartbeat to distinguish a hazard and ready parental figures or people on call [36, 37].

In summary, the recent research work of VLC in healthcare makes VLC the best alternative in healthcare replacing RF. Furthermore, VL-OCC that uses a camera as the receiver is a potential candidate for the data transmission in healthcare, due to its minimum hardware requirement and easy deployment.

### 1.2.3 Challenges in using VLC for EEG applications

This section presents the challenges while deploying VLC for EEG applications.

**(1) Field of view (FOV)**

In healthcare applications specifically EEG, due to low cost, free from EMI and reliability, several researchers have moved to VLC from RF technology. The two types of transmitter and receiver could be used in the VLC system. The transmitter can be LED, or OLED and receiver can be a photodiode or a camera. Recently in VLC systems, the OLED is replacing the conventionally used transmitter such as white LED (WLED) because OLED consists of materials of organic chemistry, comes into several shapes, low cost and flexibility. The authors in [38] demonstrated the successful transmission of the VLC system using OLED as transmitter and photodiode as receiver. VLC based LEDs/OLED system use positive-intrinsic-negative (PIN) and avalanche photodiode (APD) as the receiver (Rx) but does require hardware modification, therefore in order to provide low cost flexible wireless communications, the camera is the best solution to be deployed as a receiver in VLC systems [39, 40]. Due to the advancement in technology and rapid increase in the use of smartphones, led to the development of optical camera communication (OCC) where the camera is used as receiver, unlike traditional VLC system where photodiode is receiver [40, 41]. OCC is one of the promising technologies of OWC where the light intensity of LED is modulated to transmit the data, but the receiver is camera instead of photodiodes unlike traditional VLC system as requiring almost no additional cost [42]. The VL-OCC is known as the communication between light from the LED or OLED as transmitter and the receiver being the camera.

**(2) Angle deviation or perspective distortions**

During the brain monitoring or EEG, the patient must be still, or no movement is expected to avoid artefacts, however, in some instances due to patient movement the

data received is distorted, thus resulting in distorted images [21]. Therefore, the experimental study of angle deviation or perspective distortions is essential to determine the system performance in context to BER and link distance for the successful EEG recording.

**(3) The synchronisation between transmitters and receivers**

The synchronisation between the transmitter and camera as a receiver is a major challenge in EEG applications using VLC system. Several researchers have used, mask bits or start and stop bits before the transmission of the signal starts in order to establish the synchronisation between the tx and RX respectively [41]. The use of preamble helps in solving the synchronisation issue, however, the alignment of camera to maintain the LOS to ensure the camera is focussed and stationery is mandatory for the successful data transmission and reception of EEG signals. In this thesis in research work, preamble depending upon the size block of the OLED screen is used in experimental work to distinguish between the frames transmitted and received, thus beneficial in establishing synchronisation between transmitter and receiver.

The aim of this research work is to design a system prototype for the successful transmission of EEG to be deployed in RF restricted areas such as Hospitals. The work described in this thesis is based on the authors own research in discussion with the supervisory team at Northumbria University and Sheffield Hallam University. Any material/data adopted from other sources to make this research work more comprehensive is clearly referenced.

## 1.3 Aims and Objectives

The aim of this research is to develop an innovative VL-OCC system for transmitting EEG signals for indoor healthcare applications. The main objectives are listed below:

**1)** To conduct an in-depth literature review on the visible light communication technologies with a focus on camera communications and its applications in indoor healthcare.

**2)** Design and development of VL-OCC system using OLED as the transmitter and camera as the receiver.

**3)** Study the impacts of the block size of the low-cost OLED screen, distance, angle on the performance of the proposed VL-OCC and find the optimal pixel size for BER.

**4)** Experimental investigation of the proposed VL-OCC system to verify its performance in context to BER and link distance with respect to different pixel sizes 8, 16 and 32 of the OLED screen.

**5)** Experimental investigation of the proposed system in context to angular deviation with respect to BER and link distance at pixel size 16 pf the OLED screen.

## 1.4 Original Contributions

This thesis introduces the following original contributions to the knowledge that are summarized as follows:

- A VL-OCC system for EEG is proposed which has a great potential in hospitals and is investigated for future in-door healthcare applications. In particular, for those applications where RF is restricted, such as RF sensitive areas specifically ICUs. Establishment of the relationship between the communication performance of the OOK-NRZ modulation in VL-OCC and the key configuration parameters

of VL-OCC, including the block size of the low-cost OLED screen, distance, angle and effective link configuration between transmitter and receiver was investigated.

- The angle deviation for EEG signal transmission was proposed the first time and mentioned in this thesis illustrating the system performance in context to link distance and BER. The BER results of 16 × 16 Pixel OLED screen and Thorlabs camera, depicted that with the angle deviation, distortions in the bits increased considerably per frame with the increase in distance, hence affected the system performance in context to BER at farther distances and greater angle deviations.
- Development of a proof-of-concept VL-OCC prototype using low-cost OLED and digital single-lens reflex camera (DLSR). A 32 × 32-pixel OLED screen acts as a transmitter. Other cameras, such as the android smartphone J3 samsung galaxy and thorlabs camera, were also used for comparison. Intensive experiments were carried out to evaluate the performance of the proposed system in the indoor healthcare scenario

These original contributions are further summarised in figure 1.1. The green boxes show what has been carried out in this research work.

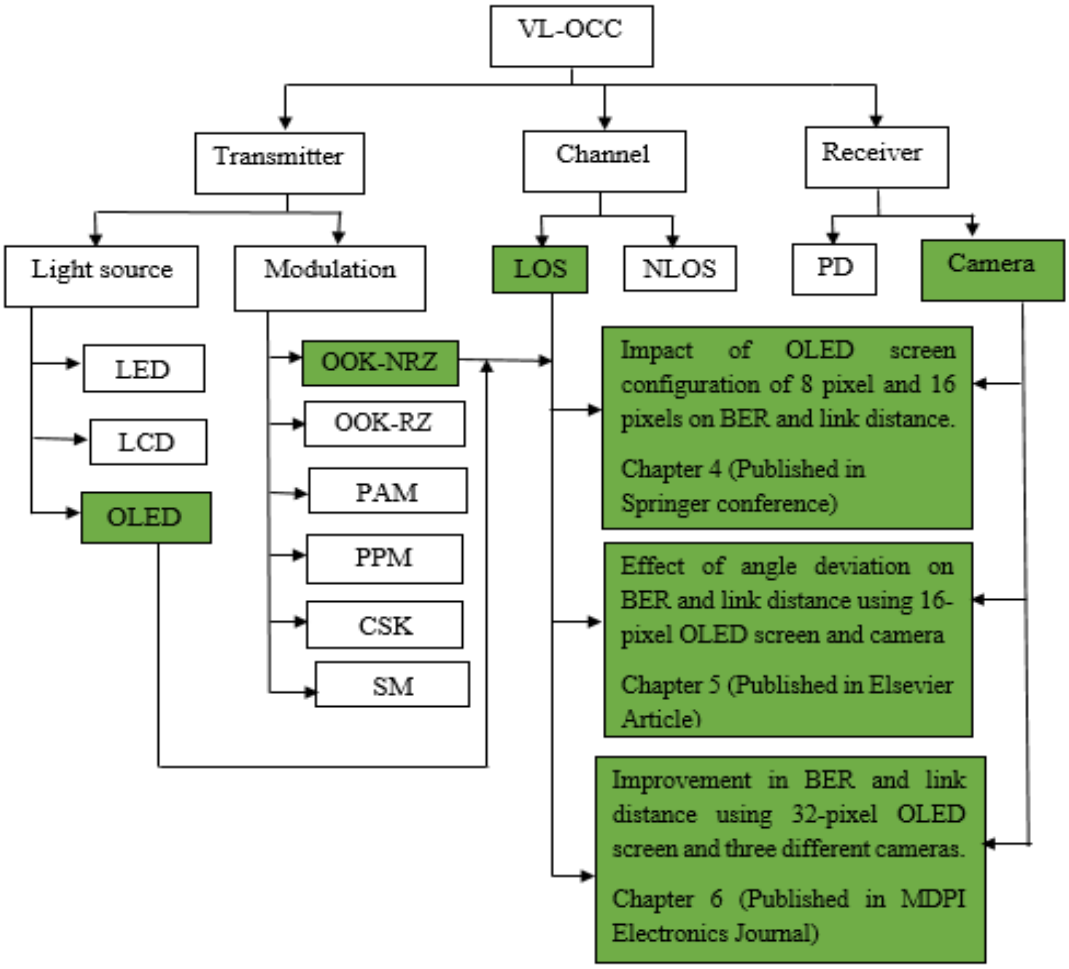


Figure 1.1 VL-OCC domain in EEG research undertaken during the PhD study.

## 1.5 Publications and Awards

### 1.5.1 Peer-reviewed Journals

[J1]. **G. Aggarwal**, X. Dai, R. Saatchi, R. Binns and A. Sikandar. Experimental Demonstration of Single-Channel EEG Signal Using 32 × 32 Pixel OLED Screen and Camera. *Electronics* **2019**, *8(7)*, 734.

[J2]. **G. Aggarwal**, X. Dai, R. Binns and R. Saatchi, "Real-time Wireless Healthcare system for Angular Transmission of EEG signal using VL-OCC". *Procedia Computer*

*Science*, *152*, International Conference on Pervasive Computing Advances and Applications – PerCAA 2019, pp.28-35.

### 1.5.2 Referred Conferences

[C1]. **G. Aggarwal**, X. Dai, R. Binns and R. Saatchi, "Wireless EEG Signal Transmission Using Visible Light Optical Camera Communication". In: Deka G., Kaiwartya O., Vashisth P., Rathee P. (eds) Applications of Computing and Communication Technologies. ICACCT 2018. Communications in Computer and Information Science, Springer, Singapore, 2018, vol 899. pp.152-161.

[C2]. **G. Aggarwal**, X. Dai, R. Binns and R. Saatchi, "Experimental Demonstration of EEG Signal Transmission Using VLC Deploying LabView," 2018 3rd International Conference and Workshops on Recent Advances and Innovations in Engineering (ICRAIE), Jaipur, India, 2018, pp. 1-6.

### 1.5.3 Poster

[P1]. Presented at EE PGR conference, 2018 at Northumbria University, UK

### 1.5.4 Awards Won

1. Won the Northumbria Student LED Teaching Award in the category of "**Outstanding Staff Member – Engineering and Environment**", 2019.
2. Won the **Annual Award 2019** at Northumbria University, UK
3. Won the Northumbria Annual Award in the category of "**Best Contribution to Student Academic Experience**", 2018.
4. Nominated for Student-Led Teaching Award in the category "**Best Postgraduate Student who teaches**", 2018.

5. Won the **Education Award** 2018 at Northumbria University, UK.

## 1.6 Thesis Organization

This thesis is mainly focused on the research work dedicated to VL-OCC system to be deployed in healthcare or hospitals specifically for EEG applications. The organization of this thesis includes the literature review, original contributions, state of art, image processing, experimental work, programming codes, conclusions, and future work divided into 7 Chapters.

**Chapter 1** gives a brief introduction to the thesis along with background and motivations behind this research, followed by aims and objectives, original contributions and research outcomes.

**Chapter 2 lists** the literature review and background on VLC along with potential applications of VLC. Thereafter, chapter 2 continues to discuss the principals of VLC, system model of VLC including different transmitters, VLC channel and different receivers. Lastly, chapter lists the basic criteria for the modulation schemes of VLC. The chapter list that the due to simplicity OOK modulation is easier to implement, hence in this thesis research work OOK-NRZ modulation scheme is deployed.

**Chapter 3** gives an overview of OCC, followed with the advantages of OCC compared with the conventional VLC system. The key components of OCC, such as transmitters of OLED screens, image sensors and channel used in communication systems and then moving on VL-OCC system. The chapter also provides the basic architecture of VL-OCC system along with different visible light i.e. LED and camera communication scenarios. Thereafter, digital image processing (DIP) along various techniques of image detection along with computer vision and necessary background

or theory is illustrated which is essential for the reader to understand the proposed system model in this thesis.

**Chapter 4** focuses on the design and implementation of the proposed system. It also lists the experimental setup and PCB hardware design. The work investigated the BER performance and system stability in LOS condition using different blocks such as 8-pixel and 16-pixel OLED screen and Thorlabs camera deploying OOK-NRZ modulation scheme.

**Chapter 5** introduces the angle deviation concept to understand the system performance and stability in context to BER and link distance. This chapter illustrates the system performance for real-time wireless healthcare system for EEG using 16-by-16-pixel OLED screen and Thorlabs camera.

**Chapter 6** focuses on the data rate improvement using the experimental set up listed in chapter 4 and chapter 5. Chapter 6 also illustrates the improvement in link distance and BER performance using a 32-pixel OLED screen. The receiver is the camera, three different cameras namely thorlabs, android smartphone samsung galaxy J3 and DSLR were tested during the experimental work to determine the BER performance and link distance. The experiments show the error-free, transmission of EEG signal up to 5.5m using DSLR camera in context to Thorlabs and an android smartphone camera.

**Chapter 7** lists the conclusions and recommendations for future work.

# Chapter 2 Literature Review

## 2.1 Background

Light has been used throughout history for enlightenment purposes, progressing from the basic utilization of flame for brightening to conventional glowing and bright light bulbs. As far back as 800 BC, Romans and the Chinese utilized flame signals to transmit messages. In addition, around 150 BC, local Indian Americans utilized smoke as a method for interchanges to send data [43]. Light was one of the earliest means of communication employed by humans since ancient times. Light is likewise broadly utilized for route purposes, for example, exploring ships through harbors. Furthermore, ancient Greeks polished their shields to reflect the sunlight as a means of providing signs to other soldiers in wars. Ancient Romans also used polished metals as mirrors to transmit information over long distances. Later, the Romans placed watchtowers on top of mountains all over the Roman Empire to transmit optical signals. In mid-1880, the world saw the introduction of the principal modern handy showing of an optical interchange's framework "Photophone" by the Scottish researcher Alexander Graham Bell shown in Figure 2.1 [44, 45]. In his experimental setup, the transmitter modulated the voice signals over the light carriers while the receiver comprised of a selenium cell that was set inside the point of convergence scope of an explanatory mirror in order to convert the optical signal received into an electrical signal.

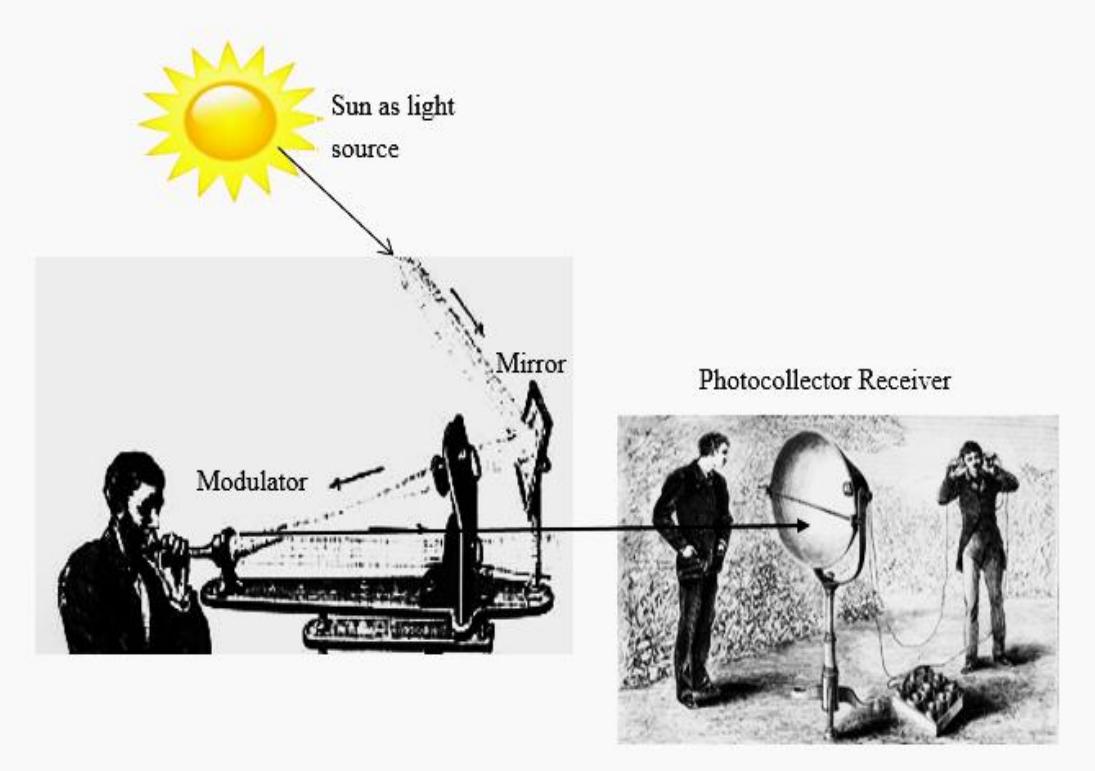


Figure 2.1. The experimental set up of Alexander Graham Bell [44, 45].

In 1962, James R. Biard and Gary E. Pittman from the Semiconductor Research and Development Laboratory in Texas Instruments developed the PN intersection infrared light-emitting diode (LED) using gallium arsenide (GaAs) as a semiconductor material thus a revolution in telecommunication started [46-49]. Nowadays, the basic principle to transmit wireless data is through RF protocols. However, the RF spectrum is currently crowded and congested, accordingly is finding it difficult to meet the data rate necessity of the users [50,51]. In [52], it has been stated that because of the expectation of the end-users in terms of data rate needs and the foreseen rise in data traffic, the RF electromagnetic spectrum is exhausted and congested, therefore will not be able to meet the data rate increase in nearer future. Hence, the alternative to meet the growing demand of data is optical wireless communication (OWC) as it has unique

advantages over RF, the foremost being the huge unlicensed bandwidth spectrum. The electromagnetic spectrum is shown in figure 2.2 [53].

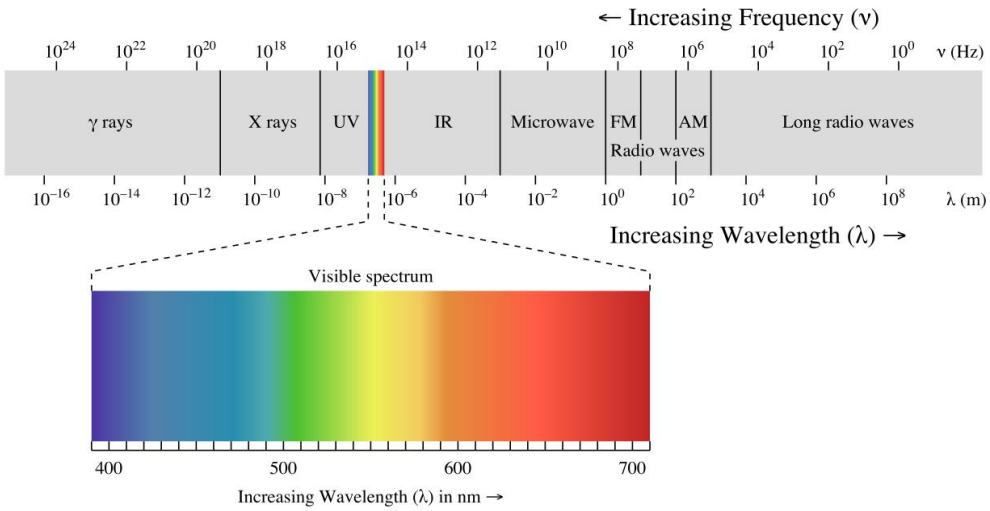


Figure 2.2. The classification of electromagnetic the spectrum [53].

The VLC spectrum ranging between 400nm and 700nm is license-free, high bandwidth, EMI free, hence is an ideal alternative for the indoor environment such as hospitals specifically in EEG applications. VLC can be utilized to supplement current RF frameworks, especially in indoor conditions where over 70% of the remote traffic begins [54]. VLC has immense potential to be deployed in an indoor environment especially hospitals due to numerous advantages of VLC over RF, IR and UV are discussed below:

**(1) Safety**

The RF negative impact on the human wellbeing is increasingly inclined to RF prohibited regions particularly in hospitals specifically ICUs. Moreover, it has been stated by world health organization (WHO) that the RF electromagnetic have the

possibility of causing a disease called cancer in humans [55, 56], hence VLC is the prime alternative in medicinal services or healthcare.

**(2) Security**

On the contrary to RF waves, the light can't enter through dividers or pass through objects, giving VLC high security against eavesdropping. This makes VLC suitable in regions of high security in healthcare while transferring the patient data [55, 56].

**(3) Low-cost implementation**

In contrast to RF, VLC utilizes the light or existing infrastructure for data communication, hence, the cost of implementation is remarkably decreased. Another advantage of VLC is that it reduces the cost of implementation being pervasive in nature [55] because VLC depends on existing frameworks offered by LED lighting sources. Another characteristic which empowers VLC to decrease the cost of implementation is the use of LED or OLED deployed as transmitters, while receivers are photodiode and camera, which are installed in smart devices [53, 56]. Therefore, VLC deployed in healthcare or hospitals would not need infrastructure modifications due to existing frameworks, which makes VLC best suited over other technologies such as RF.

**(4) Green wireless communication technology**

While the increase in population, the natural resource consumption and climate deteriorations are also increasing as a result greenhouse gas emissions have reached alarming levels that are producing significate climate changes that affect the whole ecosystem [57]. However, natural resource consumption and pollution can be significantly reduced by decreasing energy consumption. Artificial lighting, commonly provided by electric lights, represents a significant percentage of energy consumption. Worldwide, approximately 19% of electricity is used for lighting, while

electricity represents 16% of the total energy produced [57, 58]. VLC is also a green wireless communication technology because it does not use additional power for the communication as the same light which is used for illuminating is used for the data transmission. Another important advantage of VLC is the usage of LEDs which provides substantial energy savings, reducing the CO2 emissions, therefore VLC is the optimum solution in the view of shortcomings of RF in the indoor environment.

The above-discussed advantages of VLC and benefits depict that VLC is the appropriate candidate for healthcare or hospitals. The VLC being safe to patients, staff and medical equipment because of free of EMI, no eavesdropping, low power consumption and high bandwidth makes VLC the prime substitute of RF in hospitals or healthcare specifically for EEG applications. Over the years, research in context to VLC has resulted in deploying VLC in numerous applications, some of them are discussed in section 2.2. Section 2.3 discusses Principals of VLC, with subsections illustrating a typical VLC system model highlighting different transmitters and receivers used in the VLC system. Thereafter the basic criteria for the modulation schemes are listed focussing on OOK, being simple to implement, followed up with summary in section 2.4.

## 2.2 Potential applications of VLC

The advantage of VLC over other technologies listed in section 2.1 makes VLC a paramount candidate for indoor environment specifically hospitals. Furthermore, VLC can also be deployed for indoor localization, aeroplane, home or office in an indoor environment in addition to underwater and V2V, I2V communication [59]. Some of the potential applications of VLC are shown in figure 2.3.

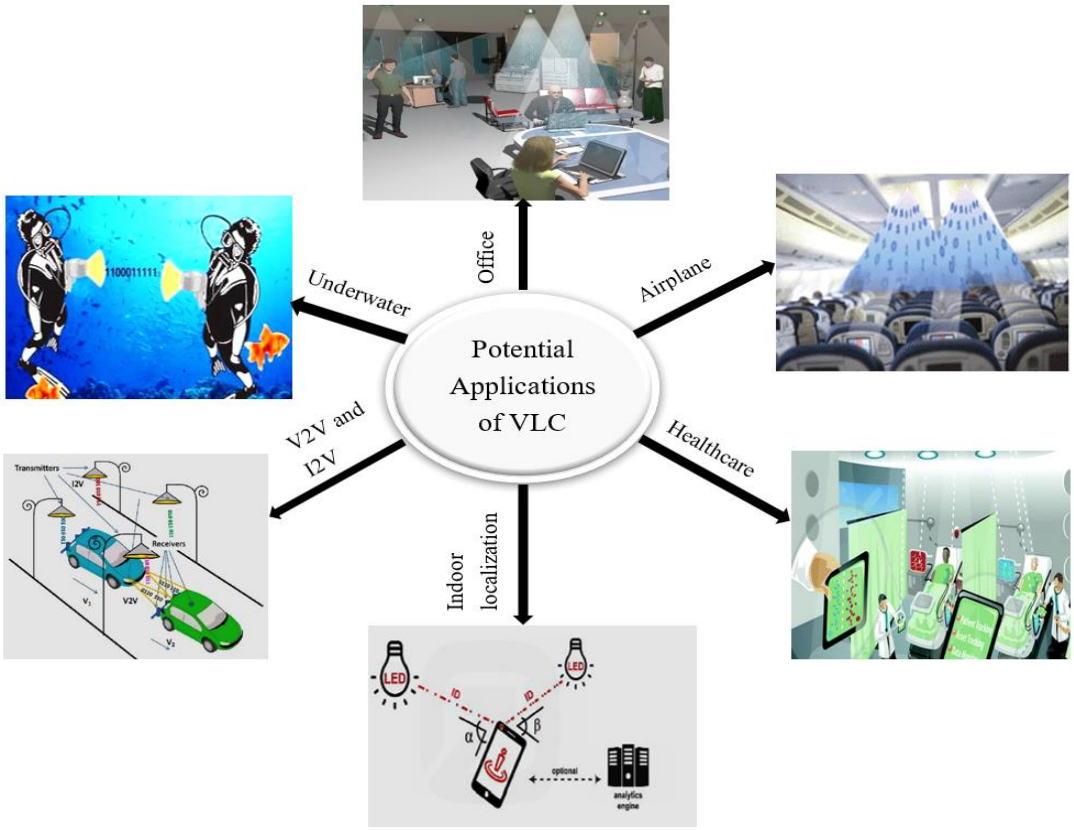


Figure 2.3. The potential applications of VLC.

**(1) Office**

Any lighting source in-home or office can be utilized to give VLC hotspots and similar correspondences. For instance, a protected and exceptionally high information rate LAN can be sent where PCs, printers, cell phones, and other cell phones are interconnected utilizing VLC. It can likewise be utilized to manage extreme interest indoor remote access to the Internet and ongoing transfer speed concentrated applications, for example, Voice over IP (VoIP), video gathering, continuous video recurrence checking, and organize joined capacity [60]. VLC using the existing infrastructure for communication can also be used in device to device (D2D) connections both at home and office, thus making VLC a suitable candidate for internet of things (IoT) or optical internet of things (IoT).

**（2）Underwater communication**

Currently, communication underwater is next to impossible because radio waves are quickly absorbed in water. In contrast, light can easily travel in water and is able to penetrate for large distances. Hence, VLC can be used to enable communication between divers, diver to mini-sub, the diver to a drilling rig, or even military communication underwater as RF waves do not travel well in seawater because of its conductivity [61-63].

**(3) Vehicle-to-Vehicle (V2V) and Infrastructure-to-Vehicles (I2V)**

VLC can be used for vehicular communication due to the presence of the vehicle lights and the existing traffic light infrastructure. The high priority applications indicated by the vehicle safety communications project include cooperative forward-collision warning, pre-crash sensing, emergency electronic brake lights, lane change warning, stop sign movement assistant, left turn assistant, traffic signal violation warning and curve speed warning [64, 65]. The LEDs used for car headlights and taillights presents a wonderful opportunity for the development and application of technologies that improve road safety by enabling vehicle to vehicle (V2V) communication using VLC. Additionally, LED traffic lights to allow more efficient traffic management systems such as continually updating cars with optimal routes to take at certain hours or with information on certain emergency events at different locations thus resulting in infrastructure to vehicle (I2V) communication [65, 66].

**(4) Indoor localization**

The global positioning systems (GPS) make use of GPS satellites in space in order to provide location data. For mobile users, this data is acquired using mobile phone

location services [67, 68]. Light can be used for indoor positioning systems by setting each light source to transmit different sets of data. Each light source can send a unique code that corresponds to specific locations. These codes are then decoded by smartphones using phone apps. Once decoded, the position of the specific light source will be found and shown on an electric map on a user's smartphone. This can be useful in a variety of situations such as an easy locator of parking spots in large parking spaces, electronic maps for museums, or even for delivery of content at retail establishments [ 68, 69]. Visible light can be used as an ID system in different places such as buildings and subways. For example, if we are standing in room seven in a certain building. A visible light ID system can be employed for identifying the room number and its building. In retail, LED lights can be used to deliver specific content to shoppers browsing through different items while in a store. The data being transmitted can be in the form of supplemental information about an item to nudge them in the right direction. These can also be advertising materials to inform customers about special offers and coupons. Catalogue information can also be provided in order to inform customers about other products the store has to offer [67-70].

**(5) Healthcare**

Many healthcare environments forbid the use of electronics, especially those that make use of radio frequencies, because these radio frequencies may interfere with sensitive hospital equipment specifically in RF restricted zone areas. It has been discovered that the activity of heart pacemaker is affected due to the electromagnetic caused by RF devices [71]. In view of shortcomings of RF, a VLC-based communication system can be deployed effectively on existing infrastructure to provide electromagnetic free safe data communication [27,29]. This can be applied in the monitoring of patients, hospital

security, storage or transport of hospital patient records, or emergency situations that necessitate instant communication

**(6) Aeroplane**

The main concern with electronics uses in airlines mid-flight is that these devices may create electromagnetic interference with sensitive radio equipment on the flight deck. VLC technology can be deployed on airlines for easier delivery of content on-board the plane while also eliminating data rates, the need for extra wiring, and radio frequency interference [72]. With the use of on-board VLC systems for data connections, airlines are able to easily deliver pre-flight instructions, deliver in-flight movies and games, and even create additional channels for communication between airline staff [43, 72].

## 2.3 Principals of VLC

The idea of VLC utilizing LEDs for data communication in addition to illumination was considered in Japan in 1999 by Pang et al. [73], In 2001, Kulhavy of Twibright Labs created RONJA (Reasonable Optical Near Joint Access) [74], a free innovation venture for solid free-space optical information joins utilizing light for communication at a link distance of 1.4 km. In recent years the are numerous activities to advance and institutionalize VLC innovation. For example, the Visible Light Communication Consortium (VLCC) [75], in Japan, was set up in November 2003 to announce and institutionalize the VLC innovation; the OMEGA (HOME Gigabit Access) venture in Europe, kept running by analysts from organizations, colleges and research foundations to build up a home/office get to arrange equipped for conveying high-data transfer capacity  administrations and substance at a transmission speed of 1-Gbps utilizing a blend of light intensity [76].

The IEEE 802.15.7 Visible Light Communication Task Group [77], started in 2009, which has finished a PHY and MAC standard for VLC. Furthermore, the Li-Fi Consortium [78], established in 2011 with the idea and guide to set up the innovation in the market. Other significant research focuses along with R&D exercises on VLC incorporating University of Oxford (U.K.), Smart Lighting Engineering Research Center (Boston University), UC-Light Center (University of California, U.S.), Keio University (Japan), and University of Edinburgh. In context to incandescent and fluorescent lights, LED lights to have longer life expectancy, low cost and no health hazards [79]. As a result of these advantages, LED selection has been rising reliably, and it is predicted by 2030 about 75% of light sources will be formed of LEDs [80]. Furthermore, the fast switching characteristic of LED gives the VLC to use LED as a transmitter for dual purpose of lightning and communication by adjusting the power of the LED light so that it is imperceptible to the human eyes, having no negative impact on the brightening usefulness [81, 82].

Illumination has come a long way from fires and candles through to the LED. Incandescent lamps are still a widely used lighting technology, however, due to high amount of useful energy being lost in the form of heat, the trend shifted towards the use of fluorescent lamps. LED is a solid-state semiconductor device which has the capability of changing electrical energy directly into light energy. The key structure in an LED is a semiconductor chip which creates a p-n junction. It contains semiconducting material doped with impurities to create a p-n junction. Charge carriers, mainly electrons and holes flow into the junction from electrodes with different voltages. On applying voltage, an electron meets a hole, and falls into a lower energy level, releasing energy in the form of photons which is seen as emitted visible

light. This effect is called electroluminescence [83,84]. LEDs have a wide range of advantages compared to traditional lighting technologies:

(1) LEDs are energy efficient and generate less heat [85]. They can reduce energy consumption by 80% in general and domestic lighting applications [86].

(2) LEDs have a longer service life and can operate for 25,000 to 50,000 hours before their output drops to 70% compared to standard incandescent bulbs having a lifetime of 6000 to 15000 hours only [87,88].

(3) They are free from hazardous substances like mercury [89].

(4) They can work under unforgiving environments and ambient lighting conditions [90].

These exciting complementary communication aspects to LED lighting have generated considerable research and industrial interest in using VLC as an alternative for RF in data transmission specifically in an indoor environment, thus reducing the implementation cost considerably due to infrastructure readily available.

### 2.3.1 VLC system model

Visible light communications using the idea of LEDs for both illumination and data communications. The LED lighting is replacing the existing incandescent lighting systems due to low cost, longer life span, low power consumption and dual functionality of lightning and data communication. VLC employs LED at transmitter section and photodiode at receiver section, where the transmitter is electro-optical device converting electrical signal to optical and photodiode is optical-electronic device thus converting the optical signal to electrical [23, 43]. The basic VLC system diagram is shown in figure 2.4.

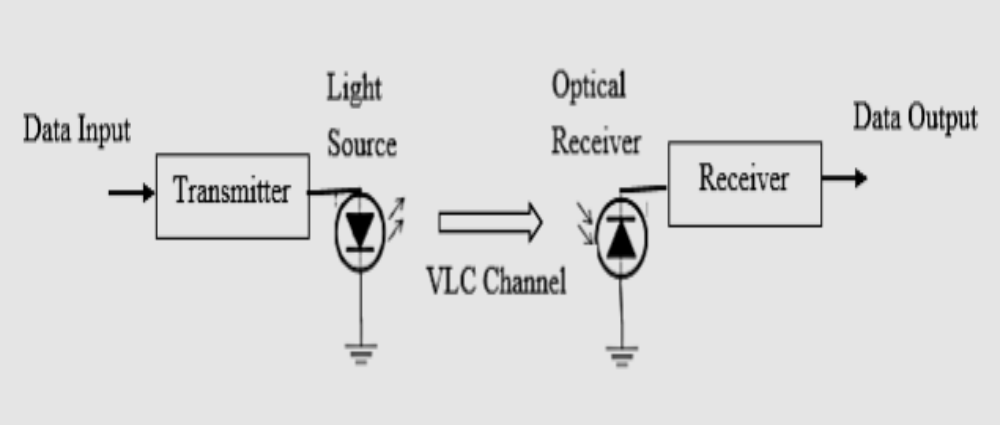


Figure 2.4. Basic VLC system block diagram.

The light intensity-modulated beam from the transmitter is transmitted over the VLC channel which could be LOS or NLOS or combination of two. At the receiver section, the incoming light signal or information is captured using an optical receiver which is further processed to reconstruct or recover the originally transmitted data.

**(1) Transmitter**

White light is the most widely used form of illumination deployed in data communication applications [43]. Therefore, the commonly used method to produce white light is with the help of blue LED as shown in figure 2.5(a), however, the modulation bandwidth is of the order of 3MHz only due to the phosphor coating relaxation time. [23, 43]. Thus, the key challenges that limit the data rate of the VLC system are the slow modulation response of LEDs and the limited bandwidth. Another method to produce white light is the combination of red-green-blue (RGB) LEDs shown in figure 2.5(b) [43].

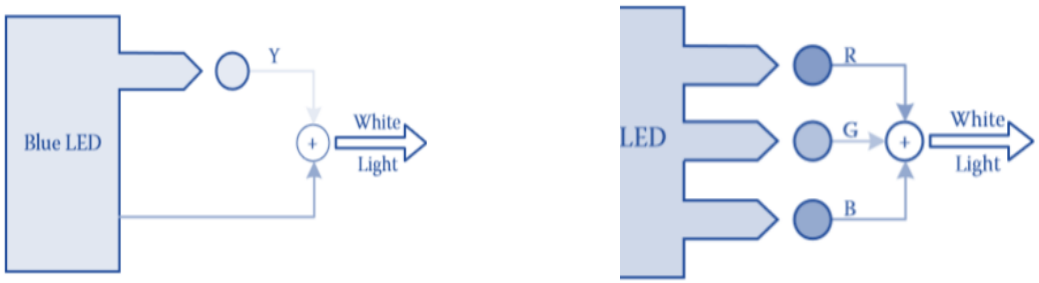


Figure 2.5. (a). Blue LED. (b) RGB LED [43].

RGB LEDs is the most common multichip LED, which contains three jointly packaged LED chips (red, green and blue) to produce white light. Therefore, by changing the light intensities of the different chips, the colour of the output light is modified and a much higher modulation bandwidth of more than 100 MHz, can be obtained [43]. However, the multi-chip LEDs still suffer from some drawbacks, such as a more complex structure, and higher costs than the traditional phosphor-based LEDs (ps-LEDs). In the past few years several LEDs have been developed to improve the data rate and modulation bandwidth thus to enhance the system performance of the VLC system, commonly used transmitters in the VLC system are discussed below:

**(a) Resonant Cavity LEDs (RC-LED)**

The extraction efficiency of conventional LEDs is poor due to the large difference in refractive index between the narrow gap semiconductor and the surrounding medium, which is typically air, however, high brightness RC-LEDs would benefit VLC for colour displays [91]. The emission of RC-LED is typically at ~650 nm with a narrow linewidth and can be modulated in excess of 100 MHz [91]. The authors in [92] demonstrated phosphor-converted white resonant-cavity light-emitting diodes (RC-LEDs) that provided the data rate of 150Mb/s. Due to fabrication issues, RC-LEDs are not used significantly.

**(b) Micro LEDs (μ-LED)**

Instead of a single LED, micro LEDs consist of arrays of micro-pixelated LED pixels, based on III-nitride technology. μ-LEDs offer better contrast, response times, longer lifetime, and energy efficiency. Furthermore, by reducing the LED active area to 100×100 $\mu m^2$ or less, the capacitance is decreased while the current density is increased, and this thereby contributes to a significant increase in the modulation bandwidth. Usually, the typical size of each individual pixel ranges from 14 to 84 $\mu m$, and the 3-dB bandwidth can reach 450 MHz, thus resulting in a data rate up to 1.5 Gb/s. Figure 2.6 shows the micro-LED reported by Islam et al. which converts electrical-to-optical bandwidths of up to 655 MHz [93].

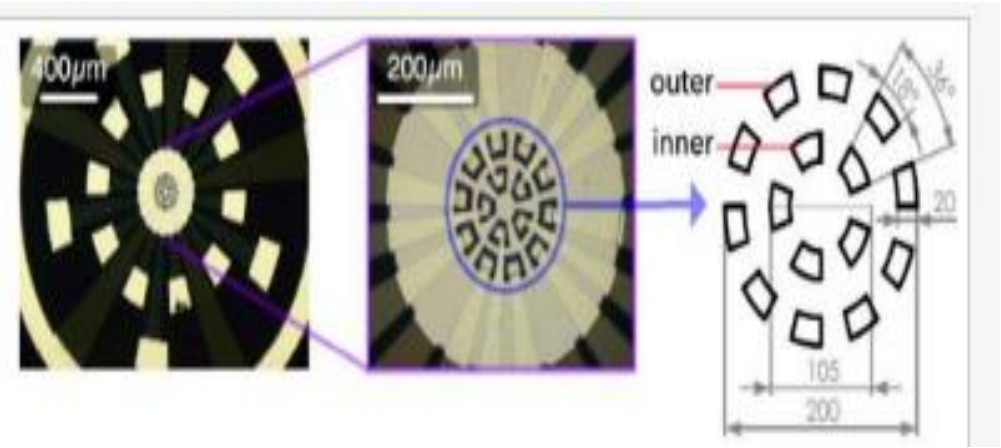


Figure 2.6. Micro LEDs [93].

Aluminium Gallium Nitride (AlGaN) based micro-light emitting diode arrays have been in development for VLC and Polymer Optical Fiber (POF) recently [94, 95]. $\mu$-LEDs have the potential to be used as display panels incorporating high-density parallel communication. These arrays typically emit light in 370–520 nm wavelength range, with the possibility of using wavelength conversion to produce white light [96,97]. The high bandwidth is possible due to the very low capacitance in the LEDs.

Recently, the University of Strathclyde, along with researchers from the University of Oxford, Edinburgh, Cambridge, and St. Andrews have begun researching into GaN-based LEDs for ultra-parallel high-density communication [98].

**(c ) Laser diodes (LDs)**

LDs are particularly impressive due to their small size, where a single LD is a much brighter light than an LED. Furthermore, LDs can handle a data bandwidth enlarged by one or two orders of magnitude greater than LEDs [43]. Additionally, the output light has the feature of coherent and collimated, which is fit for point-to-point data transmission. Thus, by leveraging the advantages mentioned above, an LD-based white VLC system is promising to outperform the ones based on LEDs. According to recent studies, multi-Gigabit data rates have been achieved in VLC systems based on III-nitride LDs [43]. However, the safety concerns involving the use of LDs are the main limitation for the rapid development of an LD-based VLC system in healthcare specifically in brain monitoring or EEG [83].

**(d) Organic light-emitting diode (OLED)**

Like an LED, an OLED is a solid-state semiconductor device that is 100 to 500 nanometres thick or about 200 times smaller than a human hair. OLEDs generate light using an organic layer sandwiched between anode and cathode as shown in figure 2.7 [99]. OLED is known as organic light emitting diode because it is formed of organic substances.

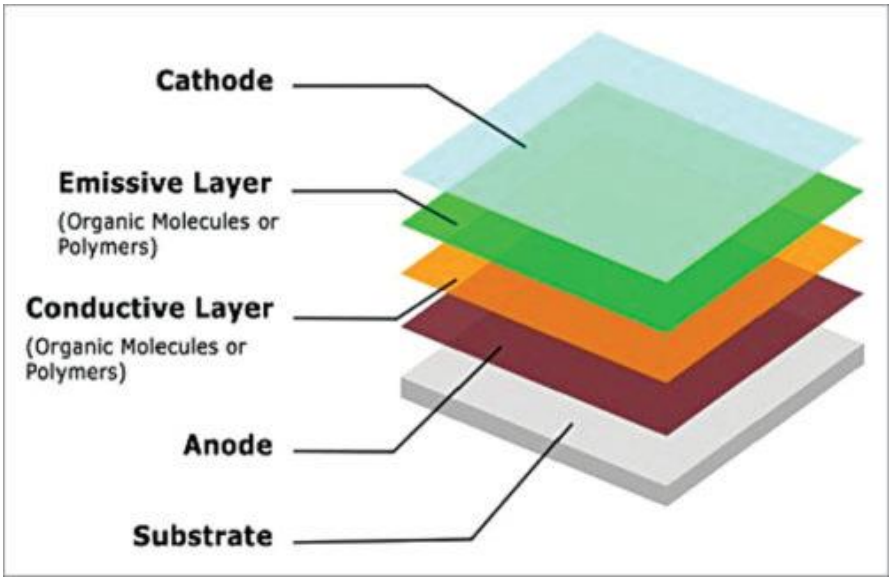


Figure 2.7. The structure of OLED [99].

In recent years there has been a growing interest in using organic light-emitting diodes (OLEDs) for illumination in indoor environments. They offer attractive features such as flexibility and large active areas at a low cost; they are energy efficient and have higher illumination levels compared to silicone-based LEDs [100-103]. In addition, the utilization of OLEDs has increased in devices such as smart mobile phones and TVs because of their low thickness. The maximum thickness of an OLED is 500 nm [104], which is ideal for thin-film devices (such as mobile phones, computers, and TVs), thus providing the potential of infrastructure-to-device (I2D) and device-to-device (D2D) communications [105]. In D2D communications, the data can be transmitted via pixels of the mobile phone display [106] and is captured using the camera(s) in smartphones [107]. Therefore, in this thesis, OLED is used as a transmitter to transmit the EEG data optically.

**(2) VLC channel**

Channel is the most important feature in VLC systems as it represents how the transmitter light ray moves through space to the receiver. The two main components

to analyse the VLC channel are the line of sight (LOS) and non-line of sight (NLOS) transmission. The NLOS transmission generally given by rays, which reflected on obstacles and, after some bounces, hit the detector/receiver. System environment and location, transmission/reflections emission, wavelength dependence and number of reflections are the general characteristics to be considered for VLC channel. The IM-DD (intensity-modulated direct detection) technique is the most used method to communicate with VLC for its low cost and simplicity. The mathematical model for the VLC optical channel is given by [43]:

$$y(t) = \Re x(t) \otimes h(t) + n(t) \tag{2.1}$$

Where $\Re$ is the responsivity of the photodetector, $y(t)$ is the photocurrent, $x(t)$ is the transmitted optical power, $n(t)$ is the channel noise comprising of shot noise or thermal noise, which is modelled as additive white gaussian noise (AWGN), $\otimes$ denotes the convolution and $h(t)$ is the impulse response of the optical channel.

**(1) Receiver**

In VLC systems, two types of detectors are commonly used at the Rx: (a) PDs; and (b) Camera consisting of image sensors or an array of PDs. This section will give a brief overview of each of the receivers.

**(a) Photodiodes (PDs)**

In VLC systems typical commercial silicon (Si)-based positive-intrinsic-negative (PIN) PDs and avalanche PDs (APDs) are used as a receiver. The PD can provide a 2 GHz of bandwidth for a photosensitive area $A$PD of ~0.00785 $mm^2$ [108]. As PD yields to the smaller photosensitive area, therefore, the higher bandwidth can be obtained but at the cost of decreased FOV thus resulting in a higher optical gain. Furthermore, at low intensity, PD does not offer the required SNR. Alternatively, APD

which provides higher gain than PD can be employed under low illumination or low-intensity conditions [109]. The commercial Si-based APDs with $A$PD = 0.0314 $mm^2$ can reach a bandwidth of 2 GHz at a wavelength of 700 nm offering a gain of 100 [110]. The other option is the single-photon avalanche PDs (SPADs), which works above the breakdown voltage and can detect a single photon. However, at the detection of a photon, the bias voltage across the SPAD drops. In order to detect the second photon, the bias voltage needs to recover and hence the "dead time". In order to mitigate the "dead time", an array of SPADs has been employed [111]. However, the APDs and SPADs are very costly and require high bias voltage levels of ~100 and ~10 V, respectively. Besides, PD-based VLC systems are for short-range links and are complex to implement for multiple access-based schemes and suffer from high-level of ambient light noise.

**(b) Camera**

Today's pervasive devices are increasingly being integrated with light-emitting elements in the form of light-emitting diode (LED) arrays, that serve the dual purpose of illumination and signage, and photo-receptor arrays in the form of pixel elements in a camera. The increasingly ubiquitous use of cameras (or photodiode arrays) in pervasive devices such as smartphones and tablets, cars, gaming consoles, etc. creates an exciting opportunity to use cameras for data communication [106,107]. In healthcare nowadays, cameras and surveillance offered by Cisco are used for monitoring patients and to provide two-way communication between the patients and relatives in emergency situations [112]. Fujitsu has created a camera that recognizes the sleep of a patient thus analyzing the intervals when the patient is in bed, out of bed, tossing in and out. In this thesis, the camera is deployed as receiver [112]. As the OLED used in the research work in this thesis is in the form of a matrix hence, the patient

information is transmitted in the form of quick response (QR) code received by a camera. The QR code obtained at the receiver section through image capture can be easily compared to the transmitted image in 2D to calculate BER and to analyze the system performance.

### 2.3.2 Modulation schemes

In the past years, several modulation techniques and have been thoroughly analyzed based on the number of constraints imposed such as the maximum average radiation, power efficiency, and transmitted power [42]. The majority of practical OWC systems employ the IM/DD scheme for indoor and outdoor applications. In RF systems, the amplitude, frequency, and phase of the carrier signal are modulated by the information signal. Whilst they cannot be applied in an optical system, the intensity of the optical carrier is modulated when the data rate is small than 2.5 Gbps. There are a number of modulation schemes that have been deployed in optical systems such as quadrature amplitude modulation (QAM) utilizing discrete multitone (DMT), binary and multi-level modulation schemes, for instance, on-off keying (OOK) modulation and multi-level pulse amplitude modulation [23,43,83]. These are suitable for VLC systems and are based on LEDs. The main metrics to select the modulation scheme are:

1. **Bandwidth efficiency:** As the receiver, bandwidth is limited by the photodetector area whereas multipath propagation confines the bandwidth of the channel. Modulation schemes also affect Inter Symbol interference (ISI). The efficiency of bandwidth $\eta_B$ is the ratio between achievable bit rate $R_b$ and bandwidth of the transceiver $B$ [43]:

$$\eta_B = \frac{R_b}{B} \tag{2.2}$$

The second parameter is known by the power efficiency which is the relationship between the bandwidth efficiency and the average duty cycle $\gamma$ [43]:

$$\eta_p = \frac{\eta_B}{\gamma} \tag{2.3}$$

2. **Transmission reliability:** Transmission reliability requires a minimum acceptable error rate. Modulation schemes should overcome several problems such as phase jitter due to signal power variations, pulse extensions and pulse distortion [43].
3. **Power efficiency:** The average transmitted optical power for each modulation technique is limited because of safety regulations and the requirement of illumination which is the main purpose of LED. The power efficiency is the ratio between the pulse energy $E_{pulse}$ and the average energy per bit $E_b$:

$$\eta_p = \frac{E_{pulse}}{E_b} \tag{2. 4}$$

The above-mentioned metrics must be taken into consideration in the selection of the modulation scheme based on bandwidth and power requirements. There are two common modulation schemes which are M-ary Pulse amplitude modulation (M-PAM) and L-pulse position modulation (L-PPM) [43]. The simplest modulation technique is OOK which is the lowest order of M-PAM and is easy to implement. The OOK technique has two sub-techniques which are return-to-zero (RZ) and non-return-to-zero (NRZ). The OOK signal can be given by [43]:

$$\emptyset_{OOK}(t) = \frac{1}{\sqrt{T}} rect\left(\frac{1}{T}\right) \tag{2.5}$$

The time-varying optical intensity is represented by:

$$x(t) \sum_{k=-\infty}^{\infty} 2P\sqrt{T}A[k] \;\; \emptyset_{OOK}(t - kT) \tag{2.6}$$

Where, $A[k] \in [0,1]$ and should be uniform. OOK-NRZ power spectral density (PSD) is different from that of the PSD of OOK-RZ, given by [43].

$$PSD_{OOK-NRZ}(f) = (P_r R)^2 T_b \, sinc^2(\pi f T_b) + (1 + R_b \, \delta(f)) \quad (2.7)$$

$$PSD_{OOK-NRZ(\gamma=0.25)}(f) = (P_r R)^2 T_b \, sinc^2(\pi f T_b) + (1 + R_b \sum_{n=-\infty}^{\infty} \delta\left(f - \frac{n}{T_b}\right)) \quad (2.8)$$

where $\delta$ () is the Dirac delta function. The power spectral density is plotted in figure 2.8 [43]. The average optical power is the same for NRZ and RZ schemes. The power efficiency $\eta_p$ is 2 for both but the bandwidth efficiency of NRZ ( $\eta_B$) is 1, whereas, for the RZ scheme, it depends on the duty cycle such as if $\gamma$=0.25, the bandwidth efficiency is 0.25 [43].

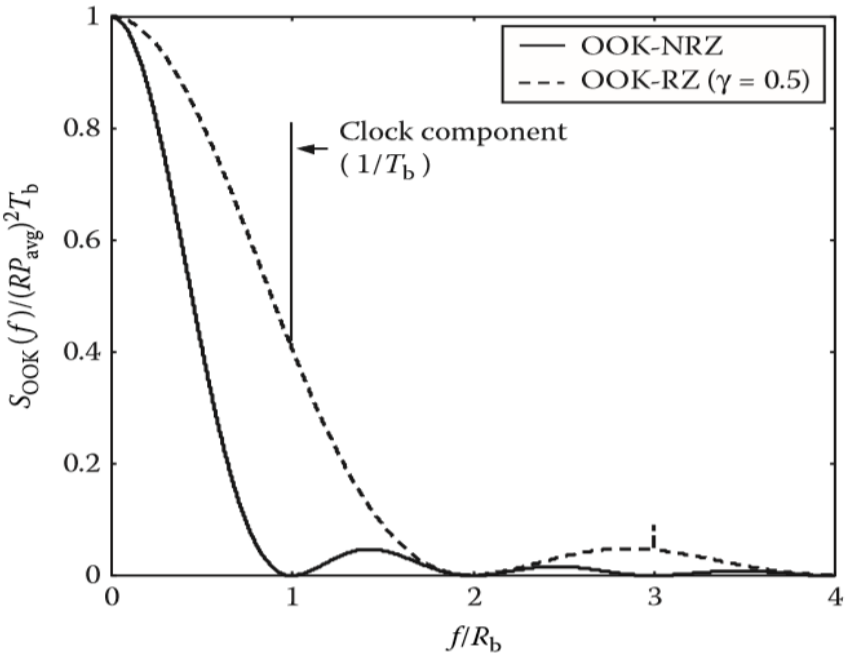


Figure 2. 8 The power spectral density (PSD) of the OOK-NRZ scheme and the OOK-RZ scheme [43].

OOK modulation can be further categorized as On-Off Keying Non-Return to Zero (OOK-NRZ) and On-Off Keying Return to Zero (OOK-RZ). As the name suggests the data is conveyed by turning the LED off and on. In its simplest form, a digital ‘1’ is represented by the light ‘on’ state and a digital ‘0’ is represented by the light ‘off’ state. The advantage of using OOK modulation is that it is simple to generate and decode, therefore in this thesis, the OOK-NRZ modulation scheme is used during the lab work and experiment. The VLC system used in this thesis employed the camera at the receiver section, thus resulting in VL-OCC system, discussed in detail in the next chapter.

## 2.4 Summary

This chapter listed the background of VLC and its advantages over other technologies specifically in indoor environments, especially in hospitals and healthcare. Thereafter, this chapter discussed the potential applications of VLC followed by principals of VLC. Additionally, this chapter illustrated the VLC system model, different transmitters and receivers. Lastly, the criteria or the necessary steps to be considered in choosing the modulation scheme was explained.

# Chapter 3 Visible Light Optical Camera Communication

## 3.1 Introduction

Nowadays, digital cameras with ISs containing many micro-scale PDs are used for photography, vision, surveillance, motion detection, augmented reality, virtual reality, localization, and data communications [113-115]. In VLC systems, with PD as receivers, the use of high-power enlarged devices improves the FOV but enhances the cost of system considerably which can be significantly reduced by using the camera at the receiver section [116, 117]. The image processing techniques and computer vision involved with the use of the camera, empower the users and researchers with an easy and convenient algorithm for data collection, analysis, BER calculation, and image extraction. Furthermore, the blurring and the undesirable ambient noise are reduced easily by inhibiting the focusing properties of the camera. Additionally, camera rotation to maintain the LOS in context to the targeted destination is effortlessly achievable without the need for extra infrastructure modifications [115-118]. Hence, camera or image sensor-based VLC is an attractive solution for both indoor environments specifically EEG applications.

This chapter aims to give the outline of OCC, related work or applications in the different fields and thereafter discuss the system model of VL-OCC followed by

different image sensors and their comparison. This chapter also illustrates the DIP techniques and computer vision used in this thesis.

### 3.1.1 Overview of OCC

Optical camera communication is a recent development of OWC and an extension of VLC, where image sensors or cameras are used for sensing the light intensity emitted from a light emitter instead of conventional photodiodes. OCC is a pragmatic version of VLC using a camera as the receiver. OCC operates in the same channel band as VLC with more advantages on receiver characteristics and has been studied in the IEEE 802.15 SG7a within the framework of optical wireless communications and considered as a candidate of IEEE 802.15.7rl [119-122]. The OCC has an inherent advantage of capturing 2-dimensional (2D) image data, compared with intensity level-based photodiodes in VLC [119, 121]. The popularity of smart devices and the camera installed in every smart device has resulted in the use of a camera as a receiver for communication purposes in VLC systems. The expansion in consumption of smart devices, furnished with inbuilt camera and light to act as a transceiver pair without the need for extra hardware ease the implementation of OWC technologies. Cameras are pervasive thus extensively been deployed for both data communication and photography. The computer vision and image processing have made communication easier with the help of QR codes. These QR codes prompt in-camera communication applications, using 2D barcodes [120, 122]. When a camera is used as a receiver, lights from different sources are separated almost perfectly on a focal plane because of several numbers of pixels in image sensor (IS) of camera, and optical signals are output separately from each pixel, which avoids signals from becoming mixed, thus permitting communication even if light signals and ambient lights such as sunlight and

streetlights are present [123]. There are numerous modulation techniques developed for OCC, such as variable pulse position modulation (VPPM), spatial 2-phase shift keying (S2-PSK), and pulse width modulation (PWM). One of the most widely used modulation techniques for OCC is under-sampled frequency shift on-off keying which was first proposed by Intel [124 - 126]. It employs two different high frequencies to simultaneously modulate data at a low frame rate. Similarly, Intel also developed VPPM for OCC where the modulated signals consist of two signalling sources, i.e., a high and a low frame rate source. The low frame rate camera is used to locate the LEDs, which modulate the data while the high frame rate camera is adopted for variable pulse position modulated data. Another well-known standardized under-sampling modulation technique for OCC is S2-PSK which uses a spatial modulation scheme [127]. A randomly sampled image can be fully demodulated by using S2-PSK due to the separation between the cameras. S2-PSK can demodulate randomly sampled images that allow it to be used for variable frame rate cameras.

Recently, several other hybrid modulation schemes are standardized which include but not limited to pulse width modulation/pulse position modulation (PWM/PPM) [128, 129], camera multiple frequency shift keying (CM-FSK) [130 - 132], on-off keying (OOK) comprising of OOK-NRZ and OOK-RZ [133], rolling shutter frequency shift keying (RS-FSK) [132, 133], asynchronous quick link (A-QL) [134], hidden asynchronous quick link (HA-QL) [134], and variable transparent amplitude shape code (VTASC) [134]. In this thesis, the OOK-NRZ modulation is used to modulate the data. The data is transmitted in two levels, high level represented by ‘1’ and low level represented by ‘0’. As OLED screen, used in experimental is a matrix of rows and columns formed depending upon the pixel size, therefore, the high level and low level are represented by white and black pixels in the image or frames. The QR code from

the OLED screen is captured by a camera in the form of videos followed by image processing to extract the original data or information and to analyse system performance.

### 3.1.2 Applications of OCC

The possible candidates for a transmitter in OCC systems are LEDs, television screens, projector screens, monitor screens, traffic lights, and the car lights are shown in figure 3.1.

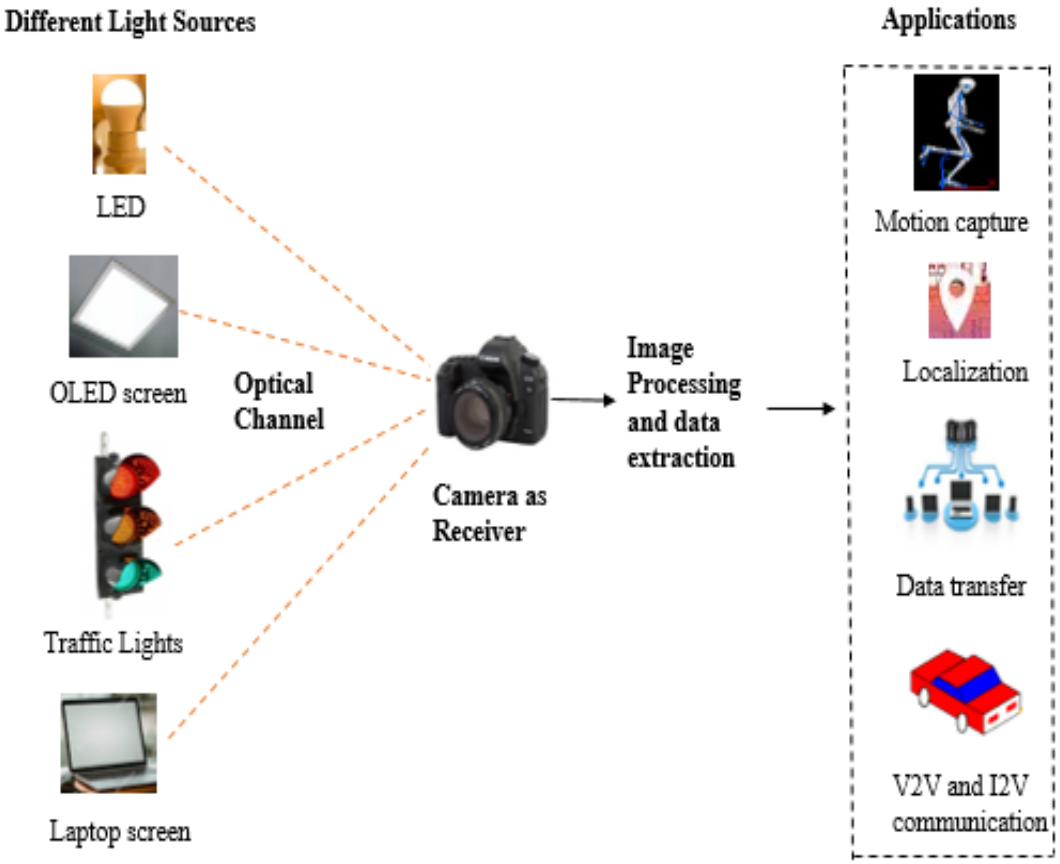


Figure 3.1. Applications of VL-OCC.

The light from all these different sources passes through the wireless channel and arrives at the lens of the receiver. Afterwards, the light passes through the shutter, which controls the exposure of the image sensor/camera. An image of the source captured is generated at the image plane of the camera, which can further be processed using image processing techniques to extract the data required for various applications [135, 136]. At the image sensors, the light is first transformed to the electronic signal, then quantized to an image, and finally compressed to a specific image format. Some of the applications of VL-OCC are discussed below:

**(1) Motion Capture**

The idea of motion capture was first introduced by Eadweard Muybridge back in 1887 where the movement of birds and animals was studied. The motion of the subject was estimated by taking the photographs at discrete time intervals. Numerous VLC based motion capture schemes have been developed [137-140] for various applications. In [141] and [142], the authors have evaluated the performance of optical and inertial motion capture systems where the optical system consists of cameras which emit light and reflective sensors placed on the subject which reflect back the light to the cameras, thus beneficial in tracking the person.

**(2) Localization**

One of the potential applications for VL-OCC is the emerging area of indoor positioning, which uses the LED-based lighting infrastructures. Provided LED lamps are given a unique identification (ID) code, a smart device with a built-in camera can be effectively used to locate people and objects within a room [143 -145].

**(3) Data Transfer**

In healthcare, VL-OCC technology has immense potential in monitoring the health of the patient because to date RF protocols have been deployed in healthcare which suffers from EMI and has limitations in RF restricted zone areas such as ICUs. and data transfer thus providing two -way communications as laptops, mobile phones have an inbuilt camera and a screen for transmission and reception of data through QR codes [145].

**(4) Intelligent transport systems (ITS)**

Intelligent transport systems (ITS) offer a great potential to enhance the road safety, improve traffic flow, and address environmental concerns by monitoring driving behaviour, communicating between vehicles and the roadside infrastructure, thus giving warnings to drivers and providing information for safe driving [146]. Dedicated short-range communication (DSRC) systems are considered to be the promising technology for enabling bidirectional communications between vehicles and the roadside infrastructures [147-149]. Apart from RF-based system alternative technology based on VL-OCC can be used to establish vehicle-to-vehicle (V2V) and vehicle-to-infrastructure (V2I) communications.

Due to the several advantages and applications of OCC deploying camera as a receiver instead of photodiodes, in VLC systems, VL-OCC is preferred where the camera is the receiver, thus reducing the hardware cost and enhancing the mobility and flexibility to secure wireless communication technology.

## 3.2 Architecture of VL-OCC

The basic simplified block diagram of VL-OCC is shown in Figure 3.2, which is comprised of three sections, namely transmitter, optical channel, and receiver.

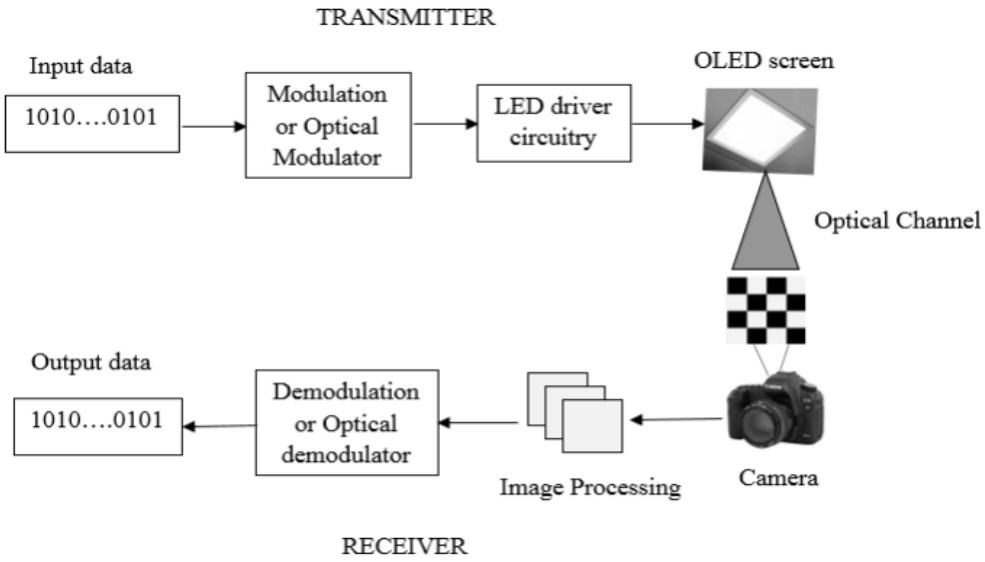


Figure 3.2. The architecture of VL-OCC.

The transmitter section is comprised of input data module, modulator, and LED driver. The input data bits can be transmitted through the LED using a modulation scheme such as OOK, UPSOOK, etc.; The LED driver circuitry is essential to drive the LED, used as a transmitter. The free-space optical channel is the second module where the intensity-modulated light signals propagate from the transmitter to the receiver. The third module is the receiver section whereby the receiver is a camera, used to capture the transmitted light signal in the form of images or video. Thereafter, the offline processing or image processing is done in MATLAB to decode the bits and to extract the originally transmitted bits, and finally to calculate BER, resulting in reliability and stability of the communication system. The image bits received have distortions that can be minimized to a large extent by accurately focusing the camera. Furthermore, the interference from neighbouring sources can be significantly mitigated using a region of interest signalling, where the source is detected at a low frame rate. Another

method to reduce the interference is the selective capturing technique, in which the selective LED region is captured by the image sensor/camera, hence minimizing the probability of interference [124]. The noise sources that could possibly affect the signal quality or image received are mentioned below:

1. Perspective distortion is a common phenomenon in daily life. When we look at an image on a rectangular screen from a certain angle, the image on the screen appears more like a trapezoid. We observe that some pixels shrink, while others expand. This same phenomenon is also observed in screen-camera links where some pixels have better visibility than others improving their communication reliability [119, 122].
2. Blurring occurs when the camera moves while capturing the display. The result of blurring is out-of-focus images where some pixels are blended together. In the frequency domain, blur can be considered a low-pass filter where high frequency attenuates much more than the low frequency [ 120-122].
3. Ambient light is a source of noise which changes the luminance of the received pixels. This can cause errors in the information encoded in the pixels, resulting in information loss at the receiver. In the frequency domain, since ambient light changes the overall luminance, it can be considered the DC component [121].

The distortion and the blurring can be reduced to a minimum or zero by focusing the camera properly. The ambient light noise is dependent on camera settings of contrast, hence by changing the camera contrast, the ambient light noise can be reduced considerably. Because of the above-mentioned reduction in noise sources easily without any additional modifications, the camera is preferred over photodiodes in communication systems. In this thesis research work autofocus is deployed to focus is employed to reduce errors and noise due to blurring, defocussing.

Predominantly, an intensity-modulated direct detection (IM/DD) scheme is used for OCC where the information signal modulates the light intensity for the transmission. The information signal is non-negative and is proportional to the intensity of the light. On the receiver side, a pixel is used as a basic unit for power detection which represents the photon count rate at the receiver area. The received signal is affected by multiple phenomena such as scattering and different types of noise. The photon's arrival rate at the receiver is a random process that is modelled by the Poisson distribution [150]. The intensity of the received signal is given as

$$I_y = hX + N_b \tag{3.1}$$

where $h$ is the channel gain, $X$ is the transmitted signal, and $N_b$ is the background noise intensity. In ideal case $h = 1$ and $N_b = N_s + N_p + N_r$ , where $N_s$ is the shot noise for photons and dark current, $N_p$ is the noise due to non-uniform photo-response in pixel output, and $N_r$ is the read noise which is a collection of noise independent of the signal. Then, the received signal in electrical form can be written as

$$Y = X + Z_b \tag{3.2}$$

where $Z_b$ represents the background noise in electrical form. The signal to noise ratio (SNR) of the received signal is written as

$$\gamma = \frac{E\{X^2\}}{\sigma_b^2} \tag{3.3}$$

Where $E\{X^2\} = \left(I_{pt}\right)^2$ and $\sigma_b^2 = \sigma_s^2 + \sigma_p^2 + \sigma_r^2$ is the variance of the background noise. t is the integration time in which Ip number of photons are aggregated by each pixel. In the following, we describe the variances for each type of noise. The variance of shot noise is given by

$$\sigma_s^2 = qt\left(I_p + I_b + I_d\right) \tag{3.4}$$

where $q$ is the quantization step, $I_b$ is the induced current due to background radiation, and $I_d$ is the dark current. Similarly, the variance of noise due to non-uniform photo-response is given as

$$\sigma_p^2 = \kappa\left(\left(I_{pt}\right)^2 + \left(I_{bt}\right)^2\right) \tag{3.5}$$

where κ is the factor value for photo-response non-uniformity. The read noise Nr consists of an analogue to digital conversion noise (AN), reset noise (RN), and source follower noise (SN), and therefore has the following variance

$$\sigma_r^2 = q^2(\sigma_{AN}^2 + \sigma_{RN}^2 + \sigma_{SN}^2) \tag{3.6}$$

Putting the values of $\sigma_s^2$, $\sigma_p^2$, and $\sigma_r^2$in (3.6) yields the SNR for OCC which depends on the pixel area, photo-current, integration time, and different types of noise sources. Moreover, the SNR can be improved by leveraging the spatial diversity (mapping of a single transmitter by combining multiple pixels into a block). Based on the SNR calculation in (3.7), the capacity of OCC is given by Shannon formula in [151] as

$$C = W\left(W_s log_2(1+\gamma)\right) \tag{3.7}$$

where $W_s$ is the bandwidth of the system. The BER performance in context to QR code or single frame and images is calculated by

$$BER = \frac{Total\ number\ of\ bits\ transmitted}{Total\ number\ of\ bits\ received} \tag{3.8}$$

In this thesis, the screen to camera communication type of VL-OCC is adopted to analyse the performance of the system, different types of VL-OCC communication systems are discussed in next section.

### 3.2.1 Different VL-OCC communication systems

VL-OCC are separated into two categories, based on systems using light sources for transmissions i.e. LCD or LED screens for transmission and camera as a receiver. In this section, we look at a special application of VLC where a screen and a camera sensor can communicate for device-to-device communication. screens and cameras are widely used in today's mobile devices such as smartphones, laptops, etc. Also, this section will list the infrastructure-to-device communication where LED luminaire serves a dual purpose of illumination and communication. On the other hand, screen-camera communication is a form of device-to-device communication where information can be encoded in display screens of the smartphone, laptops, advertisement boards, etc., and another device with a camera sensor can capture the screen and decode the data using image analysis.

**(a) Light source to camera communications**

Several research works have been carried out in the area of the light source to camera communications, where the light source can be an LED such as White Light-emitting diode (WLED), Red-green blue (RGB) LED, etc., and the receiver is the camera. The authors in [152] demonstrated an LED-to-camera communication system where the transmitter is a board containing 16 LED for data transmission where each LED consists of a red-green-blue (RGB) chip, and the Rx is a smartphone camera. The communication between transmitter and receiver was based on the colour shift keying (CSK) modulation scheme and allowing multiple users to access the network, by using

the code division multiple access (CDMA) technology. In [153], the authors presented a work based on CMOS mobile phone built-in camera sensor which was used to capture the data from a visible LED light source. The modulation scheme adopted was OOK, and the rolling shutter mechanism of the camera was used for data transmission.

Rolling shutter is a mechanism typically used in CMOS cameras for image capturing. As, different parts of the sensor are exposed to light, at different times, therefore, pixels constituting the camera sensor are split into rows, and the rows are exposed one by one to the light, consecutively from the top to the bottom in rolling shutter mechanism. The LED light flashes while transmitting a binary stream (ON for 1 and OFF for 0), whilst the camera at the receiver unit captures the data in the form of video/images. data. The authors in [154], described the system based on LED- to camera communication using, RGB LEDs to transmit data, and a smartphone built-in camera on the receiving side, used by Casio, the Japanese electronics manufacturer.

**(b) Screen to camera communications**

With major progress achieved in the light source to camera communication research alongside the dramatic increase in the LED and LCD screens in everyday life, screen to camera communication was put in the research spotlight more than a decade ago, and many works have been reported in the area. This section will expose some of these works. For instance, [155] reported a computer vision-based screen to the camera communication system, where an LCD screen and a commercial webcam were used as Tx and Rx, respectively. The work presented focuses on two main desirable aspects of the system, its simplicity and its high performance despite the presence of perspective distortions yielding from the variation of the transmitter's angle of view, see Figure 3.3.


Figure 3.3. Viewing angle in screen to camera optical wireless communication.

In this system, the tx is constituted of 256 LEDs transmitting a coloured signal over 3 channels (RGB), and each LED is an independent channel transmitting an OOK modulated signal. In order to detect the transmitter on the captured frames, four LEDs at the four corners of the tx were used as a reference. The four reference LEDs blink continuously at a rate independent from the transmitted signal. On the Rx, a Hough transform [156] based edge detection method was applied to the received frames, in order to locate the reference LEDs, thus helping to remove any perspective distortions before proceeding to data extraction. Experiments were carried out using a commercial web-camera operating at a 30-fps capturing rate. In [156], authors designed a system for 2D colour barcode streaming between low-size screens and low-speed cameras, both available on today's smartphones. Once again, the transmitting screen features four corners used for easy localization in case of blurry or distorted received images. The authors in [157] propose a system using a 32-inch LCD screen transmitter with a linkspan of 10m and data rate of 12 Mbps. In [158], authors demonstrated a camera-based VLC link within an aircraft cabin, where successive 2D visual codes were displayed on the in-flight entertainment screen and captured by the camera of passenger's smartphones thus providing the essential information to users.

In this thesis, VL-OCC system is evaluated in context to OLED screen configurations with regards to link distance and BER to analyse the system performance. Chapter 4 in this thesis discusses the 8 pixel and 16-pixel OLED screen configuration sin the LOS condition to study the system performance. Chapter 5 illustrates the concept of angle deviation in context to 16-pixel OLED screen in the LOS condition, using OOK_NRZ scheme to analyse the performance of the distance at different angles and optimum link distance. Chapter 6 experimentally demonstrates the 32-pixel OLED screen configuration, analysing the performance of the system with three different receiver cameras of 5MP, 8MP and 18 MP in context to BER and link distance.

### 3.2.2 Different Image Sensors

Presently, there are two main technologies that can be used for the image sensor in a camera, i.e. CCD (Charge-coupled Device) and CMOS (Complementary Metal-oxide Semiconductor) shown in figure 3.4 (a) and 3.4(b) respectively.

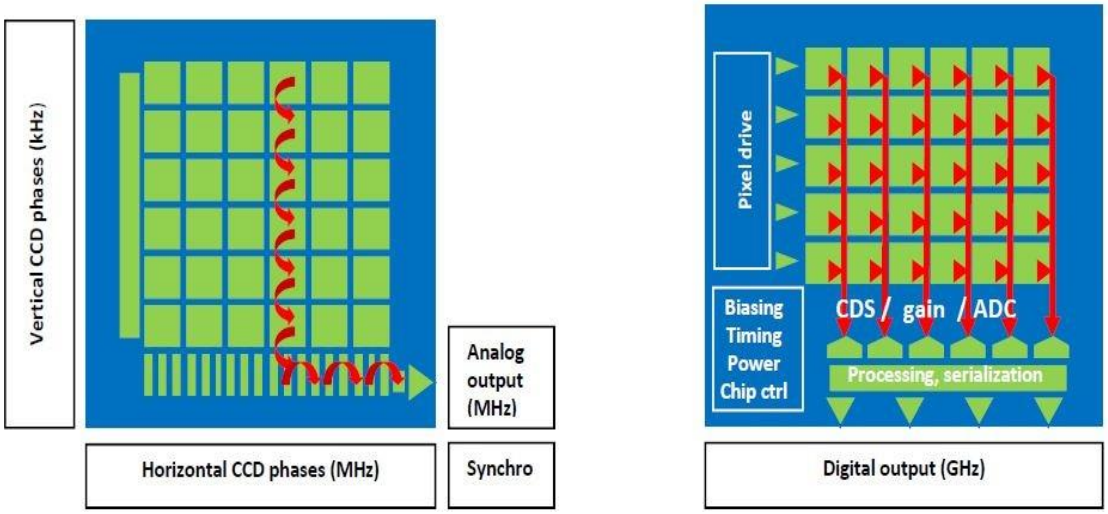


(a) (b)

Figure 3.4 (a) CCD cameras (b) CMOS cameras [159**].**

In a CCD sensor, the light (charge) that falls on the pixels of the sensor is transferred from the chip through one output node or only a few output nodes. The charges are converted to voltage levels, buffered, and sent out as an analogue signal. This signal is then amplified and converted to numbers using an analogue to digital (A/D)converter outside the sensor, as shown in Figure 3.3(a) [159, 160]. Complementary metal-oxide semiconductor (CMOS) technology is a mature technology used in a wide range of devices such as solid-state memories, CPUs, and ISs. Unlike the CCD sensor, the CMOS chip incorporates amplifiers and A/D-converters, which lowers the cost for cameras, thus each CMOS pixel contains conversion electronics. Compared to CCD sensors, CMOS sensors have better integration possibilities and more functions. CMOS sensors also have a faster readout, lower power consumption, higher noise immunity, and a smaller system size [ 159-161]. In a CMOS active pixel sensor (APS), each pixel is equipped with an amplifier, shown in figure 3.4(b) [159], providing suppressed noise generated in the signal readout path [121]. This feature of suppressing the noise of CMOS cameras is beneficial in data transfer of biomedical signals such as EEG because EEG signal has the amplitude of few microvolts ($\boldsymbol{\mu}$V) buried in noise (discussed in chapter 1). Therefore, in this thesis, CMOS cameras are deployed during the lab or experimental work.

### 3.2.3 Rolling shutter (RS) and Global shutter (GS) cameras

In global shutter cameras, all pixels are exposed to the light at the same time, while in a rolling shutter camera, the reset and readout pulses are sent to each row sequentially. Figure 3.5(a) shows the capture of a fan at RS camera and figure 3.5(b) shows the image of fan captured at GS camera.

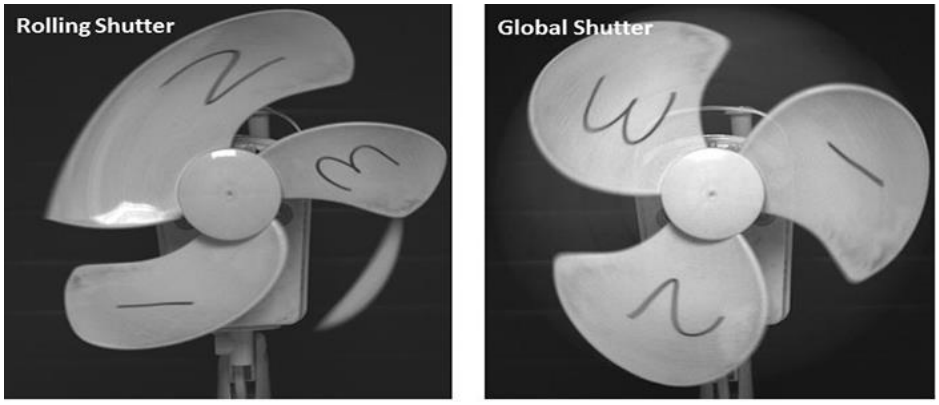


3.5(a) 3.5(b)

Figure 3.5 (a) Image of a fan at RS camera (b) Image of a fan at GS camera [162].

Due to sequential capture, RS cameras present a distorted shape of the object in the image, as shown in figure 3.5 (a) [162]. Therefore, in this thesis global shutter is deployed in cameras while capturing the images transmitted from the OLED screen.

## 3.3 Digital Image processing

The image is defined as a two-dimensional visual information that is stored and displayed. An image is created by photosensitive devices which capture the reflected light from two- dimensional surface of an object in the three-dimensional real world. Each image has intensity or grey value in the $x-y$ coordinate plane. If it is finite and discrete quantities, the image is called digital image. Digital image processing (DIP) has different techniques for processing digital images. DIP has been applying many fields with technological advances, such as medicine, geographical information technologies, space sciences, military applications, security, industrial applications [163-165]. Digital image processing helps to enhance images to make them visually pleasing or accentuate regions or features of an image to better represent the content. For example, we may wish to enhance the brightness and

contrast to make a better print of a photograph, like popular photo-processing software [165, 166]. A digital image I [M, N] described in a discrete 2D space is obtained through a sampling process of an analogue image I (x, y) in a 2D continuous space [163, 164]. This process is referred to as digitization. Figure 3.6 shows an image divided into M rows and N columns and the intersection of a row and a column is called a pixel.

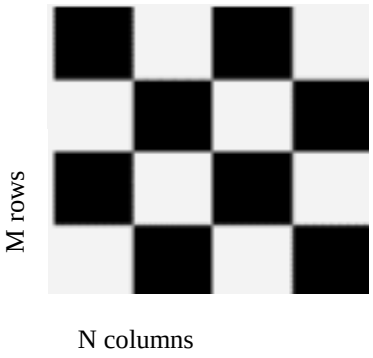


Figure 3.6 Image in the form a matrix of rows and columns.

Based on the size of the pixel, the number of rows and columns are formed on the digital image and vice versa. For instance, if the size of a pixel is small then the greater number of rows and columns, thus more data bit information while if the number of pixels is large then less number of rows and columns are formed for the same size of the image, thus fewer data bits can be transmitted.

### 3.3.1 Pixel

A pixel is the basic logical unit in digital graphics. A digital image consists of a finite number of elements. These elements are referred to as picture elements, or pixels [163, 166]. Pixels are combined to form a complete image, video, text or any other visual display. In communication systems, pixels are also known as symbols or blocks formed by a combination of rows and columns. These pixels carry useful information

about the image and convey the necessary data related to the image [164-166]. In communication systems, each pixel is used to transmit a data bit thus forming a stream of binary bits shown in figure 3.7 carrying the useful information of the signal. For instance, in the communication system in the transmitter section, the input data is converted into a binary stream. An image is then created with several blacks and white cells where '0' and '1' in the binary stream are represented with black and white cells, respectively. Initially, the input information is converted into the corresponding binary stream which is then used to create an image composed of several cells, where each cell contains several pixels, having the same intensity.

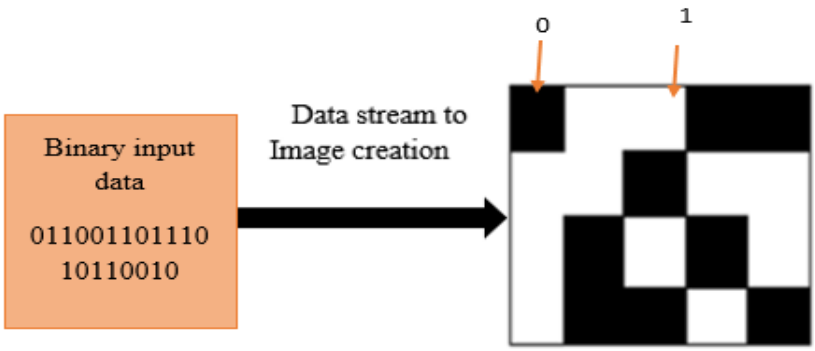


Figure 3.7 Binary data to Image creation.

In figure 3.7 the image formed of pixels with the help of rows and columns represent the binary stream in the form 0 and 1. The black pixel denotes zero and white pixel represents 1. In this manner the image processing is performed to transmit the data in communication systems, for instance in this thesis, the source of information or transmitter is OLED screen and receiver is a camera. The OLED screen itself is formed of rows and columns thus based on the pixel size the number of data is transmitted per frame of the image. The data bits are in the stream of binary data representing the image of black and white pixels depending upon high level, which is 1, represented by

white pixel and low level denoted by 0, thus forming a black pixel. In this thesis, different pixel sizes of OLED screens are studied in context to BER and link distance to determine the system performance.

### 3.3.2 Grayscale or Black and white images

As discussed above that image comprising of bits 0 and 1 represents black and white pixels. Theoretically, black and white image is a bi-dimensional array of pixels, where each pixel is represented by its grey level in image processing having the range of 0 to 255. Grey level in image processing spans the full black-to-white range within the range of as it varies between 0 and 255 shown in figure 3.8 [163-166].


Figure 3.8 Black and white image scale [165].

These black and white pixels are formed considering the sections entirely black and entirely white, though within the two-colour bits i.e. 0 and 1. In this thesis, the data information is sent through the QR code formed by the combination of black and white pixels. The QR code transmitted optically is captured by the camera through videos which are then followed by image processing to analyse the performance of the system in context to BER, OLED screen configurations, and link distance.

### 3.3.3 Border detection or edge detection of an image

Edges are the points in an image where the image brightness changes sharply or has discontinuities. Such discontinuities generally correspond to depth, surface orientation, changes in properties of material and variations in illumination. Edges are very useful

features of an image that are used in retrieving the original image. Figure 3.9 (a) shows the original image and figure 3.9(b) shows the image edge or border detection respectively [165].

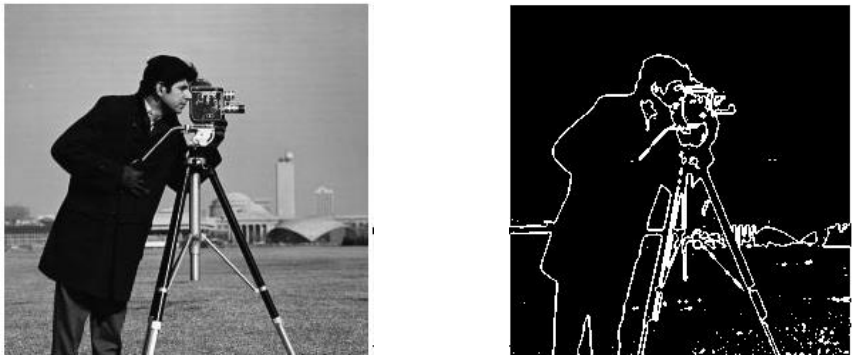

3.9 (a) 3.9 (b)

Figure 3.9 (a) original image, (b) Image of edge detection [165].

Edge detection helps in reducing the unwanted background image and helps in analysing the original images. Also, border or edge detection is also used in image processing in communication systems, to identify the size of the original image and to calculate the BER from the cropped image [165, 169]. Furthermore, with the help of edge detection points, in case the original image is moved, or communication system set up is rotated, the original image co-ordinates can be easily constructed using the points from edge detection. This technique of edge detection is significantly deployed in engineering and communication systems, thus helping in constructing the original image without any need for complicated algorithms and extra hardware requirements. In this thesis in the research work in chapter 4, chapter 5 and chapter 6, the technique of edge detection is employed to identify the border of the original image and the data bits transmitted per frame.

### 3.3.4 Computer Vision

Computer vision is an interdisciplinary scientific field that deals with how computers can be made to gain information from digital images or videos, and image processing focuses on, processing images to extract the original data from the received images/data. A typical computer vision system is shown in figure 3.10 where, computer vision system inputs an image and outputs task-specific knowledge, such as object labels and coordinates.

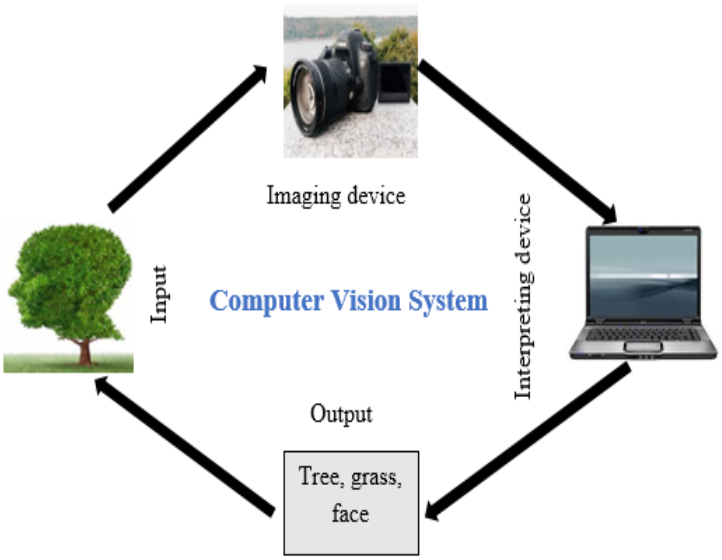


Figure 3.10. A typical computer vision system.

In figure, 3.10, the input is captured by the imaging device in the form of images, which is then passed to the interpreting device thus resulting in output. The interpreting device could be an embedded system, hardware design, image processing algorithms to extract the information from images. In this, thesis the codes used for image processing and extraction of images are listed in the section of codes. Researchers in computer vision has been developing, in parallel, mathematical techniques for recovering the three-dimensional shape and appearance of objects in imagery [167 - 169]. Computer vision is used in numerous applications such as automotive safety,

robotics, feature extraction, neuroscience, mathematics, physics, signal processing, image processing, etc as shown in figure 3.11.

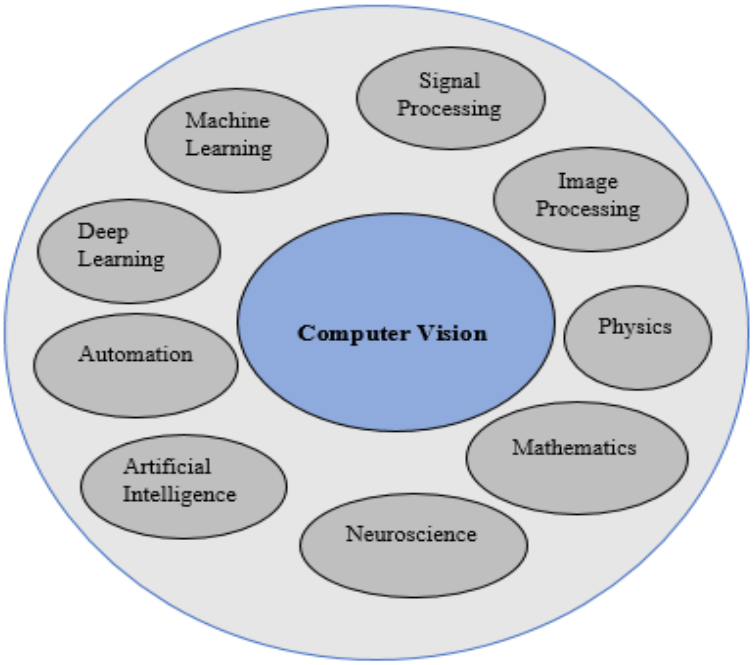


Figure 3.11. Scope of Computer vision [169].

As, computer vision has been extensively used in every field, therefore with the aid of computer vision to track a person moving against a complex background. Using computer vision, one can even, attempt to find and name all the people in a photograph using a combination of face, clothing, and hair detection and recognition. Due to the advancement in technology, several algorithms, the software has been developed for computer vision. OpenCV (Open Source Computer Vision Library) is an open-source computer vision and machine learning software library [168, 169]. OpenCV was built to provide a common infrastructure for computer vision applications and to accelerate the use of machine perception in commercial products. The library of OpenCV has numerous algorithms, which includes a comprehensive set of both classic and state-of-the-art computer vision and machine learning algorithms [168]. The Open CV has

great potential in computer vision and image processing because of its simple techniques and algorithms essential for researchers needed for image analysis. Using Open CV as a reference, in this thesis, the codes for image processing were written in MATLAB, all the codes used in experimental work and image processing are provided in the section of codes for the reader to understand the concepts and replicate the process.

## 3.4 Summary

Within this chapter, after the overview of OCC, applications of OCC were discussed. This chapter also gave a detailed description of the architecture and applications of VL-OCC. Depending upon the transmitter being LED or screen, two types of VL-OCC communication systems were also highlighted in this chapter. Thereafter, image sensors were discussed in detail and thereafter listing the noise sources and how to reduce them. This chapter also discussed the basics of digital image processing, data creation and digital image formation from binary data along with few basics which are used in communication systems for image extraction and to calculate the BER performance.

# Chapter 4 Impacts of OLED configuration VL-OCC for Wireless EEG Signal Transmission

## 4.1 Introduction

Monitoring the brain electrical activity has a great possibility to perceive brain functionality and to diagnose the brain abnormalities. The traditional Electroencephalogram (EEG) monitoring systems deploy several scalp electrodes, physically connected to the EEG recording machine however recently the wearable EEG devices have gained wide popularity due to lesser number of electrodes, ease and comfort [27]. Some of the EEG machines deploy wireless RF communication protocols like Bluetooth and ZigBee to transmit signal information wirelessly; however, both Bluetooth and ZigBee dependent EEG machines emit radio frequency signal that may interfere to other medical equipment. RF communication plays an important role in daily life such as TV, radio, Wi-Fi and so on. Furthermore, the RF signal transmitted is susceptible to contamination by other RF signals in the neighbouring environment [29].

As RF spectrum is immensely crowded, therefore, to meet the requirements of the increased bandwidth is possibly one of the biggest challenges or drawbacks of RF. In healthcare, the RF radiation may cause interference with the operation of some equipment to hospital equipment, therefore owing to shortcomings of RF, the VLC

technology is an alternative solution since VLC uses the license-free light spectrum ($380 - 780nm$) and free from electromagnetic interference with enhanced security [43, 83]. Recent reports showed that VLC communication systems LEDs have been widely adopted however the OLED is a promising area for research due to easy integration and fabrication, wide beam angle, rich colours and flexibility [170, 171]. As the latest development of VLC, OCC has shown its existence in several applications [5], hence due to advances in imaging technology and an extension of IEEE 802.15.7 standard for VLC, OCC presents a promising vision of optical communications [83]. The eruption in the usage of smart and advancement in technology over the decade unfolds the capacity of VLC implementation for the smart devices or camera with no hardware modifications [43], hence the proposed research in this paper comprises of visible light and optical camera communication between the OLED screen and image sensor of the camera.

Over the years, there has been an increase in improvement in healthcare quality at several hospitals and nursing homes thereby bringing the wireless technology due to high mobility and flexibility. However, the most important thing for the wireless technology to be adapted and used in hospitals is that it should be free from invisible EMI which tends to affect the medical equipment's and their functionality thus posing a threat to both patient's health and medical equipment. Hence, the OWC such as VLC is most suited for the environment such as hospitals as VLC is free from electromagnetic inference, highly reliable and low cost [172]. In [173], it has been stated that the usage of communication technology such as RF in medical applications, mainly EEG is flustered because of EMI hence affecting the reliability and accuracy of the transmitted data. In this chapter based on the problems associated with RF in healthcare specifically in EEG, VL-OCC system is proposed. The VL-OCC system

deploys the existing infrastructure such as lightning systems such as OLED for transmitting the data, while the camera is used in the receiver section. The OLED screen used in the experimental work is a matrix of rows and columns, hence depending upon the pixel size or configuration of OLED screen the data bits are transmitted in a single frame. Therefore, this chapter experimentally demonstrates the trade-off between the BER and data rate depending upon the pixel size, the flowchart in figure 4.1 shows the VL-OCC-EEG based system for 8 pixels and 16 pixels.

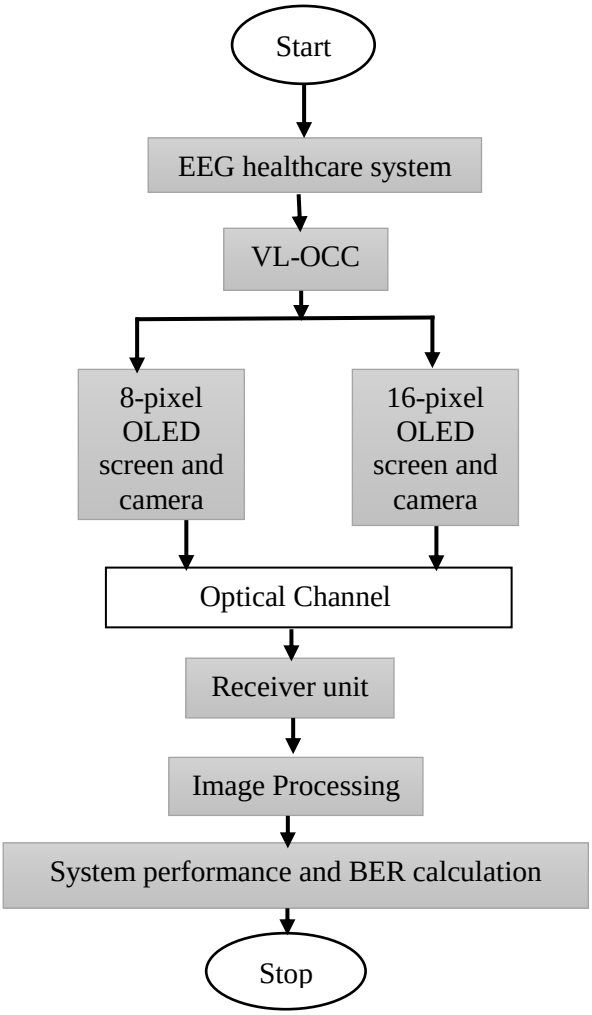


Figure 4.1. Flowchart of 8-pixel and 16-pixel VL-OCC-EEG system.

EEG has been widely adopted for brain monitoring. The transmission of the EEG signals captured from the scalp using electrodes to a displayed screen is often performed through wires utilizing RF communication technology. The wired EEG transmission restricts the patient movement during the entire EEG recordings. However, patient movement is necessary during EEG recordings in a certain medical scenario. In view of limitations of RF specifically in EMI sensitive areas such as hospitals, a subset of OWC, namely VL-OCC is the foremost alternative. Towards this end, wireless transmission of the EEG signals enables patient movements during the recordings. In this context, research work in this chapter proposes a VL-OCC system for wireless transmission of EEG signal. The signal transmission under the LOS is conducted deploying OOK-NRZ modulation scheme. The performance of VL-OCC system is evaluated by developing an experimental prototype under the realistic medical scenario. The proposed system achieves a data rate of $2kbps$ over free space at camera frame rate of 30 frames per second. OLED screen acting as transmitter converts the EEG signal into two-dimensional images by displaying the images. The experiments were performed in LOS using OOK-NRZ modulation scheme under the realistic medical scenario. During the lab work, the camera operates as the receiver and detects the images shown on the OLED screen and thereafter a computer to demodulate the EEG signal from image further processes the image received by the camera. The results of 8 pixel and 16 pixels are compared in context to BER and communication distance to test the system performance. This chapter is divided into four different sections. Section 4.2 presents the proposed system model theory. Section 4.3 discusses experiments and analysis of results followed by a conclusion presented in section 4.4.

## 4.2 Proposed System Model Theory

This section illustrates the system modelling of the optical wireless communication link as shown in figure 4.2.

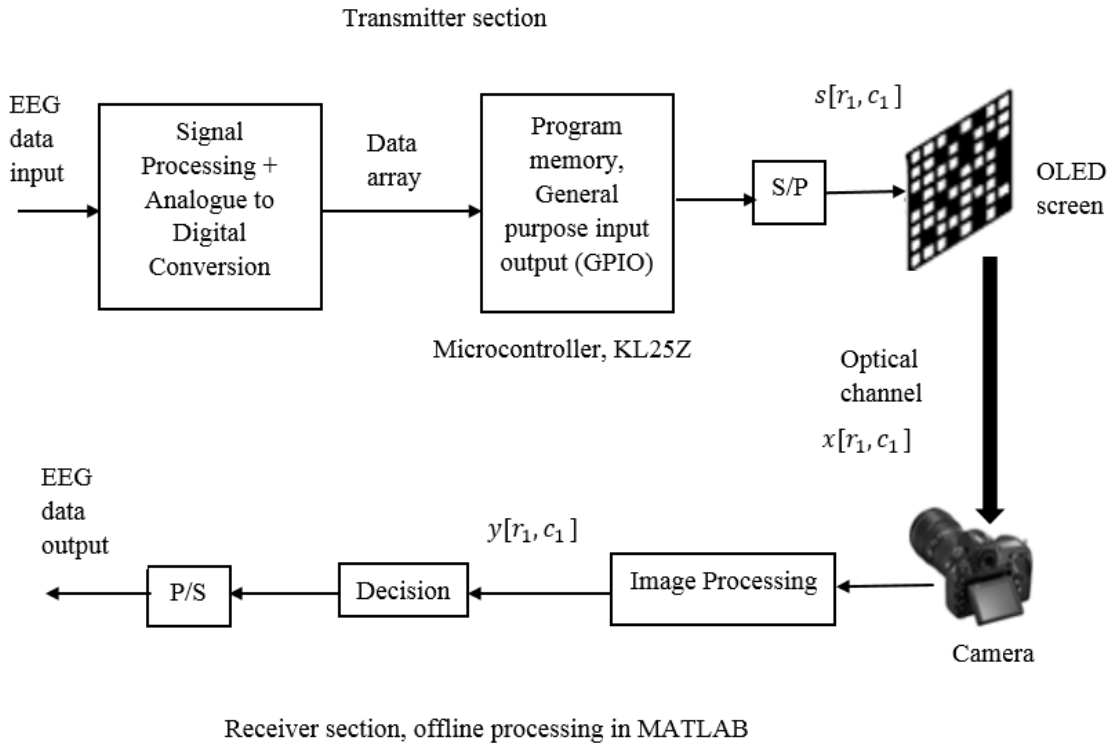


Figure 4.2. An overall system model of the proposed VL-OCC framework.

In this system, the transmitted bits in the form of OOK-NRZ is represented by $b_n$. The system has three major operational components including EEG data processing, microcontroller, and an offline processing module. The EEG signal module is responsible for generating raw data from the signal. The microcontroller takes raw EEG data as input and performs serial-to-parallel (S/P) operation on data. The offline processing module is responsible for generating final EEG output focusing on image processing, decision processing, and parallel to serial operation. The OLED screen is divided into rows and columns. The number of bits transmitted simultaneously in parallel using OOK-NRZ modulation scheme in each frame can be computed by $N =$

$R_1 \times C_1$. Thereafter, following serial to parallel conversion the signal is transmitted in dimensional form and can be written as $s^{(t)} = [n_1, n_2]$, with $n_1$ and $n_2$ representing the discrete spatial coordinates of the OLED display pixels and t denotes $t^{th}$ frame. The information bits consist of a square of pixels of size $D$. Hence, the number of bits effectively transmitted per frame changes with the value of $D$, thus a number of transmitted bits per frame $N$ given by Eq. (4.1).

$$(S_{z_{row}}/D) \times (S_{z_{column}}/D) = R_1 \times C_1 \qquad (4.1)$$

Where, $S_{z_{row}}$ and $S_{z_{column}}$ is the number of rows and number of columns respectively. Following the transit from the optical to electrical, channel the signal can be computed as given by Eq. (4.2).

$$x^{(t)}[r_1, c_1] = (s * h)^{(t)}[r_1, c_1] \qquad (4.2)$$

Where $h$ is impulse response. Hence, at receiver, the signal can be represented by Equation. (4.3).

$$y^{(t)}[r_1, c_1] = (x)^{(t)}[r_1, c_1] + (v)^{(t)}[r_1, c_1] \qquad (4.3)$$

Representing the signal received at the camera in the form of pixels of the matrix. Also, $(v)^{(t)}[r_1, c_1]$ is a realization of white gaussian noise (WGN) with mean value equal to zero, variance $\sigma^2{}_v$ and is independent of the pixels. Table 4.1. , shown below provides a description of the symbols and notations used in the system model.

Table 4.1. Nomenclature.

| **Notation** | **Description** |
|---|---|
| $N$ | Number of bits transmitted by the matrix of rows and columns formed on OLED screen |
| $D$ | Size of pixel |
| $R_1$ | Number of rows per frame |
| $C_1$ | Number of columns per frame |
| $b_n$ | Transmitted bits from microcontroller before S/P |
| $s^{(t)}$ | The dimensional signal transmitted after S/P in the t-time frame |
| $y^{(t)}$ | Received dimensional signal |
| $v^{(t)}$ | Noise realisation which is known as white noise |
| $x^{(t)}$ | The signal at the optical channel |
| S/P | Serial to parallel conversion |
| P/S | Parallel to serial conversion |

The EEG signal is extracted from EEG lab toolbox using MATLAB, thereafter signal processing and ADC is performed before uploading the data to the program memory of microcontroller thus forming patterns on OLED screen which are captured by the camera in the video form and finally the offline processing in MATLAB. The number of frames or the length of the video depends upon the pixel size and the data rate transmitted. For example: if the pixel size is 16 and the number of bits transmitted is 256 at a data rate of $256bps$ then the number of frames needed to transmit 256 $bits$ will be $256/16 = 16$.

## 4.3. Experiments and Results

This section will list the different experiments in context to 8 pixel and 16-pixel OLED screen, followed with the section of results.

### 4.3.1 Experimental Setup and Hardware

Usually the EEG has an amplitude of millivolts, however, EEG toolbox provides several features such as filtering, amplification, ERP, compression, etc, hence signal extracted from EEGlbtoolbox [174] was filtered using bandpass filter in the range of 0.5 Hz and 50Hz, and amplification of 1Volts (V). Thereafter the signal was extracted using MATLAB. Table 4.2. Illustrates the equipment and the model used for experimental set-up.

Table 4.2. Experimental equipment used.

| **Equipment** | **Model** |
|---|---|
| OLED Display Module | DD-160128FC with EVK board with a resolution of 160RGB ×128 dots |
| Microprocessor | ARM processor FRDM KL25Z |
| Thorlabs Camera | DCC 1645C |
| Language/Software used for coding Simulation | C, Matlab |
| Power Supply | EL302D Dual Power Supply 13.3 V which is regulated to 3.3 V using voltage regulator |

The optical channel transmits the optical intensity, which cannot be negative, hence the EEG signal was normalized in the range of 0 to 1. In the experiment testbed, the EEG signal transmitted shown in figure 4. 3(a) and 4. 3(b).

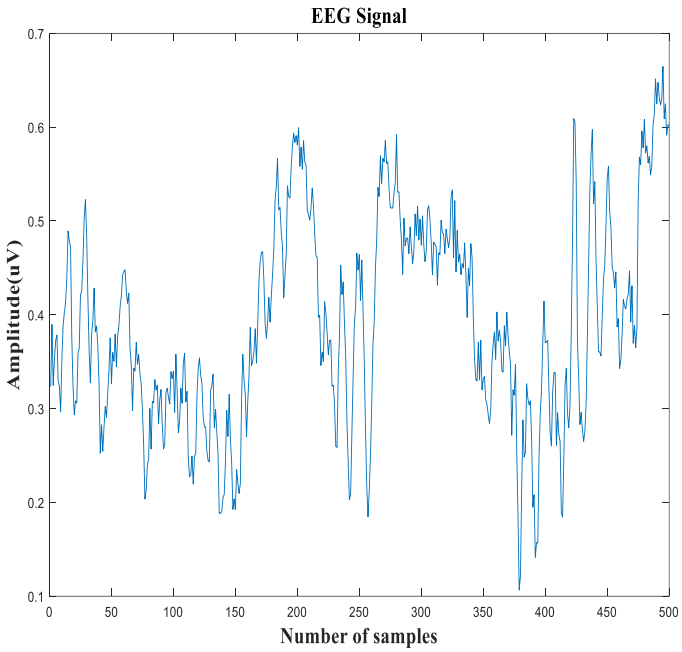


(a)

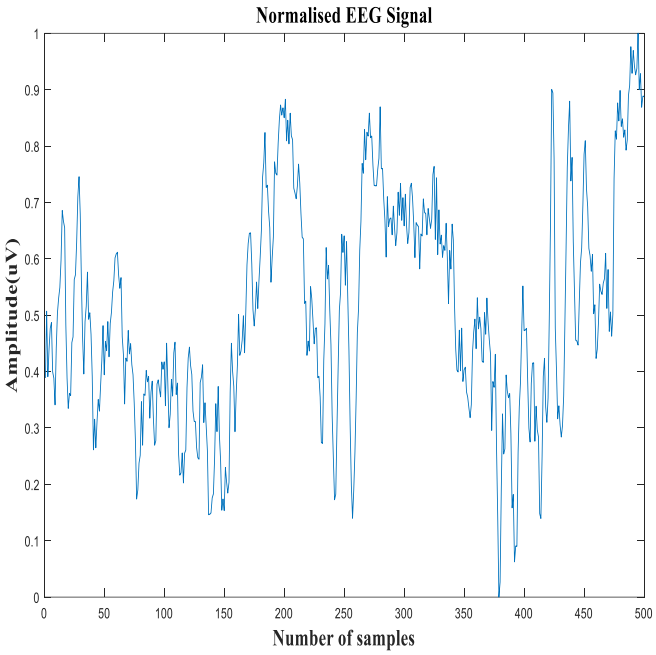


(b)

Figure 4.3 (a) EEG signal from EEG toolbox, (b) Normalized EEG signal for VLC-OCC.

The normalized EEG signal undergoes analogue to digital conversion, a $16bit$ ADC was chosen to allow for higher resolution and low quantization error. Thereafter, the signal obtained in digital form was up sampled for optical transmission to aid in the reconstruction of the original signal transmitted at the receiver (later stage). Then the useful bits obtained were transferred to the microcontroller using a USB cable.

The selected microprocessor was FRDM-KL25Z shown in Appendix C, because of high speed and low power consumption. DD-160128FC OLED [175] screen is preferred as the transmitter with an active area of 28.78 mm into 23.024 mm and a weight of $3.6g$. The evaluation board of OLED screen required a voltage of $2.8V$ to switch on the OLED screen hence, switching board designed using KICAD software having resistors forming a potential divider thus reducing the voltage level of power of the microcontroller from $3.3V$ to the voltage level of $2.8V$ required to switch on the OLED screen.

The optical camera is tested at the receiver section to capture the video of the OLED screen at several distances in LOS. Figure 4.4(a) and 4.4(b) describes the experimental hardware where microprocessor connected to the OLED screen of 8 pixel and 16 pixels respectively through the switching board and the 317 operational amplifier (op-amp) designed as a voltage regulator in order to regulate the dual power supply. The datasheets and essential voltage specifications of 317 op-amps are listed in Appendix B.

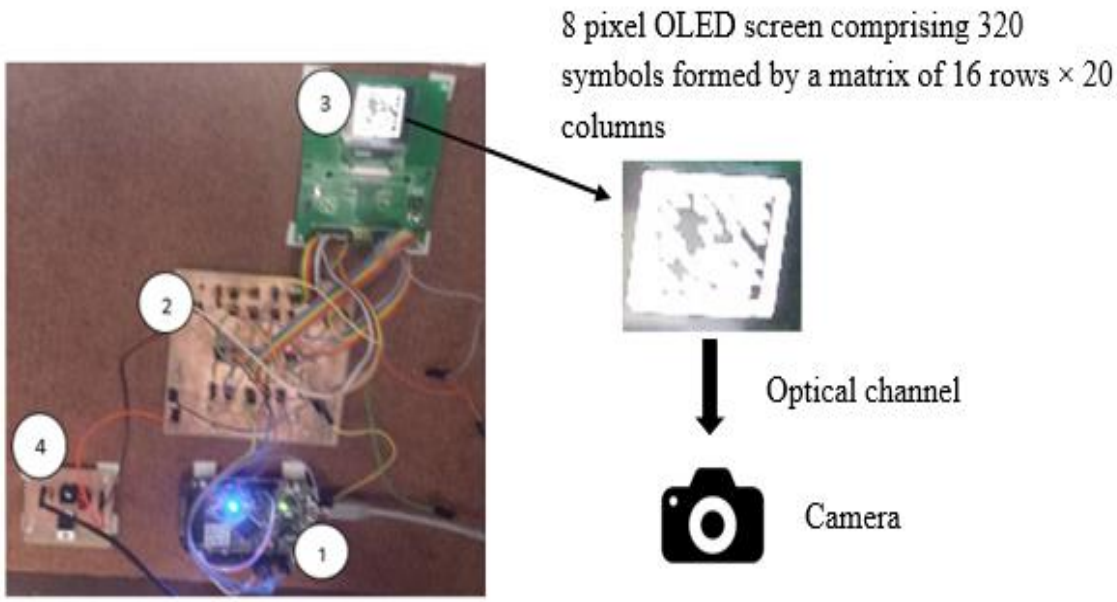


Figure 4.4 (a). Experimental set-up of 8-pixel OLED screen.

1-microcontroller, 2-switching board, 3-OLED screen, 4- voltage regulator.

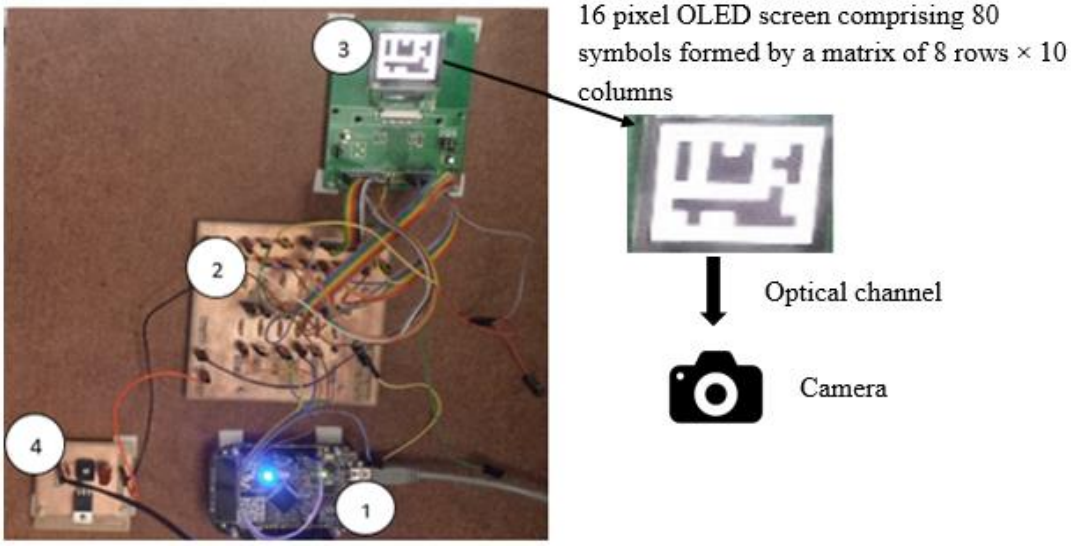


Figure 4.4 (b). Experimental set-up of 1the 6-pixel OLED screen.

1-microcontroller, 2-switching board, 3-OLED screen, 4- voltage regulator.

The OLED screen is a power-efficient operating at 2.8V hence switching board drops down the voltage coming from the microcontroller to 2.8V. The bits in the form of OOK_NRZ uploaded to the microcontroller through software written in the C

language. With the help of switching board, the patterns based on transmitted bits formed on the OLED display module, which then recorded by the camera in video form followed up by image processing to calculate the BER.

### 4.3.2 Results and Discussion

During the lab work, several measurements were taken on different distances at pixel sizes of 8 and 16. The OLED screen had a library where OLED screen divided into pixel sizes of $32, 16, 8, 4, 2$ and 1. In our experiments, in context to this chapter, we considered the pixel sizes 8 and 16, considering pixel size neither too small or too large and thereafter the Bit Error Rate (BER) was calculated to check the system performance with increase in distance for the different pixel size 8 and 16 respectively at same distance. Additionally, the experiments carried out with the pixel size of 32 of the OLED screen thus dividing the OLED screen into 5 rows and 4 columns resulting in lesser number of bits transmitted, hence was an optimum choice. On the other hand, to increase the data rate and the number of bits transmitted per frame OLED screen divided into pixel sizes such as $4, 2$ and 1 could be considered. However, due to the reduction in BER using pixel size of 4, we restricted to the experiments with OLED screen divided into pixel size 8 and 16, respectively. The number of frames required for the entire length of the video calculated by total no of bits transmitted divided by no. of bits per frame. Figure 4.5 (a) and 4.5(b) show the image processing at pixel size 16 and 8, respectively. It illustrates the transmitted information per frame captured, and the grey image conversion after the border detection and then the cropped image taking the background off.

Transmitted information Image converted to grayscale Cropped

4.5(a)

Transmitted information Image converted to grayscale Cropped

4.5(b)

Figure 4.5 Image Processing, (a) at pixel size 16, (b) at pixel size 8.

As shown in figure .4.5(a) and figure 4.5(b) the cropped image is identical to the transmitted information hence illustrating the successful optical transmission of electroencephalogram signals. After the video capture, the image processing is performed for BER calculation by comparing the bits obtained per frame and the entire video. The BER obtained at pixel size 16 was lower or better than BER obtained at pixel size as shown in figure 4.6. Though the number of bits transmitted using 8-pixel size is increased in comparison to number of bits transmitted using the pixel size 16. It is a trade-off between BER and symbol size. The increase in pixel size results in

increase bit number possibly transmitted per frame hence, the information capacity or data rate improves significantly however, processing speed increases and possibly increases the BER too.

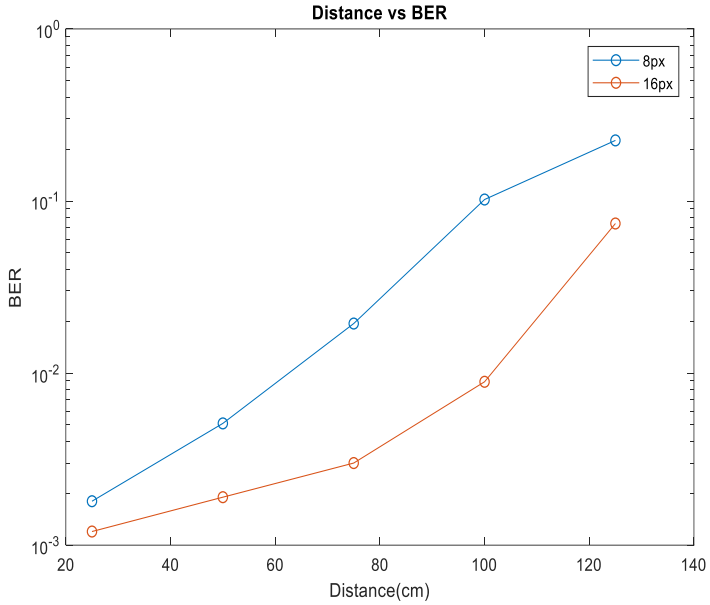


Figure 4.6. BER versus Distance.

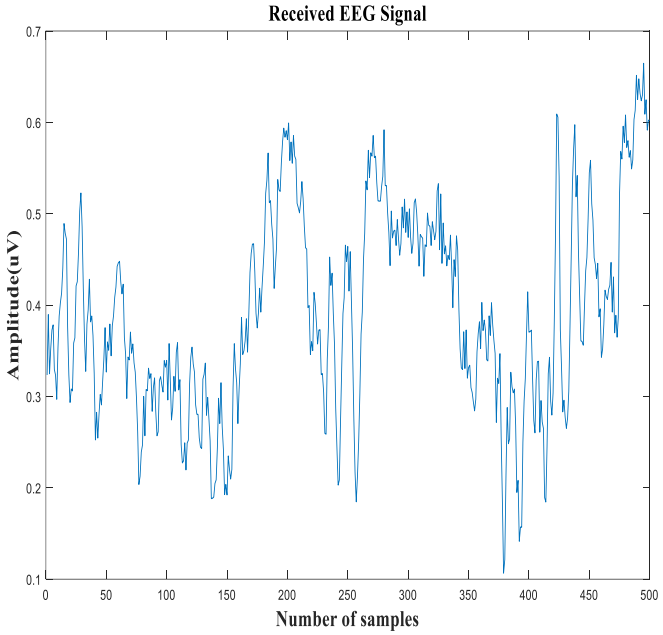


Figure 4.7. The amplitude of the received EEG signal versus number of samples.

After demodulation and digital to analogue converter, the received original transmitted EEG signal is shown in figure 4.7. The received EEG signal is same as that of transmitted EEG signal, hence implicates the successful and error-free optical transmission of EEG signal. Furthermore, the detection of transmitted bits is clearly possible for images and videos however, the BER changes with increase in distance.

## 4.4 Summary

This chapter proposed a novel technique to transmit EEG signals using VL-OCC system. The system proposed deployed in healthcare without generating any RF radiation in sensitive areas such as hospitals. Furthermore, we successfully proposed a technique that could replace current EEG systems deployed in clinical applications based on RF, which suffer from electromagnetic interference and signal loss. The BER obtained from the pixel sizes of 8 and 16 respectively at $25cm$ is of the order of $10^{-3}$. However, with the increase in distance, the BER for 8-pixel size drops considerably after $50cm$ unlike 16-pixel size where the BER obtained is of the order of $10^{-3}$ up to $75cm$ and the data rate achieved was $2kbps$ at a camera frame rate of 30 frames per second. The results in chapter 4 illustrate that the 16-pixel configuration of OLED screen yields better performance in context to 8-pixel configuration of the OLED screen. This is due to the fact in the reduction in the size of the pixels, smaller the size of the pixel, data rate is increased in comparison to 16-pixel configuration. However, the BER of the 16-pixel configuration is better than the 8-pixel configuration.

# Chapter 5 Angular Transmission of EEG signal using VL-OCC

## 5.1 Introduction

Scalp electrodes are used to capture the EEG signal and then the signal received is analysed on a displayed screen to check for epilepsy or several other diseases in context to the human brain. the placement of electrodes on the human brain or scalp is done, using the 10-20 system has been developed for placement of electrodes on the scalp during EEG recordings [18, 176,177]. The 10 and 20 refer to the per cent distances between each electrode in proportion to the size of the head. The locations on the scalp and the locations of the cerebral cortex are related together by this system[176]. The letters in figure 5.1 includes F, T, C, P, and O, which corresponds to frontal, temporal, central, parietal, and occipital, sections of the human brain respectively. Even numbers are located on the right hemisphere while odd numbers are on the left. The Z behind certain letters indicate the midline of the head [177]. As mentioned in chapter 1 that the number of electrodes required for EEG recording is entirely dependent on the EEG application, hence, to study the brain and its different sections, a number of scalp electrodes keep on varying time to time.

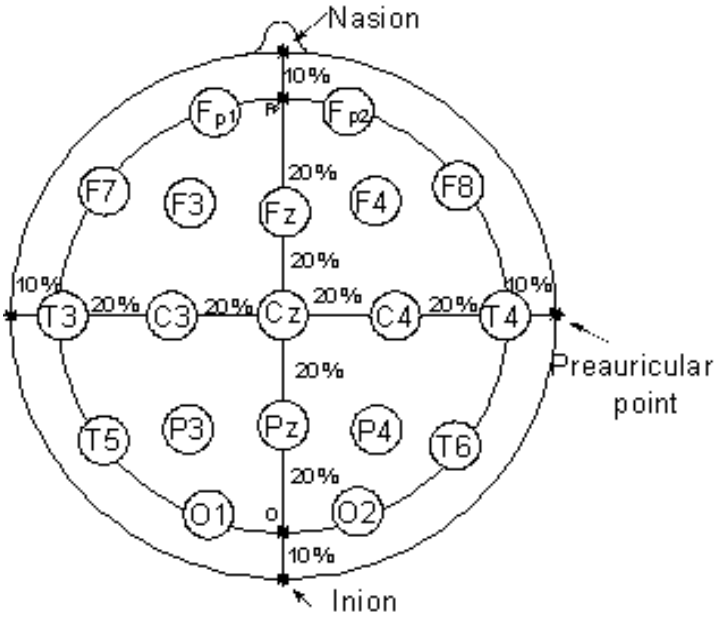


Figure 5.1. The 10-20 electrode placement system [176].

During the EEG procedure, there exists a possibility of angular transmission, thus in order to avoid inconvenience to patients, the idea is to rotate the receiver. The camera has a wide field of view (FOV) in comparison to photodiodes and can be easily rotated without any hardware or experimental setup modifications. In this chapter, the angular transmission of EEG signal is demonstrated using a 16-pixel OLED screen at the transmitter section and camera at the receiver section. The experiments were performed to maintain the LOS by rotating the camera at different angles using OOK_NRZ modulation scheme at 30 frames per second (fps).

This chapter is divided into the following sections, section 5.2 explains the proposed system in context to the angular transmission and the extraction of the EEG signal. Section 5.3 demonstrates the experiments followed by with results in section 5.4 and conclusion in section 5.5.

## 5.2 EEG signal extraction and proposed system model

This section illustrates the proposed system model and the EEG signal extraction using MATLAB.

### 5.2.1 EEG signal extraction using MATLAB

The first module of signal processing involves the conditioning of EEG signal by using filters, amplifiers and analogue to digital converter. Initially, the EEG signal was obtained from EEG toolbox [174] known as EEG lab. In our experimental work, only one channel was considered for the optical transmission of EEG signal. The single-channel namely 32 was selected in EEG lab and the EEG signal was extracted using MATLAB. The signal obtained was amplified to 1 V and filtered using bandpass filter (BPF) within a range of 0.4Hz to 40Hz. Thereafter the signal obtained in MATLAB is in the form of the continuous signal shown in figure 5.2(a). In our experiments unipolar signal was used as the light intensity in VLC systems cannot be negative, hence, the normalised EEG signal in the range of 0 and 1 is shown in figure 5.2 (b).

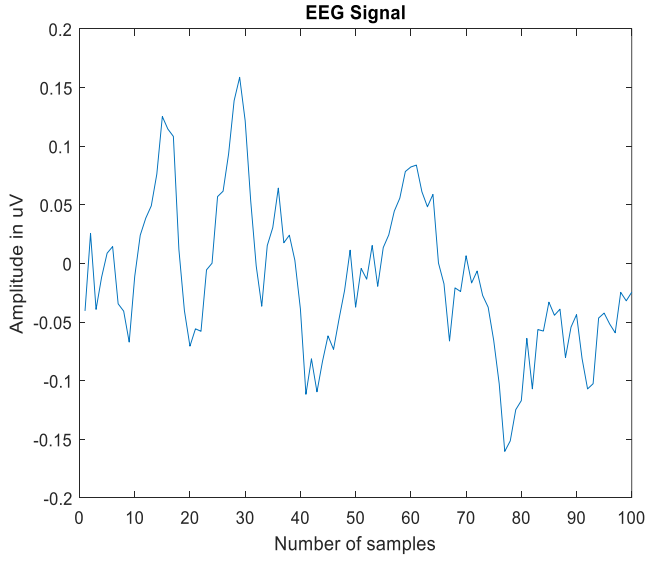


Figure 5. 2(a). EEG signal captured from EEGlab using MATLAB.

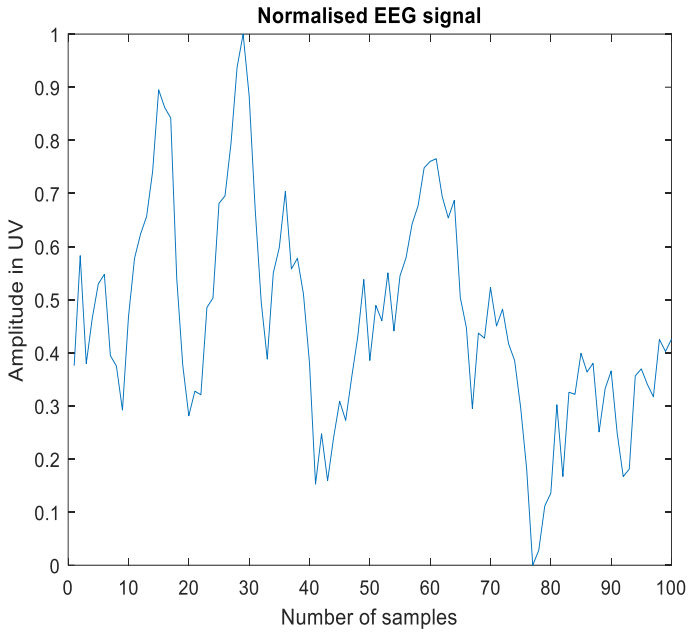


Figure 5.2(b). Normalized EEG signal.

In our experimental 100 samples of EEG signal was transmitted and analogue to digital conversion (ADC) of 16 bits was used to reduce the quantization error. A preamble of 400 bits comprising of all 1s was used to distinguish between the first and last frames during image processing and video capture. AWGN is the dominant noise, the data stream was received by a receiver unit comprising of Camera followed up by offline processing.

### 5.2.2 Proposed system model

As, this chapter is an extension of experiments in chapter 4, hence the initially proposed system modelling, figure is same as listed in section 4.3, however, the difference being the angle deviation. Hence, in this section the system modelling for the angular transmission of EEG signal using VL-OCC is explained using a flowchart shown in figure 5.3. The data bits received after ADC were up-sampled and then the received bits thorough American standard code for information exchange (ASCII) were transmitted to OLED screen using an ARM processor, FRDM KL-25Z. OLED

screen is a matrix of rows and columns, the number of bits that could be transmitted depends upon the pixel, details of OLED screen are listed in Appendix A.

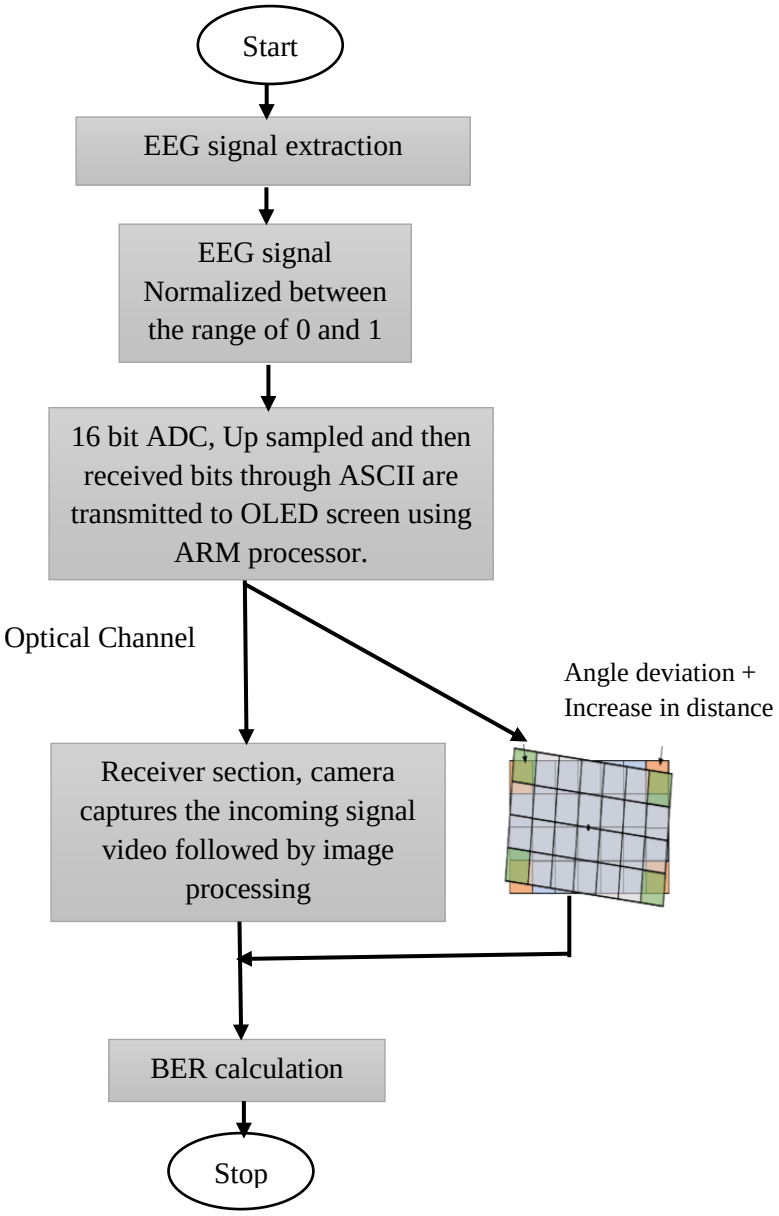


Figure 5.3 Flowchart of the proposed system.

We refer to equations 4.2 and 4.3 in chapter 4 in context to signal transmitted and received. The difference, in chapter 5 is the deployment of the concept of angular transmission with regards to 16 pixel OLED screen. The experimental set up is similar

to chapter 4, but the experiments are different. The system performance in this chapter is determined in context to 16 pixels with deviation in terms of BER, angle deviation and link distance. After the capture of images/video by the camera, image processing is done to calculate the BER and to test the system reliability and linkspan at angular transmission of EEG signal. Table 5.1 lists the description of OLED screen per pixel size and transmitted bit data information.

Table 5.1. Characterisation of OLED screen [165].

| Size of each block (in pixel) | Number of rows × columns as per the size of the block | Number of data bits can be transmitted per image/frame |
|---|---|---|
| 32 | 5×4 | 20 |
| 16 | 10×8 | 80 |
| 8 | 20×16 | 320 |
| 4 | 40×32 | 1280 |
| 2 | 80×64 | 5120 |
| 1 | 160×128 | 20480 |

In our lab work, depending upon the pattern of bits, the white section represents the transmission of ‘1’ and the black section represents the transmission of ‘0’ following the modulation scheme OOK-NRZ. At the receiver, side camera used followed by with image processing to detect the bits and to calculate the BER at different distances at different angles. n this research work of angular transmission of EEG signal, 16-pixel OLED screen was chosen because the pixel is neither too small nor too large.

## 5.3 Experimental setup and hardware description

In the experimental set up of angle deviation and hardware design consisting of Microprocessor, switching board, 16-pixel OLED and voltage regulator shown in figure 5.4.

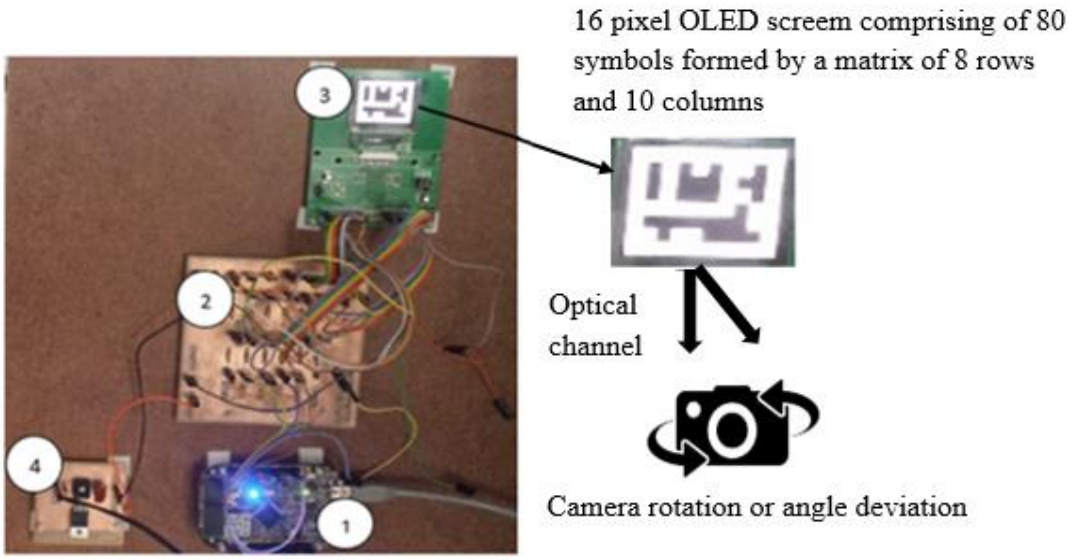


Figure 5.4. Hardware description of 16-pixel OLED screen at angle deviation.

Voltage regulator LM series used to regulate the power voltage from the dual power supply. The data sheets of OLED screen [165] and Table 5.1 illustrates that with the use of 16-pixel OLED results information of 10 rows and 8 columns, thus a total of 10×8=80 bits of information can be transmitted per frame. However, discussed in section 3.6.4 about edge detection in order to identify the images and not to lose the data and able to reconstruct back again, therefore out 80 bits per frame, the information bits transmitted were 8×6 = 48 bits per frame. Hence, the length of the video required for signal capture can be given by:

$$Video\ length = \frac{total\ data\ rate}{bit\ per\ frame} \tag{5.1}$$

Therefore,

$$Video\ length = \frac{2\ kbps}{48} = 41.6 \text{ sec} \quad (5.2)$$

From equation 5.1 and 5.2, we had calculated the time required to transmit the EEG signal is 41.6 sec, at a frame rate of 30fps at a data rate of 2 $kbps$. After the signal processing of EEG signal obtained from EEGlab the EEG signal in the form of bits uploaded to ARM processor from laptop with the help of cable USB cable wire from PC connecting the ARM processor. The OLED screen works on a voltage of 2.8 V and the ARM processor on 3.3 V, so the switching PCB board used between the OLED screen and processor, which reduces the voltage to 2.8 V from 3.3 V. The OLED transmits the bits optically through the optical, which are captured by camera at the receiver section. After the video capture, image processing is followed for further analysis. The results obtained are discussed in the next section.

## 5.4 Results and Discussion

Two different experiments were carried out 1) without angle deviation 2) at different angles i.e. angle deviation. Fig 5.5(a) explains the image processing at angle deviation while Fig 5.5(b) the image processing without angle deviation at 16-pixel symbol size respectively.

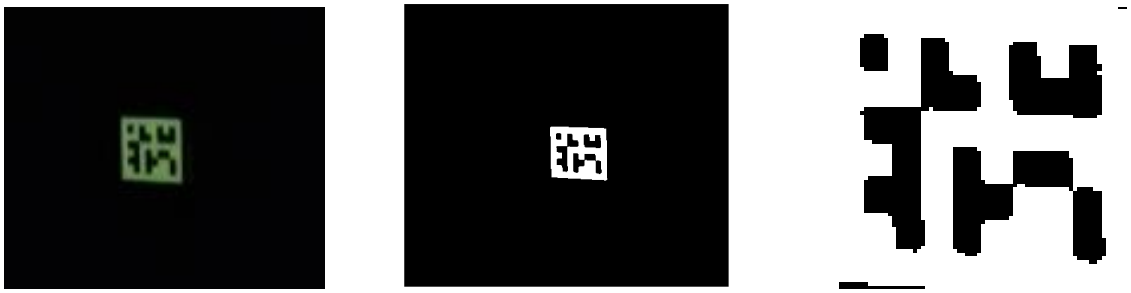

Figure 5.5(a) Image Processing at an angle deviation of pixel size 16.

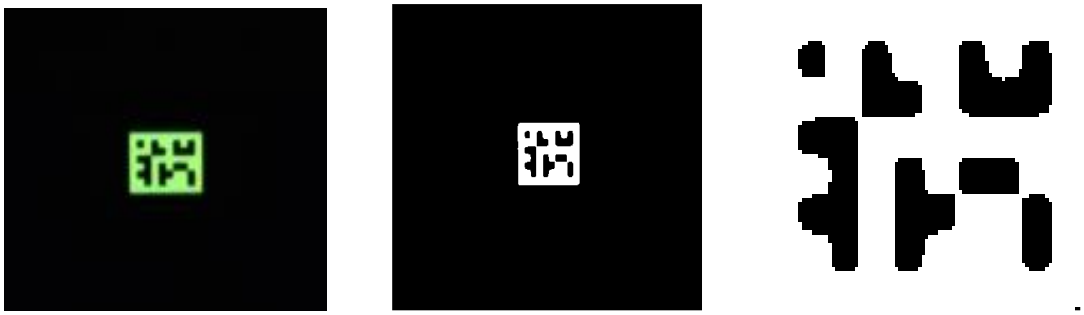

Figure 5. 5(b) Image Processing at an angle of 0-degree pixel size 16.

At angle deviation, the image received in figure 5.5(a) is tilted depending upon the angle between the normal, transmitter and receiver while figure 5.5(b) illustrates the image transmitted and received at 0-degree angle deviation. Larger angle deviation increases the image tilt thus resulting in an increase in BER as shown in figure 5.6 at 50cm. Figure 5. 7 shows the BER performance with distance and clearly states that with an increase in distance the BER increases significantly.

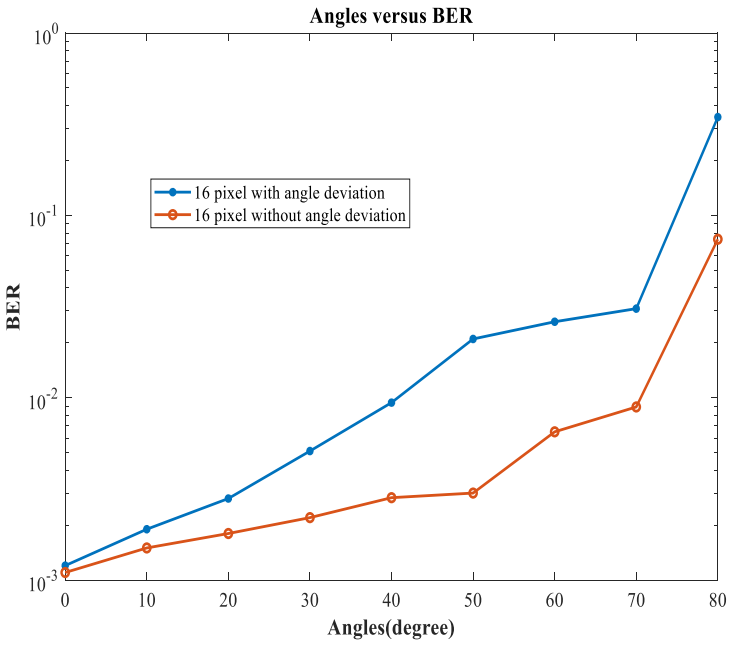


Figure 5. 6. Angles versus BER.

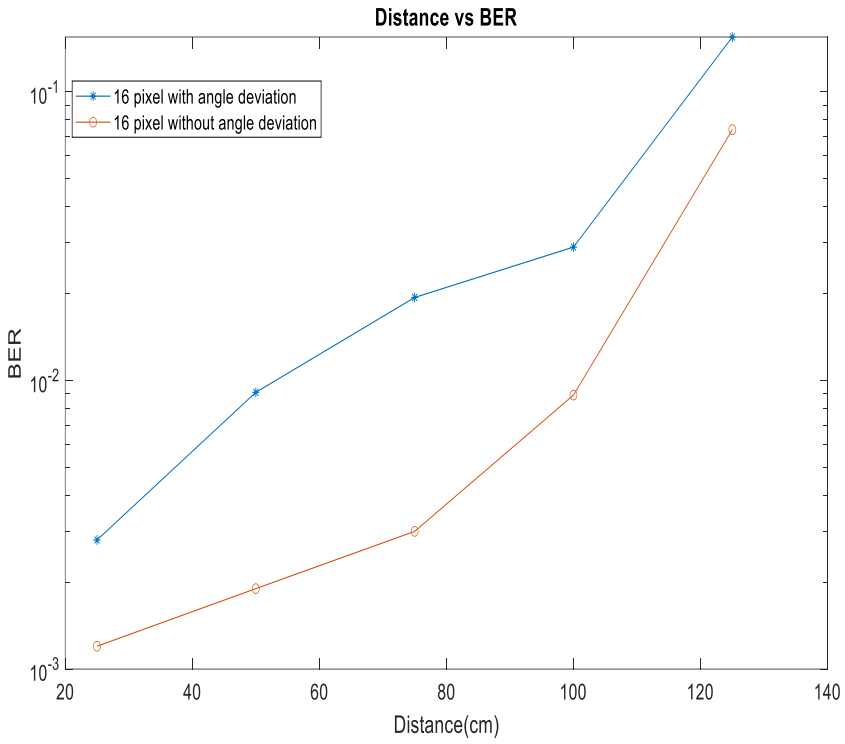


Figure 5.7. Distance versus BER.

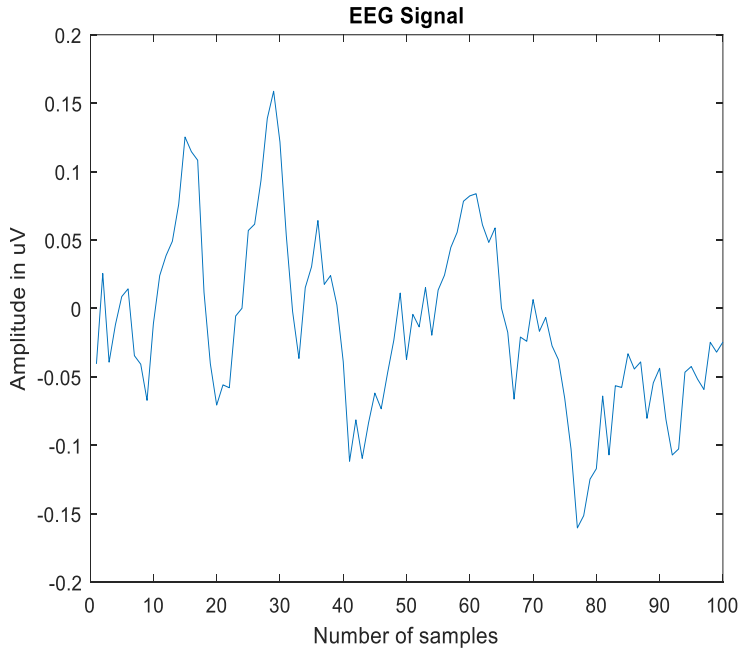


Figure 5.8 Received EEG signal.

Thus, the BER increases significantly with an increase in both distance and angle deviation respectively. The scope behind this work was to test the system performance in context to link distance and BER with regards to maximum angle deviation during EEG. The increase in distance and the higher angle deviation enhanced the BER significantly; however, during the EEG monitoring, most of the electrodes placed on the scalp follow the 10-20 system [176, 177]. Therefore, the ideal distance between two electrodes placed on the scalp is of few millimetres and the maximum angle deviation range is from 0 to 30 degree [176, 177]. As in figure 5.8, EEG signal was successfully recovered, thus illustrating the successful angular transmission of EEG signal using VL-OCC.

## 5.5 Summary

This chapter suggested and experimentally proven novel technique to be deployed in hospitals for angular transmission of EEG signals using wireless VL-OCC system. The data rate achieved in the experimental work was of 2kbps using the 16-pixel OLED and camera frame rate of 30 fps. The BER obtained from the size of the block of OLED screen in pixel size 16 irrespective of angle deviation is $10^{-3}$ at 50 cm, thus demonstrating a successful angular transmission of EEG signal using VL-OCC system. The achievable data rate is enough to detect EEG signal in applications where instant recording is required from a couple of seconds to a few minutes to detect the brain activity. This chapter illustrates that the research work could be helpful in healthcare applications especially brain monitoring at angle deviations where camera rotation is essential.

# Chapter 6 Experimental Demonstration of EEG Signal Transmission using 32 Pixel OLED screen and Camera

## 6.1 Introduction

VL-OCC has enormous potential in many applications, once such an application area is healthcare, where OLED screen is the transmitter and camera used as the receiver. As mentioned in chapter 1 and 2, that the VLC system uses different types of LED for communication, however, OLED is preferred over LED due to flexibility and nanometres in thickness, hence can be easily used in screens such as laptops, smart devices. In comparison to chapter 4 and chapter 5, this chapter demonstrates a wireless healthcare system for EEG using Visible Light Optical Camera Communication (VL-OCC) where 32-pixel OLED screen acts as transmitter and receiver section consists of several different cameras such as DLSR, android smartphone and Thorlabs camera. The experiments were performed in LOS deploying OOK modulation at several distant measurements to determine the system reliability and stability through BER performance. The proposed system results depict that DSLR camera outperforms smartphone and Thorlabs camera as is capable to transmit error-free bit rate of 2.8 kbps

at 30fps up to 5.5m. Figure 6.1 describes the block diagram of VL-OCC, where OLED screen is installed on the ceiling and the light intensity used for the dual purpose of lightning and communication.

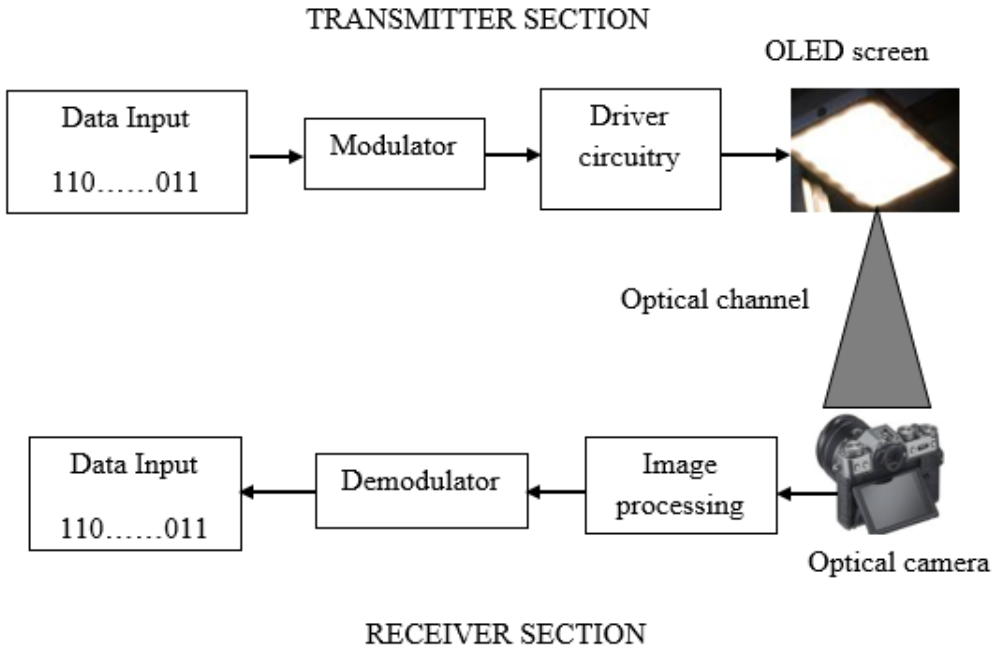


Figure 6.1 Block diagram of VL-OCC.

In the above figure, the data input is modulated and then transferred to light for transmission through the optical channel, where the camera records the video/image of the transmitted signal. This video/image is them offline processed using image processing and computer vision to extract the data bits, compare them with the input data and calculate BER. In some of the communications, driver circuitry is needed to drive the transmitter, therefore depending upon the type of LED or OLED used, the driver may vary. The popularity of smart devices and the camera installed in every smart device has resulted in the use of a camera as a receiver for communication purposes in VLC systems. In conventional VLC systems, PD is the receiver which requires hardware modification due to filters and amplifiers; however, with the receiver being the camera the cost of implementation is considerably reduced due to inbuilt filters and

focusing properties, reducing the unwanted noise. BER is calculated by comparing the transmitted and received data bits through images such as The QR code obtained at receiver section through image capture can be easily compared to the transmitted image in 2D to calculate BER and to analyse the system performance. The concept of transmitting a 1D signal in the digitized form using OOK-NRZ modulation scheme in a 2D image, with an OLED screen as transmitter and a camera as the receiver makes VLC a good alternative to RF communications for data transmission in healthcare. The captured images or videos by the camera are processed further using digital image processing for BER calculation.

Hence, the research work in this chapter proposes a novel VL-OCC-based wireless healthcare system for EEG using a 32-pixel OLED screen. Experiments were carried out in LOS using OOK_NRZ modulation in a realistic medical scenario. The camera, having a wider FOV than conventional photodiodes, can scan a larger area, hence the patient can be anywhere within the room. Furthermore, rotating the camera to maintain the LOS is easily feasible, unlike conventional VLC systems deploying photodiodes. The proposed system's experimental results of transmitting the EEG signal in 1D to a 2D image shows that that the system can communicate up to distance of 5.5 m at a camera frame rate of 30 fps, achieving a bit rate of 2.8 kbps. This chapter is divided into following section, where section 6.2 explains the proposed system modelling followed by with section experimental description in section 6.3. section 6.4 lists the results and discussion and section 6.5 concludes the paper.

## 6.2 System modelling

The focus in this chapter and experimental work was to improve the data rate, link distance and BER. The data was improved to 2.8 kbps from 2kbps in chapter 4 and

chapter 5. As stated in chapter 4 that EEGlab toolbox [164] was designed for lab research work by the US, consists of several features, algorithms, filters, Event-related potentials (ERP) etc, Therefore, the improvement in data rate was achieved by compressing the data using EEGlab before extracting the EEG signal from the toolbox. Figure 6.2 explains the system modelling with the help of the flowchart.

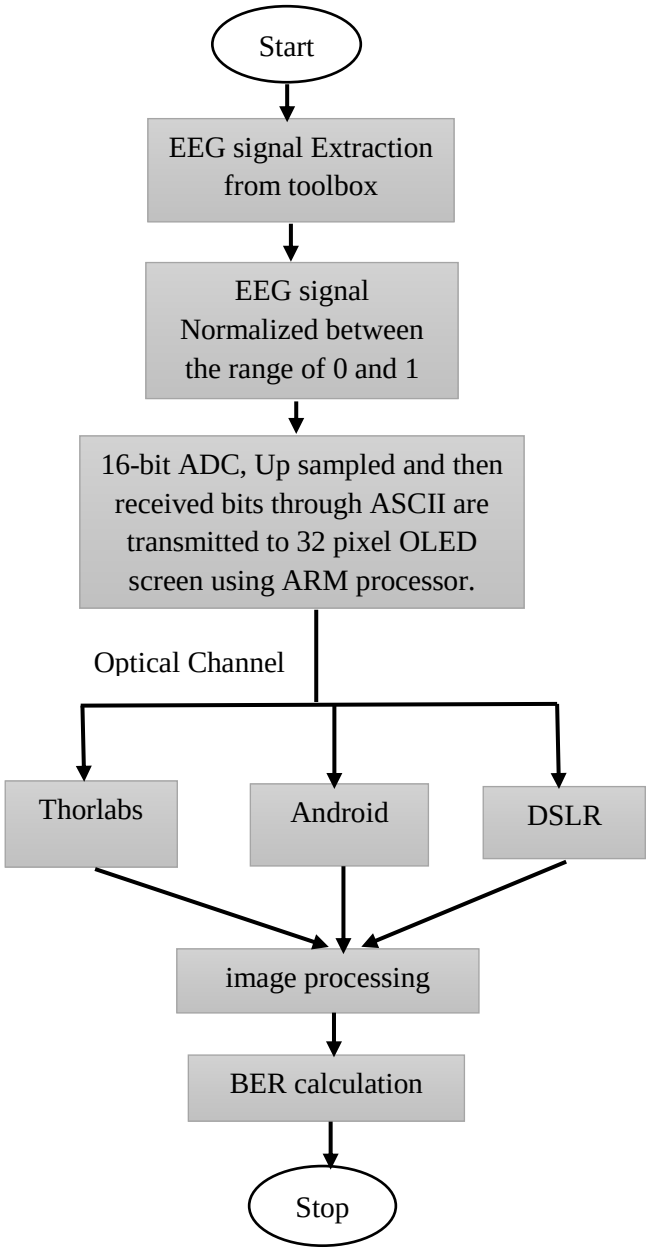


Figure 6.2 Flowchart of the proposed system.

In context to chapter 4 and chapter 5, results from 8 pixel and 16-pixel OLED screen depicted that the smaller the pixel size, more bits transmitted however affects the BER affective communication link distance. Therefore, in order to improve the BER and communication link distance, 32 pixel OLED was made a choice to be used in the experimental work in this chapter.

It is clear from table 5.1 and Appendix A that 32-pixel OLED can transmit 30 bits of information per from, formed by 5 rows and 4 columns. Therefore, the number of bits transmitted with 32 pixels per frame is less than in comparison to 8 pixels and 16 pixel OLED screen respectively, however, results illustrate the improvement in BER and link distance. The experiments were performed in LOS using OOK_NRZ modulation scheme, using three different cameras, namely thorlabs, android smartphone Samsung J3 and DSLR at the receiver section. After the up sampling, the bits are transferred to 32-pixel OLED screen through ARM processor using usb cable. We refer to equations 4.2 and 4.3 in chapter 4 for the transmission of the EEG signal optically.

## 6.3 Experimental description

This section illustrates the experimental work, PCB and hardware design. EEG signal is shown in figure 6.3(a) is downloaded from the EEG toolbox [178] using MATLAB. figure 6.3 (b). shows the Normalised EEG signal i.e EEG signal has values between 0 and 1. AWGN is the dominant noise, which is ignored in the experimental work.

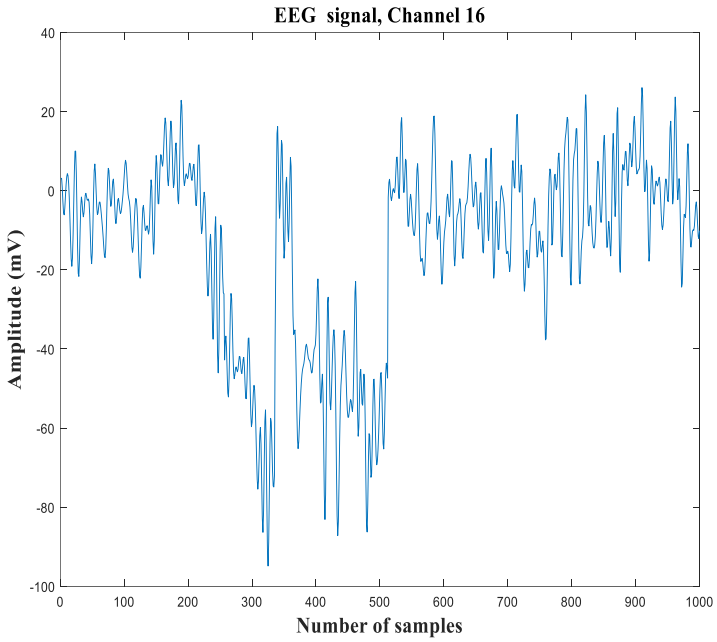


Figure 6.3(a) EEG signal from the EEG toolbox.

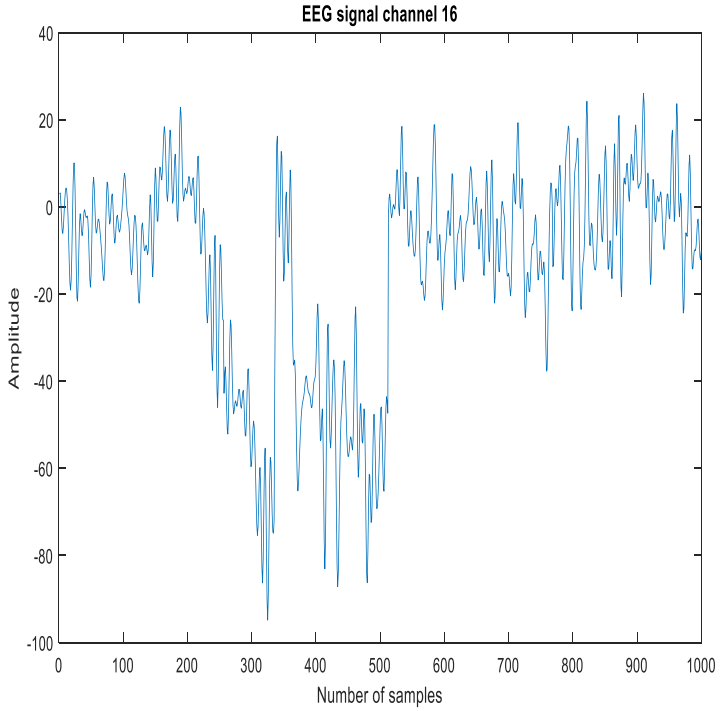


Figure 6.3 (b) Normalized EEG signal.

The input EEG data stream from the OLED screen as transmitter was received by a receiver unit comprising of Camera followed up by offline processing. The EEG data bits after signal processing in MATLAB are uploaded to the microcontroller using USB cable through MBED software by the laptop. software, the hardware design is shown in figure 6.4.

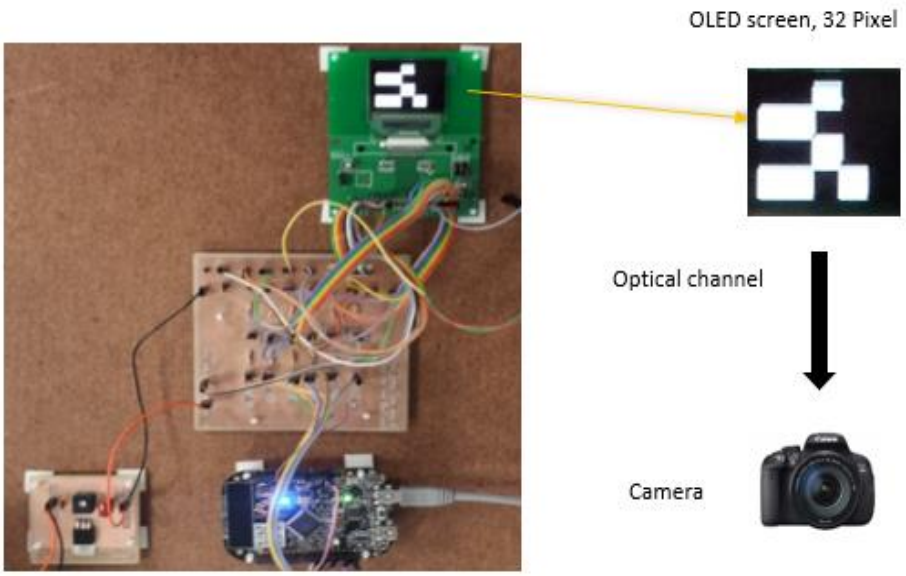


Figure 6.4. Hardware description of the 32-pixel OLED screen.

If the pixel size is 32 then based on the datasheets, OLED screen will be formed of 5 rows and 6 columns thus forming a total of 30 blocks in one single frame of OLED screen. The 30 blocks can be named as symbols where each symbol or block represents a single binary bit transmitted using OOK modulation. The experimental equipment used is listed in table 6.1. The uploaded bits are sent through switching board or potentiometer to the OLED screen. Switching Board acts as a bridge between microcontroller and OLED screen. The voltage regulator is designed using KICAD software and LM series

op-amp is used due to simplicity and readily available. Voltage regulator used to regulate the dual supply voltage to the 3.3 V for the evaluation board of the OLED screen through +VDD and –VDD.

Table 6.1 Experimental equipment.

| **Equipment** | **Model** |
|---|---|
| OLED screen | DD-160128FC-1A |
| ARM Processor | 30 fps |
| Camera | Canon, android, Thorlabs |
| Voltage Power Supply | 2.8V for logic |
| Coding and design software requirement | KICAD, C, MATLAB |

Hence, in a single frame of OLED screen with pixel size 32, a total of 30 symbols or data bits can be transmitted. The transmitted bits go through the optical channel, received by a camera in video form, followed by image processing in MATLAB to calculate BER and system reliability. The length of the video captured by a camera given by

$$video\ length = \frac{Total\ number\ of\ bits\ to\ be\ transmitted}{number\ of\ bits\ that\ can\ be\ transmitted\ per\ frame} \quad (6.1)$$

For example, for 2.8 $kbps$ data rate and 30 symbols or bits per frame length of video required will be

$$video\ length = \frac{2.8\ kbps}{30}$$

$$= 93.33\ \text{sec}\ or\ 1.56\ minutes \quad (6.2)$$

The camera parameters of three different cameras deployed at the receiver section are listed in table 6.2.

Table 6.2. Camera parameters.

| **Type of camera** | **Thorlabs camera** | **Android (Smartphone), J3 Samsung Galaxy** | **DSLR** |
|---|---|---|---|
| Camera resolution | 8MP | 5MP | 18MP |
| Camera frame rate | 30fps | 30 fps | 30 fps |
| Autofocus | Manual | Manual | Manual |
| Data rate achieved | 2.8 kbps | 2.8 kbps | 2.8 kbps |
| Link distance at error-free | 2.25m | 1.75m | 5.5m |
| Exposure mode | Rolling shutter | Rolling shutter | Rolling shutter |

For image processing and to detect the border of the image or frames, in order to convert the frame comprising of 5 rows and 6 columns into 4 rows and 5 columns thus the useful bit information transmitted through OLED screen confines to 20 bits or symbols in one single frame. Therefore, in this experimental work, the useful bits transmitted per single frame of 32-pixel size are counted as 20 comprising of 4 rows and 5 columns because remaining bits which will be used for border detection in image processing, therefore the length of video required is given by:

$$Length\ of\ video = \frac{2.8\ kbps}{20}$$

$$= 140\ \text{sec}\ or\ 2.3 minutes \qquad (6.3)$$

The length of video helps in determining the time the video has to be on thus saving the memory of the device.

## 6.4 Results analysis and Discussion

During the experimental work, the three different sets of experiments were carried out with three different cameras to calculate the BER at several distances and to check the reliability of the system. Figure 6.5 shows the image processing of the OLED screen at pixel size 32*32.

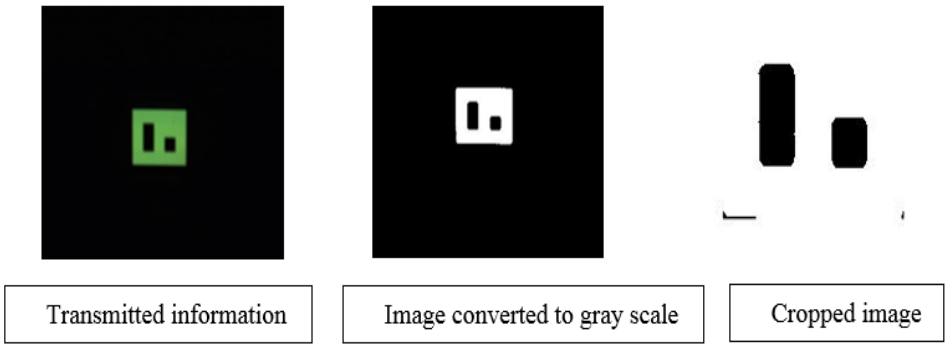


Figure 6.5 Image processing of 32-pixel OLED screen.

During the image, processing in our experimental work, the two bits 0 and 1 used representing low and high levels. If the symbol or block is black, then represents 0 bit and if the block is white represents 1 as shown in the cropped in grey image in the figure. The cropped image is used to calculate the BER by comparing the bits transmitted and bits received. The camera frame rate of 30 fps was fixed for all the respective camera; however, the distances were varied. The graph in figure 6.6 shows that DSLR outperforms Thorlabs and Android smartphone camera. The error-free link distance covered by DSLR camera is 5.5 m unlike the Thorlabs camera the link distance is 2.25m, smartphone camera is 1.75 m.

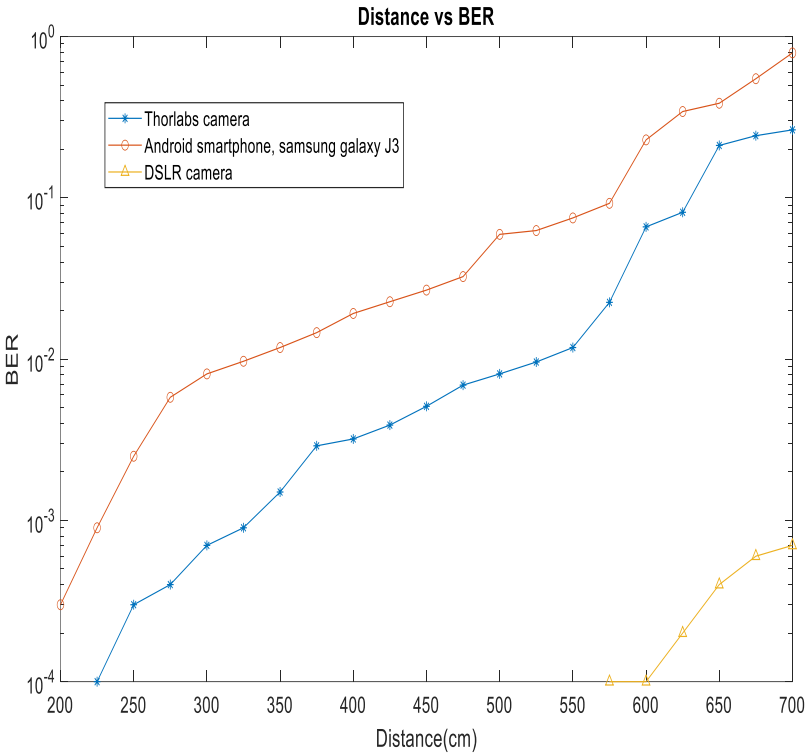


Figure 6.6 Distance versus BER.

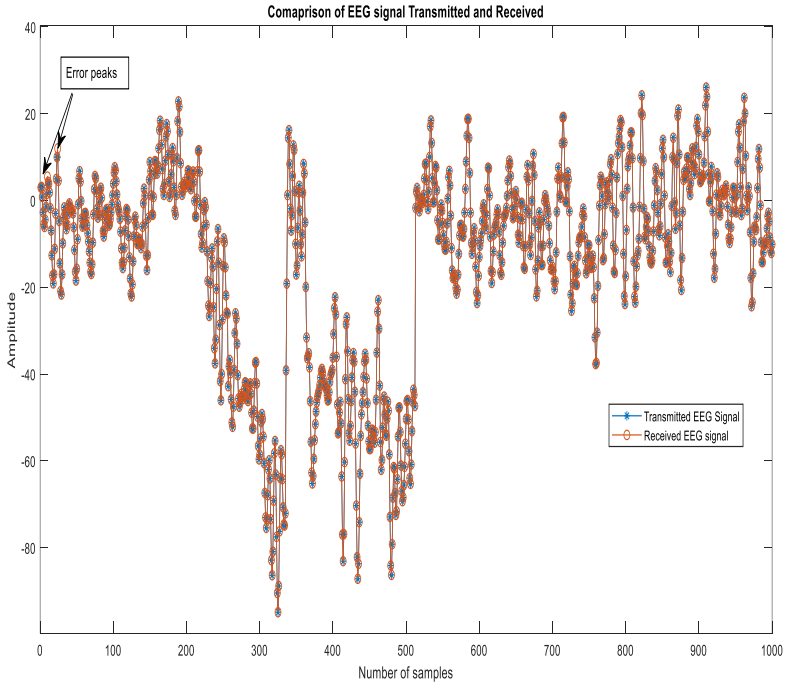


6.7 (a).

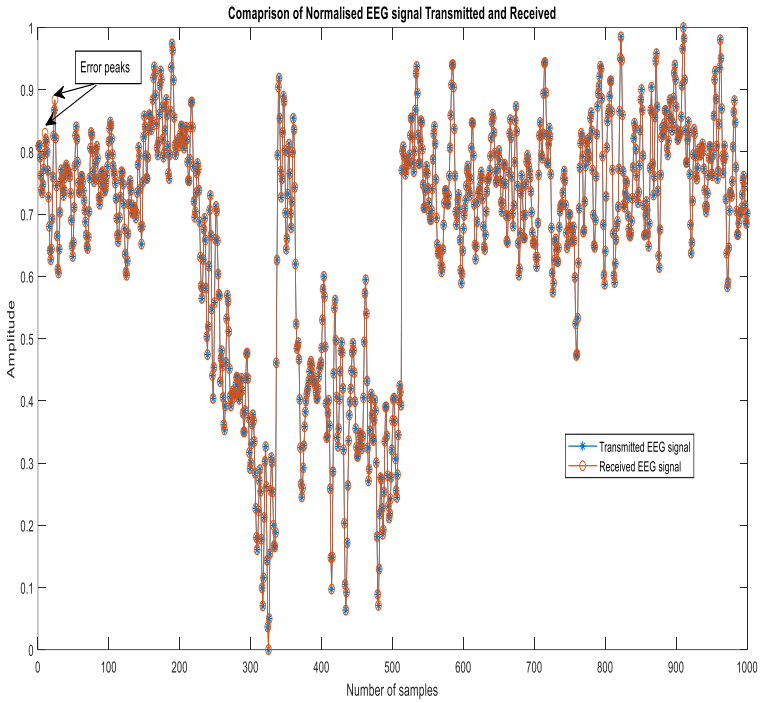


6.7 (b).

Figure 6.7(a) and 6.7(b). Comparison of EEG signal Transmitted, Received, Comparison of Transmitted, and Received Normalized EEG signal

The figure 6.7(a), and 6.7(b) shows the comparison of received EEG signal and transmitted EEG signal, thus illustrating the successful optical transmission of EEG signal and the detection of transmitted bits through images and videos, hence reducing the hardware cost in communication systems where the photodiode is used as a receiver. The results implicate the successful error-free optical transmission of EEG signal up to 5.5m using DSLR camera however the BER increases with an increase in distance.

## 6.5 Summary

The work in this paper suggested and experimentally proven novel technique to be deployed in hospitals for transmission of EEG signal using 32-pixel OLED screen. The

results of BER obtained show that in comparison to available literature the error-free link distance of 5.5m was achieved using DLSR camera and a 32-pixel OLED screen for wireless EEG signal monitoring through VL-OCC system. This chapter showed that deploying the camera with higher MP yields in better system performance both in context to link distance and BER. Therefore, DSLR camera shows better performance in comparison to thorlabs and android smartphone, samsung J3 devices. Furthermore, in comparison to the literature review, the data rate achieved in our experimental work is 2.8 kbps without any harmful radiation and successful transmission of EEG signal. The achievable data rate is enough to detect EEG signal both in applications where instant recording is required from seconds to few minutes to detect the brain activity or in applications where brain activity is recorded in the form of video, stored and analysed at later time intervals. This research work will be helpful in wireless, low-cost secure healthcare applications long-distance brain monitoring based on technology free from EMI and safe to human health and medical equipment.

# Chapter 7 Conclusions and Future work

## 7.1 Conclusions

This thesis focused on designing a prototype to be deployed in healthcare replacing the current RF system. The combination of two of the OWC technologies namely VLC and OCC, known as VL-OCC was proposed for EEG Applications. The use of the proposed system will vary depending upon the specific application and the brainwave categorization of EEG. The proposed system also, focused on system prototype using existing infrastructure and without any hardware modifications.

The objective of this research work was to design a prototype based on VL-OCC for the transmission of EEG signal free from EMI, to be deployed in hospitals. The main emphasis of this research work was to determine the performance of the proposed VL-OCC system in context to BER and link distance with respect to pixel size. This thesis highlighted the technical challenges, motivations behind conducting this study and the contributions made to knowledge in Chapter 1. Chapter 2 discussed the literature review, in context to VLC, advantages of VLC over other technologies such as RF, and potential applications of VLC. Chapter 2 also discussed the typical system model of VLC along with different forms of transmitters and receivers. Furthermore, the basic and foremost criteria to follow in choosing the modulation scheme for VLC was also listed in chapter 2.

In, chapter 3 after the brief introduction and overview of OCC, the typical VL-OCC system was discussed. Different types of VL-OCC communication systems, different image sensors, and shutter mechanism were also discussed in chapter 3. Chapter 3 also discussed the basics of DIP necessary for readers to understand the processing of images. Finally, Computer vision, scope and applications were listed, also giving brief introduction of software tools readily used for image processing in computer vision. In chapter 4, a novel technique based on VL-OCC was discussed for EEG. This research/thesis focuses and propose a new optical/electrical front-end and experimental system for EEG-VL-OCC system and compares the system performance of the traditional visible light communications system deploying LED at the transmitter and PD at the receiver. The experiments were performed in LOS using 8 pixel and 16-pixel OLED screen to be transmitter and Thorlabs camera to be a receiver. The results depicted that there is a trade-off between the pixel size and the BER obtained with an increase in distance. As with 16-pixel OLED screen, less bit information is transmitted but BER achieved was better in comparison to BER obtained with 8-pixel OLED screen at the same distance. Chapter 5 listed the angle deviation criteria and checked the system performance with 16-pixel OLED screen as transmitter and thorlabs camera to be a receiver. The results depicted that with an increase in angle deviation BER increases significantly with an increase in distance. Chapter 6 focused on EEG signal transmission using 32-pixel OLED screen as transmitter and three different cameras namely, canon, thorlabs and samsung J3 at the receiver section. This chapter showed that deploying the camera with higher megapixel results in improvement in system performance both in context to link distance and BER. Therefore, DSLR camera shows better performance in comparison to thorlabs and android smartphone, samsung J3 devices. Due to system on chip solution, low cost,

low power design, free from EMI, the proposed system prototype has the potential to be deployed in RF sensitive areas such as hospitals for remote or wireless brain monitoring amongst patients for EEG applications in brain-computer interface.

## 7.2 Future Work

This research completed the objectives listed in Chapter 1. However, the amount of time and work required to complete the system development to its full potential is out of the scope of this work. Hence, the following topics are suggested to extend the research **work reported in this thesis.**

### 7.2.1 MIMO (Multiple Input Multiple Output)

In this research, work single-channel EEG signal transmission was discussed. The future work comprising of multi-channel transmission using each pixel as an individual LED transmitting data shown in figure 7.1, would greatly enhance data rate.

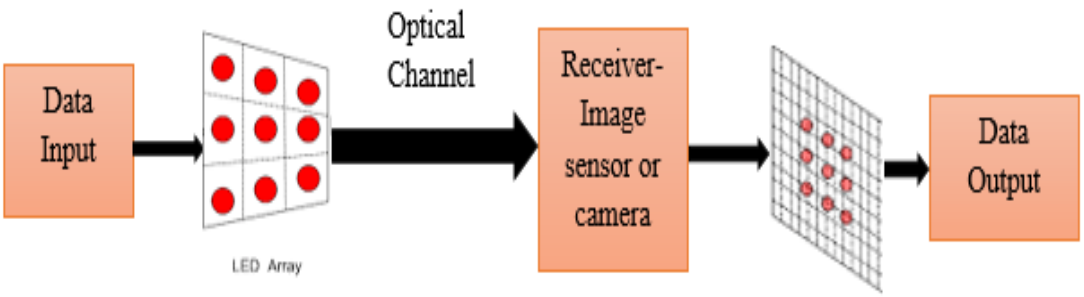


Figure 7.1. MIMO VL-OCC system.

In figure 7.1 the data input stream is transmitted using LED array, thus each LED in screens made up of rows and columns or pixel forms an individual LED to transmit the data. Each pixel is considered as an independent LED, used to transmit independent data streams irrespective of neighbouring or other pixels thus increasing the data rate.

The data is transmitted through an optical channel, received by an image sensor or camera. The received data capture by camera or image sensor is in the form of video or image which can be processed further both offline and online to calculate BER and system performance of the communication system. Deploying, MIMO will result in multiple EEG channel transmission, which is the future work.

### 7.2.2 RGB-WDM (Red Green Blue -Wavelength Division Multiplexing)

In the nearer future, the data rate requirement for the indoor wireless systems will be gradually increased due to the Internet of Things (IoT) and Optical Internet of things ( OIoT) connectivity. Currently, OWC specifically VL-OCC is considered as an alternative technology for wireless communication applications. Therefore, the red-green Blue (RGB) LEDs offer the possibility for wavelength division multiplexing (WDM). In RGB-WDM, multi-coloured LEDs or screens such as OLED screen could be used to send data at three independent frequencies simultaneously in the form of three independent data streams to overcome the challenge of low data rate in OCC. Three colours i.e Red, Green and Blue could be used to send simultaneously different frequency signals thus increasing the data rate to 3 times. Thus, the research work mentioned in the thesis could be extended further by using RGB-WDM. In colour images, each pixel is represented by three colour components, red, green and blue. Any colour can be created by mixing the correct amount of red, green and blue lights. Each one of the components ranges between 0 and 255 and can be stored in 8 bits. In image processing, every pixel is represented by a three-dimensional vector (r, g, b) that provides the colour intensity of each component, for instance, a black colour is represented by (0, 0, 0), (255, 255, 255) represents white, (255, 0, 0) denotes pure red etc [162, 163]. As, every pixel in a colour image can be represented by 24 bits (3 bytes),

thus more data bits could be transmitted using colour images when considering the communication systems. The most widespread method to give RGB colour sensitivity to image sensors is the application of a Colour Filter Array (CFA) on top of a black & white imager. In most cases a 3-colour Red-Green-Blue (RGB) pattern is used, although others exist too. Bayer colour filter array [178] is the most popular format for digital acquisition of colour images. The pattern of the colour filters varies in the sequence of the colours that are filtered using the Bayer filter shown in figure 7.2.

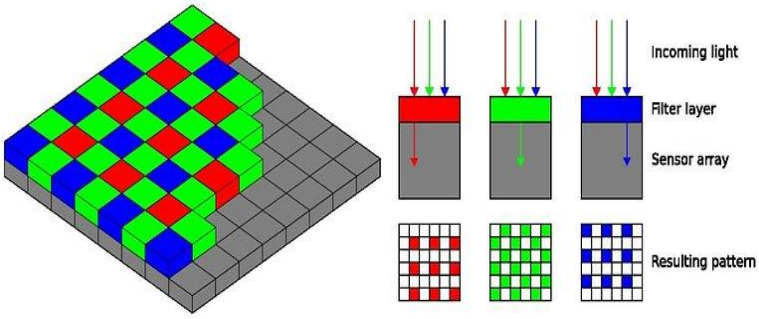


Figure 7.2 Colour image with its Bayer filter [178].

To form a colour image, we need to collect information at RGB wavelengths for all the pixels or sensors. Instead of capturing all RGB information at each pixel, with Bayer filter, we are only storing one colour information (either R, G or B) at each pixel which reduces the computation time and cost while maintaining the image quality [178]. Therefore, the use of RGB pattern will hence the data rate using VL-OCC and is recommended to be future work deployed in multiple EEG channel data transmission.

### 7.2.3 Geometric Operations

Today, there is almost no area of technical endeavour that is not impacted in some way by digital image processing. Geometrical operations change the spatial relationships between image pixels and may be used to correct distortions due to recording geometry, scale changes and rotations.

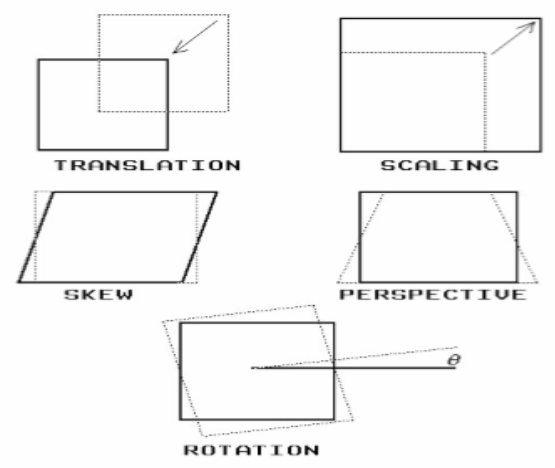


Figure 7.3. Geometric operations.

In this research, without angle deviation and angle deviation/rotation were discussed in context to BER calculation, system performance and link distance. The other geometric operations shown in figure 7.3, could be studied as the next step of this research work, analysing the BER and link distance evaluation with the change in pixels.

### 7.2.4 Blurring and defocusing

Blurring is greatly enhanced if the camera is not focused on the target or camera is in motion thus studying the effect of defocusing on signal transmission, thereby its effect on BER performance. Blurring happens when the camera is defocused or shaking during the image or video capture. The impact of blurring and defocusing and its effect on linkspan and BER in communication systems form the future work.

## Codes

### 1) Image processing at pixel size 8

```
clc
clear
close all

%%frame=0;%used as loop counter

%%LedVid = VideoReader('MVI_1667.MOV') % Place file in current folder and alter
file name accordingly
%%LedVid = VideoReader('F:\EEG\MatlabCode\32pix video a.avi');
%% convert video to image
%%vid=mmreader('video.avi');

% %% reading the video
vid=VideoReader('F:\EEG\MatlabCode\32pix video e.avi');
%     vid=VideoReader('C:\Users\Geet\Desktop\PhD_Thesis\codes_EEG\16px   vide
a\16pix video a.avi')
%
% %% read in all video frames
%  numFrames = vid.NumberOfFrames;
%  n=numFrames;
%  for i = 1:2:n
%  frames = read(vid,i);
%  imwrite(frames,['Image' int2str(i), '.jpg']);
%  im(i)=image(frames);
%  end

% read the selected frame/image 33 out of video a of 32 pixel
I       =       imread('C:\Users\Geet\Desktop\PhD_Thesis\codes_EEG\8px       video
a\image23.jpg');
% C:\Users\Geet\Desktop\PhD_Thesis\codes_EEG\8px video a

%convert it to grayscale
I = rgb2gray(I);

%calculate the binarization threshold
th = graythresh(I);

%binarize the image and display it
I = im2bw(I,th);
imshow(I)

%extract the size of the image
[a b] = size(I);

%threshold
```

```
th_row=0.1; % good for image 51
th_col=0.1; % good for image 51

%calculate first border (line0)
for i=1:a     % for image 49 i=1:a, the others are i=1:a/2
  for j=1:b
     %somma(j)=sum(I(i,:));
     if sum(I(i,:))>th_row*b
        line0 = i;
         i=0;
          break

     end
  end
  if i==0
     break

  end
end

%calculate second border (line1)
for i=a:-1:a/2
  for j=1:b
     if sum(I(i,:))>th_row*b
        line1 = i;
         i=0;
          break

     end
  end
  if i==0
     break

  end
end

%calculate third border (line2)
for i=1:a
  for j=1:b/2
     if sum(I(:,j))>th_col*a
        line2 = j;
         i=0;
          break

     end
  end
  if i==0
     break

  end
```

```
end

%calculate fourth border (line3)
for i=1:a
  for j=b:-1:b/2
     if sum(I(:,j))>th_col*a
        line3 = j;
         i=0;
          break

     end
  end
  if i==0
     break

  end
end

I = imcrop(I,[line2,line0,line3-line2,line1-line0]);
figure
imshow(I)

%extract the size of the resulting image
[c d] = size(I);
%calculate the number of pixels in each cell
numpixpercell = c*d/20;

%round number of pixels in each cell
patch = round(sqrt(numpixpercell));

offset=patch/2;

kk=1;
for i= offset+ patch:patch:c - (patch+offset)
   for j=offset+ patch:patch:d-(patch+offset)
      bits(kk)=I(i,j);
      kk=kk+1;
   end
end


%read the image 41 of video a 32 pixel
I = imread ('F:\EEG\MatlabCode\image53.jpg');

%convert it to grayscale
I = rgb2gray(I);

%calculate the binarization threshold
th = graythresh(I);
```

```
%binarize the image and display it
I = im2bw(I,th);
imshow(I)

%extract the size of the image
[a b] = size(I);

%threshold
th_row=0.1; % good for image 41
th_col=0.1; % good for image 41




%calculate first border (line0)
for i=1:a     % for image 49 i=1:a, the others are i=1:a/2
  for j=1:b
     %somma(j)=sum(I(i,:));
     if sum(I(i,:))>th_row*b
        line0 = i;
         i=0;
          break

     end
  end
  if i==0
     break

  end
end

%calculate second border (line1)
for i=a:-1:a/2
  for j=1:b
     if sum(I(i,:))>th_row*b
        line1 = i;
         i=0;
          break

     end
  end
  if i==0
     break

  end
end

%calculate third border (line2)
for i=1:a
  for j=1:b/2
```

```
      if sum(I(:,j))>th_col*a
         line2 = j;
          i=0;
           break

      end
   end
   if i==0
      break

   end
end

%calculate fourth border (line3)
for i=1:a
   for j=b:-1:b/2
      if sum(I(:,j))>th_col*a
         line3 = j;
          i=0;
           break

      end
   end
   if i==0
      break

   end
end

I = imcrop(I,[line2,line0,line3-line2,line1-line0]);
figure
imshow(I)

%extract the size of the resulting image
[c d] = size(I);
%calculate the number of pixels in each cell
numpixpercell = c*d/20;

%round number of pixels in each cell
patch = round(sqrt(numpixpercell));

offset=patch/2;

for i= offset+ patch:patch:c - (patch+offset)
    for j=offset+ patch:patch:d-(patch+offset)
       bits(kk)=I(i,j);
       kk=kk+1;
    end
 end
```

```
%read the image 63 of video a 32 pixel
I = imread ('F:\EEG\MatlabCode\image63.jpg');

%convert it to grayscale
I = rgb2gray(I);

%calculate the binarization threshold
th = graythresh(I);

%binarize the image and display it
I = im2bw(I,th);
imshow(I)

%extract the size of the image
[a b] = size(I);

%threshold
th_row=0.1; % good for image 63
th_col=0.1; % good for image 63




%calculate first border (line0)
for i=1:a     % for image 49 i=1:a, the others are i=1:a/2
  for j=1:b
     %somma(j)=sum(I(i,:));
     if sum(I(i,:))>th_row*b
        line0 = i;
         i=0;
          break

     end
  end
  if i==0
     break

  end
end

%calculate second border (line1)
for i=a:-1:a/2
  for j=1:b
     if sum(I(i,:))>th_row*b
        line1 = i;
         i=0;
          break

     end
```

```
  end
  if i==0
     break

  end
end

%calculate third border (line2)
for i=1:a
  for j=1:b/2
     if sum(I(:,j))>th_col*a
        line2 = j;
         i=0;
          break

     end
  end
  if i==0
     break

  end
end

%calculate fourth border (line3)
for i=1:a
  for j=b:-1:b/2
     if sum(I(:,j))>th_col*a
        line3 = j;
         i=0;
          break

     end
  end
  if i==0
     break

  end
end

I = imcrop(I,[line2,line0,line3-line2,line1-line0]);
figure
imshow(I)

%extract the size of the resulting image
[c d] = size(I);
%calculate the number of pixels in each cell
numpixpercell = c*d/20;

%round number of pixels in each cell
patch = round(sqrt(numpixpercell));
```

```
offset=patch/2;

for i= offset+ patch:patch:c - (patch+offset)
    for j=offset+ patch:patch:d-(patch+offset)
       bits(kk)=I(i,j);
       kk=kk+1;
    end
 end

%read the image 73 of video a 32 pixel
I = imread ('F:\EEG\MatlabCode\image73.jpg');

%convert it to grayscale
I = rgb2gray(I);

%calculate the binarization threshold
th = graythresh(I);

%binarize the image and display it
I = im2bw(I,th);
imshow(I)

%extract the size of the image
[a b] = size(I);

%threshold
th_row=0.1; % good for image 73
th_col=0.1; % good for image 73




%calculate first border (line0)
for i=1:a     % for image 49 i=1:a, the others are i=1:a/2
  for j=1:b
     %somma(j)=sum(I(i,:));
     if sum(I(i,:))>th_row*b
        line0 = i;
         i=0;
          break

     end
  end
  if i==0
     break

  end
end
```

```
%calculate second border (line1)
for i=a:-1:a/2
  for j=1:b
     if sum(I(i,:))>th_row*b
        line1 = i;
         i=0;
          break

     end
  end
  if i==0
     break

  end
end

%calculate third border (line2)
for i=1:a
  for j=1:b/2
     if sum(I(:,j))>th_col*a
        line2 = j;
         i=0;
          break

     end
  end
  if i==0
     break

  end
end

%calculate fourth border (line3)
for i=1:a
  for j=b:-1:b/2
     if sum(I(:,j))>th_col*a
        line3 = j;
         i=0;
          break

     end
  end
  if i==0
     break

  end
end

I = imcrop(I,[line2,line0,line3-line2,line1-line0]);
figure
```

```
imshow(I)

%extract the size of the resulting image
[c d] = size(I);
%calculate the number of pixels in each cell
numpixpercell = c*d/20;

%round number of pixels in each cell
patch = round(sqrt(numpixpercell));

offset=patch/2;

for i= offset+ patch:patch:c - (patch+offset)
    for j=offset+ patch:patch:d-(patch+offset)
       bits(kk)=I(i,j);
       kk=kk+1;
    end
 end
```

**2) Image processing at pixel size 16**

```
%% SECTION 1 - Load video file into matlab
%%LedVid = VideoReader('MVI_1667.MOV') % Place file in current folder and alter
file name accordingly
%%LedVid = VideoReader('F:\EEG\MatlabCode\16pix video a.avi');
%% convert video to image
%%vid=mmreader('video.avi');

% %% reading the video
% vid=VideoReader('F:\EEG\MatlabCode\16pix video a.avi');
%
% %% read in all video frames
%  numFrames = vid.NumberOfFrames;
%  n=numFrames;
%  for i = 1:2:n
%  frames = read(vid,i);
%  imwrite(frames,['Image' int2str(i), '.jpg']);
%  im(i)=image(frames);
%  end

[ bits1 ] = exp16pixel( 'image33.jpg');
[ bits2 ] = exp16pixel( 'image53.jpg');
[ bits3 ] = exp16pixel( 'image73.jpg');
[ bits4 ] = exp16pixel( 'image93.jpg');
[ bits5 ] = exp16pixel( 'image113.jpg');

bits=[ bits1 bits2 bits3 bits4 bits5];

er=0;
Lb=length(bits);
```

```
for i=1:Lb
   if(TrBits(i)~=bits(i))
      er=er+1;
   end
end


BER=er/Lb;

function [ bits ] = exp16pixel( VideoName, Folder)
%UNTITLED Summary of this function goes here
%   Detailed explanation goes here
% read the selected frame/image 33 out of video a of 32 pixel

%Name='image113.jpg';
%Folder='F:\EEG\MatlabCode\';
Path= strcat(Folder, VideoName);
I = imread(Path);

%convert it to grayscale
I = rgb2gray(I);

%calculate the binarization threshold
th = graythresh(I);

%binarize the image and display it
I = im2bw(I,th);
imshow(I)

%extract the size of the image
[a b] = size(I);

th_row=0.07;   % good for image 45
th_col=0.07;  % good for image 45

%calculate first border (line0)
for i=1:a     % for image 49 i=1:a, the others are i=1:a/2
  for j=1:b
     %somma(j)=sum(I(i,:));
     if sum(I(i,:))>th_row*b
        line0 = i;
         i=0;
          break

     end
  end
  if i==0
     break

  end
```

```
end

%calculate second border (line1)
for i=a:-1:a/2
  for j=1:b
     if sum(I(i,:))>th_row*b
        line1 = i;
         i=0;
          break

     end
  end
  if i==0
     break

  end
end

%calculate third border (line2)
for i=1:a
  for j=1:b
     if sum(I(:,j))>th_col*a
        line2 = j;
         i=0;
          break

     end
  end
  if i==0
     break

  end
end

%calculate fourth border (line3)
for i=1:a
  for j=b:-1:1
     if sum(I(:,j))>th_col*a
        line3 = j;
         i=0;
          break

     end
  end
  if i==0
     break

  end
end
```

```
I = imcrop(I,[line2,line0,line3-line2,line1-line0]);
figure
imshow(I)

%extract the size of the resulting image
[c d] = size(I);
%calculate the number of pixels in each cell
%numpixpercell = c*d/20;


numpixpercell = round(c*d/80); % 8x10 symbols per Frame

%round number of pixels in each cell
patch = round(sqrt(numpixpercell));

offset = floor(patch/2);
kk=1;
for i=patch+offset:patch:c - (patch + offset)
   for j=patch+offset:patch: d - (patch + offset)
      bits(kk)=I(i,j);
      kk=kk+1;
   end
end
```

**3) Image processing at pixel size 32**

```
%% SECTION 1 - Load video file into matlab
%%LedVid = VideoReader('MVI_1667.MOV') % Place file in current folder and
alter file name accordingly
%%LedVid = VideoReader('F:\EEG\MatlabCode\32pix video a.avi');
%% convert video to image
%%vid=mmreader('video.avi');

% %% reading the video
% vid=VideoReader('F:\EEG\MatlabCode\32pix video a.avi');
%
% %% read in all video frames
%  numFrames = vid.NumberOfFrames;
%  n=numFrames;
%  for i = 1:2:n
%  frames = read(vid,i);
%  imwrite(frames,['Image' int2str(i), '.jpg']);
%  im(i)=image(frames);
%  end

[ bits1 ] = exp32pixel( 'image33.jpg');
[ bits2 ] = exp32pixel( 'image53.jpg');
[ bits3 ] = exp32pixel( 'image73.jpg');
[ bits4 ] = exp32pixel( 'image93.jpg');
```

```
[ bits5 ] = exp32pixel( 'image113.jpg');

bits=[ bits1 bits2 bits3 bits4 bits5];

er=0;
Lb=length(bits);
for i=1:Lb
   if(TrBits(i)~=bits(i))
      er=er+1;
   end
end


BER=er/Lb;



function [ bits ] = exp32pixel( Name)
%UNTITLED Summary of this function goes here
%   Detailed explanation goes here
% read the selected frame/image 33 out of video a of 32 pixel

%Name='image113.jpg';
Folder='F:\EEG\MatlabCode\';
Path= strcat(Folder, Name);
I = imread(Path);

%convert it to grayscale
I = rgb2gray(I);

%calculate the binarization threshold
th = graythresh(I);

%binarize the image and display it
I = im2bw(I,th);
imshow(I)

%extract the size of the image
[a b] = size(I);

%threshold
th_row=0.1; % good for image 33
th_col=0.1; % good for image 33

%calculate first border (line0)
for i=1:a     % for image 49 i=1:a, the others are i=1:a/2
  for j=1:b
     %somma(j)=sum(I(i,:));
     if sum(I(i,:))>th_row*b
        line0 = i;
```

```
            i=0;
             break

        end
    end
    if i==0
        break

    end
end

%calculate second border (line1)
for i=a:-1:a/2
    for j=1:b
        if sum(I(i,:))>th_row*b
            line1 = i;
             i=0;
              break

        end
    end
    if i==0
        break

    end
end

%calculate third border (line2)
for i=1:a
    for j=1:b/2
        if sum(I(:,j))>th_col*a
            line2 = j;
             i=0;
              break

        end
    end
    if i==0
        break

    end
end

%calculate fourth border (line3)
for i=1:a
    for j=b:-1:b/2
        if sum(I(:,j))>th_col*a
            line3 = j;
             i=0;
              break
```

```
        end
    end
    if i==0
        break

    end
end

I = imcrop(I,[line2,line0,line3-line2,line1-line0]);
figure
imshow(I)

%extract the size of the resulting image
[c d] = size(I);
%calculate the number of pixels in each cell
numpixpercell = c*d/20;

%round number of pixels in each cell
patch = round(sqrt(numpixpercell));

offset=patch/2;

kk=1;
for i= offset+ patch:patch:c - (patch+offset)
    for j=offset+ patch:patch:d-(patch+offset)
        bits(kk)=I(i,j);
        kk=kk+1;
    end
end

end
```

```
    import cv2 as cv
import numpy as np

from matplotlib import pyplot as plt

img = cv.imread('sudoku.png',0)

img = cv.medianBlur(img,5)

ret,th1 = cv.threshold(img,127,255,cv.THRESH_BINARY)

th2 = cv.adaptiveThreshold(img,255,cv.ADAPTIVE_THRESH_MEAN_C,\

cv.THRESH_BINARY,11,2)

th3 = cv.adaptiveThreshold(img,255,cv.ADAPTIVE_THRESH_GAUSSIAN_C,\

cv.THRESH_BINARY,11,2)

titles = ['Original Image', 'Global Thresholding (v = 127)',
```

'Adaptive Mean Thresholding', 'Adaptive Gaussian Thresholding']

images = [img, th1, th2, th3]

for i in xrange(4):

plt.subplot(2,2,i+1),plt.imshow(images[i],'gray')

plt.title(titles[i])

plt.xticks([]),plt.yticks([])

plt.show(

is an image segmentation method. It compares pixel values with a threshold value and updates it accordingly. OpenCV supports multiple variations of thresholding. A simple thresholding function can be defined like this:

if Image(x,y) > threshold , Image(x,y) = 1

otherswise, Image(x,y) = 0

*Thresholding can only be applied to grayscale images.*

A simple application of image thresholding could be dividing the image into it's foreground and background.

```
#importing the required libraries
import numpy as np
import cv2
import matplotlib.pyplot as plt
%matplotlib inline

#here 0 means that the image is loaded in gray scale format
gray_image = cv2.imread('index.png',0)

ret,thresh_binary = cv2.threshold(gray_image,127,255,cv2.THRESH_BINARY)
ret,thresh_binary_inv = cv2.threshold(gray_image,127,255,cv2.THRESH_BINARY_INV)
ret,thresh_trunc = cv2.threshold(gray_image,127,255,cv2.THRESH_TRUNC)
ret,thresh_tozero = cv2.threshold(gray_image,127,255,cv2.THRESH_TOZERO)
ret,thresh_tozero_inv = cv2.threshold(gray_image,127,255,cv2.THRESH_TOZERO_INV)

#DISPLAYING THE DIFFERENT THRESHOLDING STYLES
names = ['Oiriginal Image','BINARY','THRESH_BINARY_INV','THRESH_TRUNC','THRESH_TOZERO','THRESH_TOZERO_INV']
images = gray_image,thresh_binary,thresh_binary_inv,thresh_trunc,thresh_tozero,thresh_tozero_inv
```

```
for i in range(6):
    plt.subplot(2,3,i+1),plt.imshow(images[i],'gray')
    plt.title(names[i])
    plt.xticks([]),plt.yticks([])

plt.show()
```

```
#import the libraries

import numpy as np

import matplotlib.pyplot as plt

import cv2

%matplotlib inline


#ADAPTIVE THRESHOLDING

gray_image = cv2.imread('index.png',0)


ret,thresh_global = cv2.threshold(gray_image,127,255,cv2.THRESH_BINARY)

#here 11 is the pixel neighbourhood that is used to calculate the threshold value

thresh_mean = cv2.adaptiveThreshold(gray_image,255,cv2.ADAPTIVE_THRESH_MEAN_C,cv2.THRESH_BINARY,11,2)


thresh_gaussian = cv2.adaptiveThreshold(gray_image,255,cv2.ADAPTIVE_THRESH_GAUSSIAN_C,cv2.THRESH_BINARY,11,2)


names = ['Original Image','Global Thresholding','Adaptive Mean Threshold','Adaptive Gaussian Thresholding']

images = [gray_image,thresh_global,thresh_mean,thresh_gaussian]


for i in range(4):

    plt.subplot(2,2,i+1),plt.imshow(images[i],'gray')
```

```
        plt.title(names[i])
        plt.xticks([]),plt.yticks([])


    plt.show()
```

**4) Mbed to camera communications**

```
#include "OLEDSeps525f.h"

#include "mbed.h"

//Serial pc1(USBTX, USBRX); // tx, rx


using namespace mbed;
OLEDSeps525f::OLEDSeps525f(PinName mosi, PinName miso, PinName clk, PinName cs, PinName rst, PinName rs)
      : _spi(mosi, miso, clk)
      , _cs(cs)
      , _rst(rst)
      , _rs(rs) {
  _row = 0;
  _column = 0;
  _width = _physical_width;
  _height = _physical_height;
  _rotation = 0;
  _columns = _width/8;
  _rows = _height/8;
  _tablength = 4;
  _writing_pixels = 0;
  foreground(0x00FFFFFF);
  background(0x00000000);
  reset();
}

void OLEDSeps525f::reset() {

  unsigned int i=0,j,k;
  const unsigned char init_commands[]= {
     0x06, // Display off
     0x00,

     //Osc control
     //Export1 internal clock and OSC operates with external resistor
     0x02,
```

```
0x01,

//Reduce current
0x04,
0x00,

//Clock div ratio 1: freq setting 90Hz
0x03,
0x30,

//Iref controlled by external resistor
0x80,
0x00,

//Precharge time R
0x08,
0x01,
//Precharge time G
0x09,
0x01,
//Precharge time B
0x0A,
0x01,

//Precharge current R
0x0B,
0x0A,
//Precharge current G
0x0C,
0x0A,
//Precharge current B
0x0D,
0x0A,

//Driving current R = 82uA
0x10,
0x52,
//Driving current G = 56uA
0x11,
0x38,
//Driving current B = 58uA
0x12,
0x3A,

//Display mode set
//RGB,column=0-159, column data display=Normal display
0x13,
0x00,

//External interface mode=MPU
```

```
0x14,
0x01,

//Memory write mode
//6 bits triple transfer, 262K support, Horizontal address counter is increased,
//vertical address counter is increased. The data is continuously written
//horizontally
0x16,
0x76,

//Memory address setting range 0x17~0x19 to width x height
0x17,  //Column start
0x00,
0x18,  //Column end
_physical_width-1,
0x19,  //row start
0x00,
0x1A,  //row end
_physical_height-1,

//Memory start address set to 0x20~0x21
0x20,  //X
0x00,
0x21,  //Y
0x00,

//Duty
0x29,
0x00,

//Display start line
0x29,
0x00,

//DDRAM read address start point 0x2E~0x2F
0x2E,  //X
0x00,
0x2F,  //Y
0x00,

//Display screen saver size 0x33~0x36
0x33,  //Screen saver columns start
0x00,
0x34,  //Screen saver columns end
_physical_width-1,
0x35,  //screen saver row start
0x00,
0x36,  //Screen saver row end
_physical_height-1,
```

```
        //Display ON
        0x06,
        0x01,

        //End of commands
        0xFF,
        0xFF
    };

    //Initialize interface and reset display driver chip
    _cs = 1;
    wait(0.01);
    _rst = 0;
    wait(0.001);
    _rst = 1;
    wait(0.01);
    _spi.format(8);
    _spi.frequency(10000000);

    //Send initialization commands
    for (i=0; ;i+=2) {
        j=(int)init_commands[i];
        k=(int)init_commands[i+1];
        if ((j==0xFF) && (k==0xFF)) break;

        command(j);
        data(k);
    }
}

void OLEDSeps525f::command(int value) {

    _writing_pixels=(value == 0x22);
    _rs = 0;
    _cs = 0;
    _spi.write(value);
    _cs = 1;
    _rs = 1;
}

void OLEDSeps525f::data(int value) {
    _rs = 1;
    _cs = 0;
    _spi.write(value);
    _cs = 1;
}

inline
void OLEDSeps525f::rgbdot(int r, int g, int b)
{
```

```
    _rs = 1;
    _cs = 0;
    _spi.write(r);
    _cs = 1;
    _cs = 0;
    _spi.write(g);
    _cs = 1;
    _cs = 0;
    _spi.write(b);
    _cs = 1;
}

void OLEDSeps525f::_window(int x, int y, int width, int height) {
    int x1, x2, y1, y2, start_x, start_y;
    switch (_rotation) {
        default:
        case 0:
            x1 = x;
            y1 = y;
            x2 = x + width - 1;
            y2 = y + height - 1;
            break;
        case 1:
            x1 = _physical_width - y - height;
            y1 = x;
            x2 = _physical_width - y - 1;
            y2 = x + width - 1;
            break;
        case 2:
            x1= _physical_width - x - width;
            y1= _physical_height - y - height;
            x2= _physical_width - x - 1;
            y2= _physical_height - y - 1;
            break;
        case 3:
            x1 = y;
            y1 = _physical_height - x - width;
            x2 = y + height - 1;
            y2 = _physical_height - x - 1;
            break;
    }
    //Limit values
    if (x1 < 0) x1=0;
    if (x1 >= _physical_width) x1=_physical_width-1;
    if (x2 < 0) x2=0;
    if (x2 >= _physical_width) x2=_physical_width-1;
    if (y1 < 0) y1=0;
    if (y1 >= _physical_height) y1=_physical_height-1;
    if (y2 < 0) y2=0;
    if (y2 >= _physical_height) y2=_physical_height-1;
```

```
/*    if ((width > 100) || (height > 100))
    {

pc1.printf("x=%d\ty=%d\twidth=%d\theight=%d\tx1=%d\tx2=%d\ty1=%d\ty2=%d\n
",x,y,width,height,x1,x2,y1,y2);
    }
*/
    command(0x19);  // Y start
    data(y1);
    command(0x1A);  // Y end
    data(y2);
    command(0x17);  // X start
    data(x1);
    command(0x18);  // x end
    data(x2);

    switch (_rotation) {
       default:
       case 0:
          start_x=x1;
          start_y=y1;
          break;
       case 1:
          start_x=x1;
          start_y=y2;
          break;
       case 2:
          start_x=x2;
          start_y=y2;
          break;
       case 3:
          start_x=x2;
          start_y=y1;
          break;
    }

    command(0x20);  // memory accesspointer x
    data(start_x);
    command(0x21);  // memory accesspointer y
    data(start_y);

}

inline
void OLEDSeps525f::_putp(int colour) {
    static int colour_prev=0xF000000, r=0, g=0, b=0;

    //Start "write data" command if not done already
```

```
    if ( ! _writing_pixels )
    {
        command(0x22);
    }
    //Only calculate rgb values if colour has changed
    if (colour_prev != colour)
    {
        r=(colour & 0xFF0000) >> 16;
        g=(colour & 0x00FF00) >> 8;
        b=colour & 0xFF;
        colour_prev=colour;
    }

    rgbdot(r,g,b);
}

void OLEDSeps525f::orientation(int o) {
        _rotation=o & 3;

        //Set write direction
        command(0x16);
        switch(_rotation) {
            case 0:
            default:
                //HC=1, VC=1, HV=0
                data(0x76);
                _width=_physical_width;
                _height=_physical_height;
                break;
            case 1:
                //HC=0, VC=1, HV=1
                data(0x73);
                _width=_physical_height;
                _height=_physical_width;
                break;
            case 2:
                //HC=0, VC=0, HV=0
                data(0x70);
                _width=_physical_width;
                _height=_physical_height;
                break;
            case 3:
                //HC=1, VC=0, HV=1
                data(0x75);
                _width=_physical_height;
                _height=_physical_width;
                break;
        }
        _columns = _width/8;
        _rows = _height/8;
```

```
}


const unsigned char FONT8x8[97][8] = {
}; // DEL

void OLEDSeps525f::locate(int column, int row) {
   _row = row;
   _column = column;
}

void OLEDSeps525f::newline() {
   _column = 0;
   _row++;
   if (_row >= _rows) {
      _row = 0;
   }
}

void OLEDSeps525f::tablength(int l) {
   _tablength = l;
}

int OLEDSeps525f::_putc(int value) {
   int x = _column * 8;  // FIXME: Char sizes
   int y = _row * 8;

   //Interpret some ASCII control codes
   if (value < 0x1F)
   {
      switch (value)
      {
         //Backspace
         case 0x08:
            _column--;
            if (_column < 0) {
               _column = 0;
               _row--;
               if (_row < 0) {
                  _row = _rows - 1;
               }
            }
            break;
         //Tab
         case 0x09:
            _column=((_column / _tablength) * _tablength) + _tablength;
            if (_column > _columns) {
               newline();
            }
            break;
```

```
            //Line feed
            case 0x0A:
               newline();
               break;
            //Vertical tab
            case 0x0B:
               _row++;
               if (_row >= _rows) {
                  _row = 0;
               }
               break;
            //Carriage return
            case 0x0D:
               _column = 0;
               break;
            //Default ignore
            default:
               break;
         }
      } else
      {
         if (value < 128)
         {
            bitblit(x + 1, y + 1, 8, 8, (char*)&(FONT8x8[value - 0x1F][0]));

            _column++;
         }
      }

      if (_column < 0) _column=0;
      if (_column >= _columns) {
         _row++;
         _column = 0;
      }

      if (_row < 0) _row=0;
      if (_row >= _rows) {
         _row = 0;
      }
   return value;
   }

   void OLEDSeps525f::cls() {
      fill(0, 0, _width, _height, _background);
      _row = 0;
      _column = 0;
   }

   int OLEDSeps525f::width() {
      return _width;
```

```
}

int OLEDSeps525f::height() {
   return _height;
}

int OLEDSeps525f::columns() {
   return _columns;
}

int OLEDSeps525f::rows() {
   return _rows;
}

int OLEDSeps525f::tablength() {
   return _tablength;
}

int OLEDSeps525f::orientation() {
  return(_rotation);
}

int OLEDSeps525f::foreground() {
   return(_foreground);
}

int OLEDSeps525f::background() {
   return(_background);
}

void OLEDSeps525f::window(int x, int y, int width, int height) {
   _window(x, y, width, height);
}

void OLEDSeps525f::putp(int colour) {
   _putp(colour);
}

void OLEDSeps525f::pixel(int x, int y, int colour) {
   _window(x, y, 1, 1);
   _putp(colour);
}

void OLEDSeps525f::fill(int x, int y, int width, int height, int colour) {
   int r, g, b;

   _window(x, y, width, height);
   //Start "write data" command if not done already
   if ( ! _writing_pixels )
   {
```

```
        command(0x22);
    }
    r=(colour & 0xFF0000) >> 16;
    g=(colour & 0x00FF00) >> 8;
    b=colour & 0xFF;
    for (int i=0; i<width*height; i++) {
        rgbdot(r, g, b);
    }
    _window(0, 0, _width, _height);
}


void OLEDSeps525f::blit(int x, int y, int width, int height, const int* colour) {
    _window(x, y, width, height);
    for (int i=0; i<width*height; i++) {
        _putp(colour[i]);
    }
    _window(0, 0, _width, _height);
}

void OLEDSeps525f::foreground(int v) {
    _foreground = v;
}

void OLEDSeps525f::background(int v) {
    _background = v;
}

void OLEDSeps525f::bitblit(int x, int y, int width, int height, const char* bitstream) {
    _window(x, y, width, height);
    for (int i=0; i<height*width; i++) {
        int byte = i / 8;
        int bit = i % 8;
        int colour = ((bitstream[byte] << bit) & 0x80) ? _foreground : _background;
        _putp(colour);
    }
    _window(0, 0, _width, _height);
}




/*/*
 OLED to Camera Communications.
*/
#include "string.h"
#include "mbed.h"
#include "OLEDSeps525f.h"
//OLEDSeps525f lcd(p5, p6, p7, p8, p9, p10); mosi - SPI data out, miso - SPI data in,
not used, clk  - SPI clock, cs   - Chip Select, rst  - reset, rs   - command/data select
```

```
OLEDSeps525f lcd(PTD2, PTD3, PTD1, PTD0, PTE0, PTE1);  //PTD3, miso, not used  (D11, D12, D13, )

int main() {

   // Initialization
   lcd.background(0x000000);  // return black background
   lcd.cls(); // fills all the display with background

   int symS; // simbols size in pixels
   int Nsym; // number of symbols per frame
   symS = 16; // simbols size in pixels, possible options: {total symbols transmitted 20480 that is symbol size 1x1, 5120 2x2, 1280 4x4, 320 8x8, 80 16x16, 20 32x32}
   Nsym = (lcd.width()/symS)*(lcd.height()/symS); //depends on the size of the screen, our case is 160x128

   // symS = 16x pixels per symbol, 8x10 symbols, information bits 6x8 48 per Frame
   //const int Nbits=1000; //  number of transmitted information bits
   const int Nbits=1056;  //MULTIPLE OF 48, which are the information bits per Frame
   int bits[Nbits]= {};  // array inizialization

   //int n_column = 10;

   // initialization of display, with cornice of squared white symbols
   int jj =0; // column counter
   int ii =0; // row counter
   for(int j=0; j<lcd.height();  j+=symS) {  // scan on the rows, incremented by symS
         for(int i=0; i<lcd.width();  i+=symS) {  // scan on the column

            // cornice of white
            if((ii>=0 && ii<10) && (jj==0 || jj==7)){
               lcd.fill(i, j ,symS, symS, 0xFFFFFF);  // fill with white
            }

            if((ii==0 || ii==9) && (jj>0 && jj<7)){
               lcd.fill(i, j ,symS, symS, 0xFFFFFF);  // fill with white
            }

         ii+=1;
      }
   jj+=1;
   ii=0;
   }


   int count=0;  // counter

   while(1){ // while there are still bit to transmit
```

```
      if(count == Nbits){
         count=0; // restart
 //        lcd.background(0x000000);  // black background,
 //        lcd.cls();
      }

//       if(count == 256){ // count == information bits per frame
 //          lcd.background(0x000000);  // black background, change to white only for the symbols related to bit 1
 //          lcd.cls();
 //      }

      for(int j=1*symS; j<7*symS;  j+=symS) {   // scan on the rows, incremented by symS
          for(int i=1*symS; i<9*symS;  i+=symS) {  // scan on the column

                if(bits[count]==1){    // check bits

            lcd.fill(i, j ,symS, symS, 0xFFFFFF);  // fill with white

            }
            if(bits[count]==0){    // check bits

            lcd.fill(i, j ,symS, symS, 0x000000);  // fill with white


            }
            count+=1;
          }
      }
   wait(1);
   } // end while}
```

**5) EEG signal**

```
Data = textread('Data.txt');
N = length(Data);
figure;
plot(Data);
DataBinary = zeros(1,N);

% To make the data to binary stream
mean = sum(Data)/N;
M=0;
for i = 1:N
   if Data(i) >= mean;
      DataBinary(i) = 1;
      M = M+1;
   else
      DataBinary(i) = 0;
```

```
        M=M;
    end
end
M
hold on;
% figure;
plot(DataBinary);
axis([0 1000 -0.4 1.1]);
save DataBinary.txt -ascii DataBinary


s=EEG_Normalised_1000
min_s=min(s)
max_s=max(s)
S=(s-min_s)/(max_s-min_s)
plot(S)
clc
clear

%% Data load

load('OOK_NRZ.txt') % load dataTx

Volt = load('test1.txt'); %load dataRx

%% Resampling and Alignment

RxUpRaw = resample(Volt, 10000, 100000); % resampling

D = finddelay(OOK_NRZ, RxUpRaw); % correlation

RxDataUp = RxUpRaw(D+1:D+length(OOK_NRZ)); % Alignment

%% downsampling

RxDataNoise = RxDataUp(5:10:end); %downsample DataRx

TxData = OOK_NRZ(5:10:end); %downsample DataRx

%% data recovery

plot(RxDataUp);

th = 0.7;

RxData = RxDataNoise>th;

BER = sum(RxData(RxData~=TxData))/length(RxData);
clc
clear
```

```
%% Load the data

load('data.mat');

DataAnlg = EEG_Normalised_1000;

%% Initialization

NumBits = 4; % number of quantization levels
numItt = 2 ^ NumBits;

dataMax = max(DataAnlg);
dataMin = min(DataAnlg);

intrvl = 1.01 * dataMin : 1.01 * (dataMax - dataMin)/(numItt-1) : 1.01 * dataMax;

DataDig = [];

%% Digitization
for i = 1 : length(DataAnlg)

   Chk = 0;
   j = 0;

   while(j < numItt && Chk == 0)

      j = j + 1;

      if DataAnlg(i)>= intrvl(j) && DataAnlg(i)< intrvl(j+1)

         DataDig = [DataDig, dec2bin(j-1, NumBits)];

         Chk = 1;

      end

   end

end

DataOut=[];

for i = 1 : length(DataDig)

   DataOut = [DataOut double(DataDig(i))-48];

End

plot(eeg1000)
```

```
%%


%% signal normalized between 0 and 1
maxS = max(eeg1000);
minS = min(eeg1000);
SignalNormalized = (eeg1000 - minS)/(maxS - minS);
S=double(SignalNormalized);
plot(S)

%%
plot(eeg1000errorpeaks)
%% signal normalized between 0 and 1
maxSr = max(eeg1000errorpeaks);
minSr = min(eeg1000errorpeaks);
SignalNormalizedr1 = (eeg1000errorpeaks - minS)/(maxS - minS);
Sr1=double(SignalNormalizedr1);
plot(Sr1)

%% comparison

plot(eeg1000, '*-')
hold on;
plot(eeg1000errorpeaks,'o-')
hold off;
xlabel('Number of samples')
ylabel('Amplitude')
title('Comaprison of EEG signal Transmitted and Received')

%%


plot(S, '*-')
hold on;
plot(Sr1,'o-')
hold off;
xlabel('Number of samples')
ylabel('Amplitude')
title('Comaprison of Normalised EEG signal Transmitted and Received')

clc
clear
close all

%%frame=0;%used as loop counter

%% SECTION 1 - Load video file into matlab
%%LedVid = VideoReader('MVI_1667.MOV') % Place file in current folder and
alter file name accordingly
%%LedVid = VideoReader('F:\EEG\MatlabCode\32pix video a.avi');
```

```
%% convert video to image
%%vid=mmreader('video.avi');

% %% reading the video
vid=VideoReader('F:\EEG\MatlabCode\32pix video e.avi');
%  vid=VideoReader('C:\Users\Geet\Desktop\PhD_Thesis\codes_EEG\16px vide
a\16pix video a.avi')
%
% %% read in all video frames
%  numFrames = vid.NumberOfFrames;
%  n=numFrames;
%  for i = 1:2:n
%  frames = read(vid,i);
%  imwrite(frames,['Image' int2str(i), '.jpg']);
%  im(i)=image(frames);
%  end

% read the selected frame/image 33 out of video a of 32 pixel
I = imread('C:\Users\Geet\Desktop\PhD_Thesis\codes_EEG\8px video
a\image23.jpg');
% C:\Users\Geet\Desktop\PhD_Thesis\codes_EEG\8px video a

%convert it to grayscale
I = rgb2gray(I);

%calculate the binarization threshold
th = graythresh(I);

%binarize the image and display it
I = im2bw(I,th);
imshow(I)

%extract the size of the image
[a b] = size(I);

%threshold
th_row=0.1; % good for image 51
th_col=0.1; % good for image 51

%calculate first border (line0)
for i=1:a     % for image 49 i=1:a, the others are i=1:a/2
  for j=1:b
     %somma(j)=sum(I(i,:));
     if sum(I(i,:))>th_row*b
        line0 = i;
         i=0;
          break

     end
  end
```

```
  if i==0
     break

  end
end

%calculate second border (line1)
for i=a:-1:a/2
  for j=1:b
     if sum(I(i,:))>th_row*b
        line1 = i;
         i=0;
          break

     end
  end
  if i==0
     break

  end
end

%calculate third border (line2)
for i=1:a
  for j=1:b/2
     if sum(I(:,j))>th_col*a
        line2 = j;
         i=0;
          break

     end
  end
  if i==0
     break

  end
end

%calculate fourth border (line3)
for i=1:a
  for j=b:-1:b/2
     if sum(I(:,j))>th_col*a
        line3 = j;
         i=0;
          break

     end
  end
  if i==0
     break
```

```
  end
end

I = imcrop(I,[line2,line0,line3-line2,line1-line0]);
figure
imshow(I)

%extract the size of the resulting image
[c d] = size(I);
%calculate the number of pixels in each cell
numpixpercell = c*d/20;

%round number of pixels in each cell
patch = round(sqrt(numpixpercell));

offset=patch/2;

kk=1;
for i= offset+ patch:patch:c - (patch+offset)
   for j=offset+ patch:patch:d-(patch+offset)
      bits(kk)=I(i,j);
      kk=kk+1;
   end
end


%read the image 41 of video a 32 pixel
I = imread ('F:\EEG\MatlabCode\image53.jpg');

%convert it to grayscale
I = rgb2gray(I);

%calculate the binarization threshold
th = graythresh(I);

%binarize the image and display it
I = im2bw(I,th);
imshow(I)

%extract the size of the image
[a b] = size(I);

%threshold
th_row=0.1; % good for image 41
th_col=0.1; % good for image 41
```

```
%calculate first border (line0)
for i=1:a     % for image 49 i=1:a, the others are i=1:a/2
  for j=1:b
     %somma(j)=sum(I(i,:));
     if sum(I(i,:))>th_row*b
        line0 = i;
         i=0;
          break

     end
  end
  if i==0
     break

  end
end

%calculate second border (line1)
for i=a:-1:a/2
  for j=1:b
     if sum(I(i,:))>th_row*b
        line1 = i;
         i=0;
          break

     end
  end
  if i==0
     break

  end
end

%calculate third border (line2)
for i=1:a
  for j=1:b/2
     if sum(I(:,j))>th_col*a
        line2 = j;
         i=0;
          break

     end
  end
  if i==0
     break

  end
end

%calculate fourth border (line3)
```

```
for i=1:a
  for j=b:-1:b/2
     if sum(I(:,j))>th_col*a
        line3 = j;
         i=0;
          break

     end
  end
  if i==0
     break

  end
end

I = imcrop(I,[line2,line0,line3-line2,line1-line0]);
figure
imshow(I)

%extract the size of the resulting image
[c d] = size(I);
%calculate the number of pixels in each cell
numpixpercell = c*d/20;

%round number of pixels in each cell
patch = round(sqrt(numpixpercell));

offset=patch/2;

for i= offset+ patch:patch:c - (patch+offset)
    for j=offset+ patch:patch:d-(patch+offset)
       bits(kk)=I(i,j);
       kk=kk+1;
    end
 end


%read the image 63 of video a 32 pixel
I = imread ('F:\EEG\MatlabCode\image63.jpg');

%convert it to grayscale
I = rgb2gray(I);

%calculate the binarization threshold
th = graythresh(I);

%binarize the image and display it
I = im2bw(I,th);
imshow(I)
```

```
%extract the size of the image
[a b] = size(I);

%threshold
th_row=0.1; % good for image 63
th_col=0.1; % good for image 63




%calculate first border (line0)
for i=1:a     % for image 49 i=1:a, the others are i=1:a/2
  for j=1:b
     %somma(j)=sum(I(i,:));
     if sum(I(i,:))>th_row*b
        line0 = i;
         i=0;
          break

     end
  end
  if i==0
     break

  end
end

%calculate second border (line1)
for i=a:-1:a/2
  for j=1:b
     if sum(I(i,:))>th_row*b
        line1 = i;
         i=0;
          break

     end
  end
  if i==0
     break

  end
end

%calculate third border (line2)
for i=1:a
  for j=1:b/2
     if sum(I(:,j))>th_col*a
        line2 = j;
         i=0;
          break
```

```
      end
   end
   if i==0
      break

   end
end

%calculate fourth border (line3)
for i=1:a
   for j=b:-1:b/2
      if sum(I(:,j))>th_col*a
         line3 = j;
          i=0;
           break

      end
   end
   if i==0
      break

   end
end

I = imcrop(I,[line2,line0,line3-line2,line1-line0]);
figure
imshow(I)

%extract the size of the resulting image
[c d] = size(I);
%calculate the number of pixels in each cell
numpixpercell = c*d/20;

%round number of pixels in each cell
patch = round(sqrt(numpixpercell));

offset=patch/2;

for i= offset+ patch:patch:c - (patch+offset)
    for j=offset+ patch:patch:d-(patch+offset)
       bits(kk)=I(i,j);
       kk=kk+1;
    end
 end

%read the image 73 of video a 32 pixel
I = imread ('F:\EEG\MatlabCode\image73.jpg');

%convert it to grayscale
```

```
I = rgb2gray(I);

%calculate the binarization threshold
th = graythresh(I);

%binarize the image and display it
I = im2bw(I,th);
imshow(I)
%extract the size of the image
[a b] = size(I);
%threshold
th_row=0.1; % good for image 73
th_col=0.1; % good for image 73
%calculate first border (line0)
for i=1:a     % for image 49 i=1:a, the others are i=1:a/2
  for j=1:b
     %somma(j)=sum(I(i,:));
     if sum(I(i,:))>th_row*b
        line0 = i;
         i=0;
          break

     end
  end
  if i==0
     break

  end
end

%calculate second border (line1)
for i=a:-1:a/2
  for j=1:b
     if sum(I(i,:))>th_row*b
        line1 = i;
         i=0;
          break

     end
  end
  if i==0
     break

  end
end

%calculate third border (line2)
for i=1:a
  for j=1:b/2
     if sum(I(:,j))>th_col*a
```

```
          line2 = j;
           i=0;
            break

      end
   end
   if i==0
      break

   end
end

%calculate fourth border (line3)
for i=1:a
   for j=b:-1:b/2
      if sum(I(:,j))>th_col*a
         line3 = j;
          i=0;
           break

      end
   end
   if i==0
      break

   end
end

I = imcrop(I,[line2,line0,line3-line2,line1-line0]);
figure
imshow(I)

%extract the size of the resulting image
[c d] = size(I);
%calculate the number of pixels in each cell
numpixpercell = c*d/20;

%round number of pixels in each cell
patch = round(sqrt(numpixpercell));

offset=patch/2;

for i= offset+ patch:patch:c - (patch+offset)
    for j=offset+ patch:patch:d-(patch+offset)
       bits(kk)=I(i,j);
       kk=kk+1;
    end
 end
```

# Appendix

# Appendix A

SEPS525

---

**160 RGB x 128 Dots, 262K Colors PM-OLED Display Driver and Controller**

---

**1. Product Preview**

▪ 262k colors OLED single chip display driver IC

▪ Data Interface

- Parallel interface : 68/80series MPU(8/9/16/18-bit)

- Serial interface : SPI 4-wire interface

- RGB interface : 18/16/6-bit interface

▪ Driver Output

- 160× RGB columns(480), 128 rows

▪ Display RAM Capacity

- 160 × 18(RGB) × 128 = 368,640 bits

▪ Various Instructions Set

- Power save mode

- Reduced current driving available

- Window mode

- Partial display : programmable panel display size

- Vertical scroll & Horizontal panning

▪ OLED Column Drive

- Driving current control : 8-bit, 0uA ~ 255uA by 1uA step control

- Pre_charge current control : 8-bit, 0uA ~ 2040uA by 8uA step control

- Pre_charge time control : programmable pre_charge time(0clock ~ 15clocks) based on internal oscillator clock

▪ OLED Row Drive

- Current sink : Max 120mA

▪ Internal Oscillator Circuit

- Internal / External clock selectable

- Frame rate : 90 frames/sec( 75.0 ~ 150.0 frames/sec adjustable)

▪ Supply Voltage

- VDD : 2.4 ~ 3.3V

- VDDH : 8.0 ~ 18.0V

- VDDIO : 1.6 ~ 3.3V

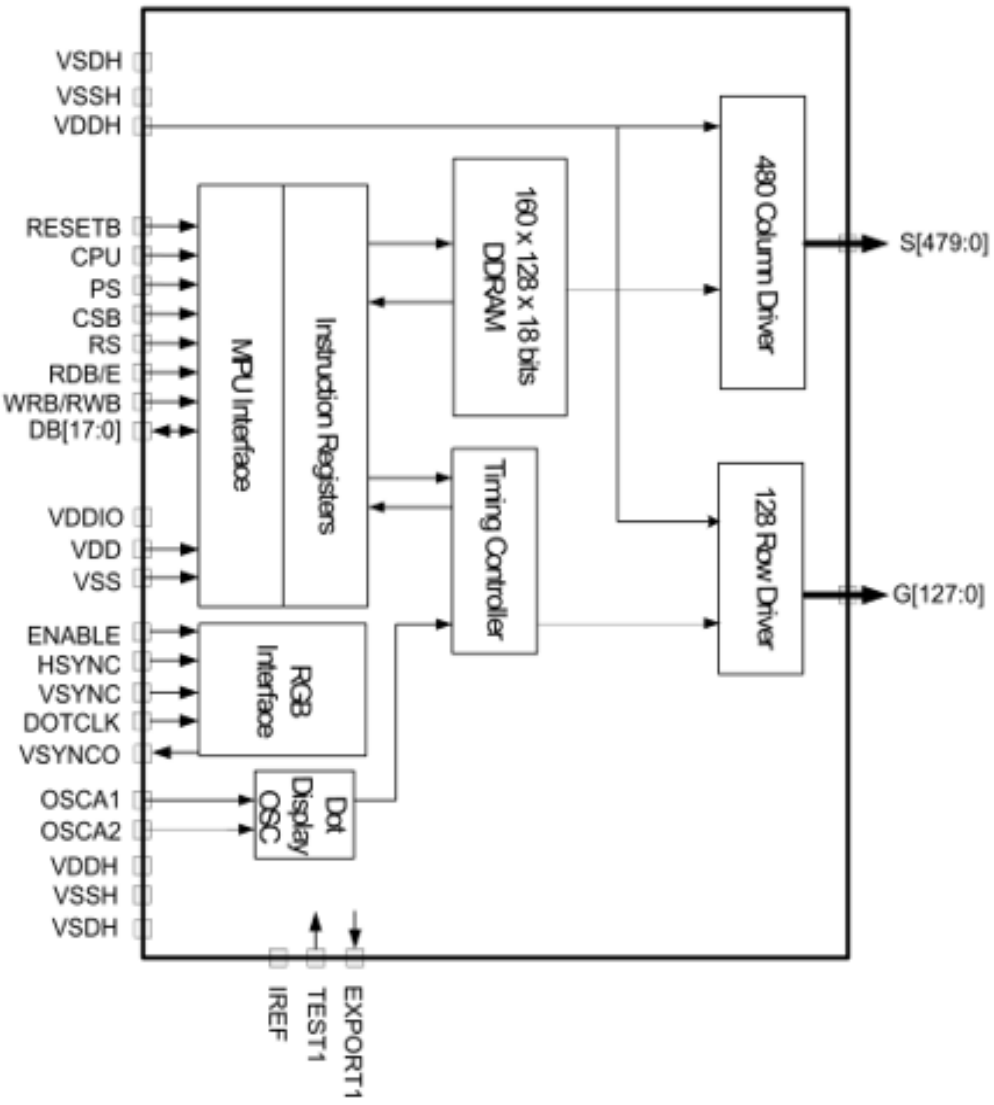


## Pin Description

| Pin Name | Number Of Pins | I/O | Connected To | Description |
|---|---|---|---|---|
| CPU | 1 | I | VSS or VDD | Selects the CPU type<br>Low : 80-Series CPU, High : 68-Series CPU |
| PS | 1 | I | VSS or VDD | lects parallel/Serial interface type Low :<br>serial, High : parallel |
| CSB | 1 | I | MPU | Selects the SEPS525.<br>Low : SEPS525 is selected and can be accessed<br>High : SEPS525 is not selected and cannot be accessed |

<table>
<tr><td>RS</td><td>1</td><td>I</td><td>MPU</td><td>Selects the data / command<br>Low : command, High : parameter / data</td></tr>
<tr><td>RDB/E</td><td>1</td><td>I</td><td>MPU</td><td>For an 80-system bus interface, read strobe signal(active low)<br>r an 68-system bus interface, bus enable strobe(active high) When using SPI, fix it to VDD or VSS level</td></tr>
<tr><td>WRB/RWB</td><td>1</td><td>I</td><td>MPU</td><td>For an 80-system bus interface, write strobe signal(active low)<br>For an 68-system bus interface, read/write select<br>Low : Write, High : Read<br>When using SPI, fix it to VDD or VSS level</td></tr>
<tr><td>DB[17:0]</td><td>18</td><td>I/O</td><td>MPU</td><td>Serves as a 18_bit bi-directional data bus
<table>
<tr><th>PS</th><th>Description</th></tr>
<tr><td>1</td><td>8_bit bus : DB[17:10]<br>9_bit bus : DB[17:9]<br>16_bit bus : DB[17:10], DB[8:1] 18_bit bus : DB[17:0]</td></tr>
<tr><td>0</td><td>DB[17] SCL : Synchronous clock input<br>DB[16] SDI : Serial data input<br>DB[15] SDO : Serial data output</td></tr>
</table>
Fix unused pins to the VSS level</td></tr>
<tr><td>OSCA1</td><td>1</td><td>I</td><td rowspan="2">Oscillation-Resistor</td><td rowspan="2">Fine adjustment for oscillation<br>Tie TBD kΩ ohms to OSCA1 between OSCA2<br>hen the external clock mode is selected, OSCA1 is used external clock input</td></tr>
<tr><td>OSCA2</td><td>1</td><td>O</td></tr>
<tr><td>RESETB</td><td>1</td><td>I</td><td>MPU</td><td>Reset SEPS525(active low)</td></tr>
<tr><td>S[479:0]</td><td>480</td><td>O</td><td>PANEL</td><td>SEPS525 Display column outputs</td></tr>
<tr><td>G[127:0]</td><td>128</td><td>O</td><td>PANEL</td><td>SEPS525 Display row outputs</td></tr>
<tr><td>VDDH</td><td>2</td><td>-</td><td>POWER</td><td>Data, Scan Driver Power Supply(8V ~ 18V)</td></tr>
<tr><td>VSSH</td><td>2</td><td>-</td><td>POWER</td><td>Scan Driver Ground</td></tr>
<tr><td>VSDH</td><td>2</td><td>-</td><td>POWER</td><td>Data Driver Ground</td></tr>
<tr><td>VDDIO</td><td>1</td><td>-</td><td>POVER</td><td>MPU I/F PAD Power Supply(1.6 ~ 3.3V)</td></tr>
<tr><td>VDD</td><td>1</td><td>-</td><td>POWER</td><td>Logic power supply(2.4V ~ 3.3V)</td></tr>
<tr><td>VSS</td><td>1</td><td>-</td><td>POWER</td><td>Logic ground.</td></tr>
</table>

## Reset Status

The **SEPS525** is initialized as following description when RESETB terminal is set to “L”. Usually RESETB terminal is connected reset terminal of MPU, so that the chip can be initialized simultaneously with MPU. The **SEPS525** should be initialized when the power is on.

**INITIAL SETTING CONDITION (default setting)**

1. Frame frequency : 90Hz
2. OSC : internal OSC
3. Internal OSC : ON
4. DDRAM write horizontal address : MX1 = 00h, MX2 = 9Fh
5. DDRAM write vertical address : MY1 = 00h, MY2 = 7Fh
6. Display data RAM write : HC = 1, VC = 1, HV = 0
7. RGB data swap : OFF
8. Row scan shift direction : G0, G1, … , G126, G127
9. Column data shift direction : S0, S1, … , S478, S479
10. Display ON/OFF : OFF
11. Panel display size : FX1 = 00h, FX2 = 9Fh, FY1 = 00h, FY2 = 7Fh
12. Display data RAM read column/row address : FAC = 00h, FAR = 00h
13. Precharge time(R/G/B) : 0 clock
14. Precharge current(R/G/B) : 0 uA
15. Driving current(R/G/B) : 0 uA

POWER ON SEQUENCE

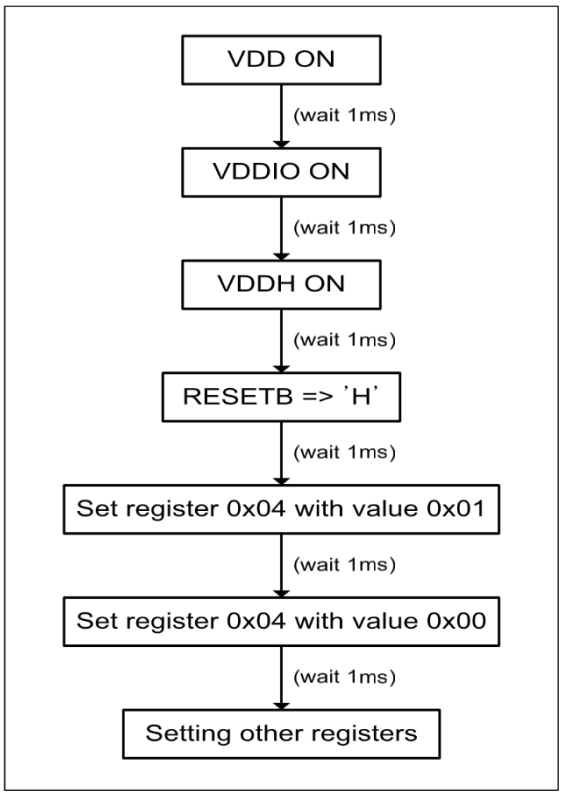


## RGB Interface

When the RGB_IF register bit0 is set to "0", SEPS525 enters into the RGB interface mode and DDRAM write cycle is synchronized by DOTCLK.

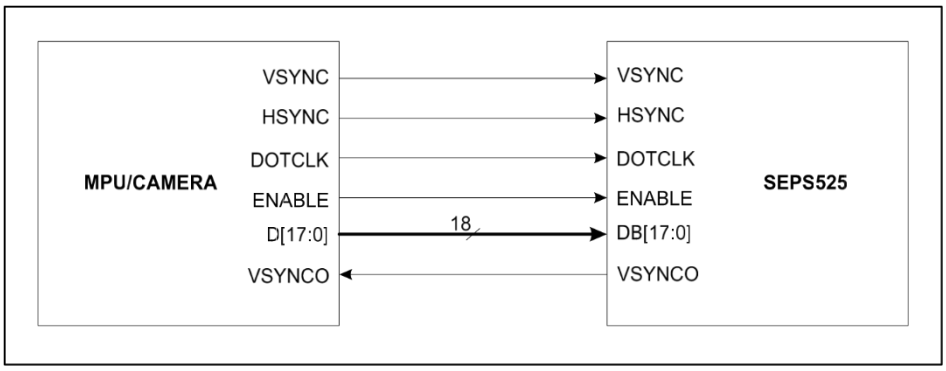


### 18-bit RGB interface

The 18-bit RGB interface is selected by setting RIM[1:0] bits to "00". DDRAM write operation is Synchronized with DOTCLK and ENABLE. Display data are transmitted

to DDRAM in synchronization with 18-bit RGB data bus(DB[17:0]) and the data enable(ENABLE).

**DDRAM Write**

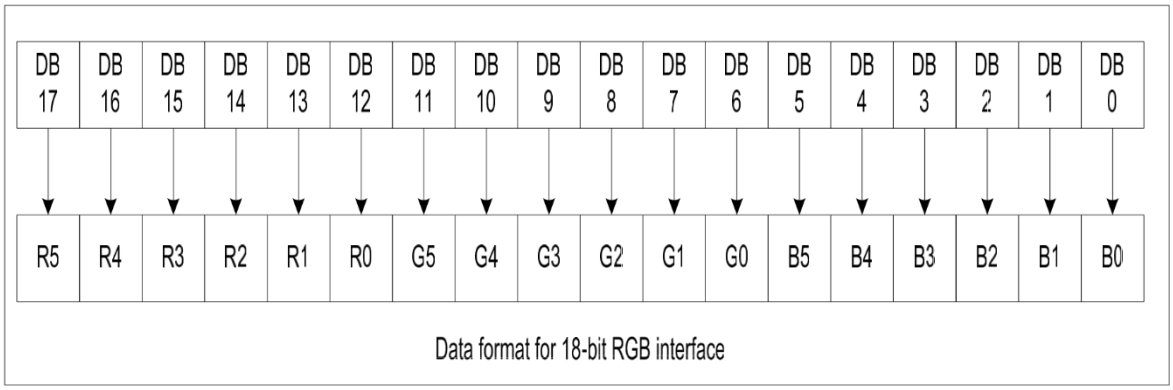

Data format for 18-bit RGB interface

**16-bit RGB interface**

The 16-bit RGB interface is selected by setting RIM[1:0] bits to “01”. DDRAM write operation is Synchronized with DOTCLK and ENABLE. Display data are transmitted to DDRAM in synchronization with 16-bit RGB data bus(DB[17:10], DB[8:1]) and the data enable(ENABLE).

**MPU Interface**

The SEPS525 has three high-speed system interface : a 68-system, an 80-system 8/9/16/18 bit bus, and a clock synchronous serial(SPI : Serial Peripheral Interface). Among the interface modes, a specific mode is selected by the setting of PS pin and MEMORY_WRITE_MODE register(16h). The SEPS525 has 3-type registers : an index register(IR) 8-bits, a write data register(WDR), and a read data register(RDR). The IR stores index information for the control registers and the DDRAM. The WDR temporarily stores data to be written into control registers and the DDRAM, and the RDR temporarily stores data read from the DDRAM.

Data written into the DDRAM from the MPU is first written into the WDR and then it is automatically written into the DDRAM by internal operation. Data is read through the RDR when reading from the DDRAM, and the first read data is invalid and the second and the following data are valid.

**Electric Characteristics**

1) Absolute Maximum Rating

| ITEM | SYMBOL | CONDITION | PORT | RATINGS | UNIT |
|---|---|---|---|---|---|
| Supply voltage | VDD | VSS/VSSH/ VDSH(0V) Reference Ta = +25℃ | VDD | - 0.3 ~ +4.0 | V |
| | VDDH | | VDDH | - 0.3 ~ +19.5 | V |
| | VDDIO | | VDDIO | - 0.3 ~ +4.0 | V |
| Input voltage | VI | | *1 | - 0.3 ~ +VDD+0.3 | V |
| Storage temperature | Tstg | | | - 65 ~ +150 | ℃ |

*1 : DB[17:0], CPU, PS, CSB, RS, RDB, WRB,

RESETB.

2) Recommended Operation Conditions

| ITEM | SYMBOL | PORT | MIN | TYP | MAX | UNIT | REMARK |
|---|---|---|---|---|---|---|---|
| Supply voltage | VDD | VDD | 2.4 | 2.8 | 3.3 | V | |
| | VDDH | VDDH | 8.0 | 16 | 18.0 | V | |
| | VDDIO | VDDIO | 1.6 | - | 3.3 | V | |
| Operating voltage | VDC | S[479:0] | 0 | 16 | 18.0 | V | |
| Operation temperature | Topr | | - 40 | | 85 | ℃ | |

## Appendix B

### LM317 Voltage regulator

The LM317 is an adjustable 3−terminal positive voltage regulator capable of supplying in excess of 1.5 A over an output voltage range of 1.2 V to 37 V. This voltage regulator is exceptionally easy to use and requires only two external resistors to set the output voltage. Further, it employs internal current limiting, thermal shutdown and safe area compensation, making it essentially blow−out proof. The LM317 serves a wide variety of applications including local, on card regulation. This device can also be used to make a programmable output regulator, or by connecting a fixed resistor between the adjustment and output, the LM317 can be used as a precision current regulator.

Features

• Output Current in Excess of 1.5 A

• Output Adjustable between 1.2 V and 37 V

• Internal Thermal Overload Protection

• Internal Short Circuit Current Limiting Constant with Temperature

• Output Transistor Safe−Area Compensation

• Floating Operation for High Voltage Applications

• Eliminates Stocking many Fixed Voltages

• Available in Surface Mount D2PAK−3, and Standard 3−Lead Transistor Package

• NCV Prefix for Automotive and Other Applications Requiring Unique Site and Control Change Requirements; AEC−Q100 Qualified and PPAP Capable • These Devices are Pb−Free, Halogen Free/BFR Free and are RoHS Compliant

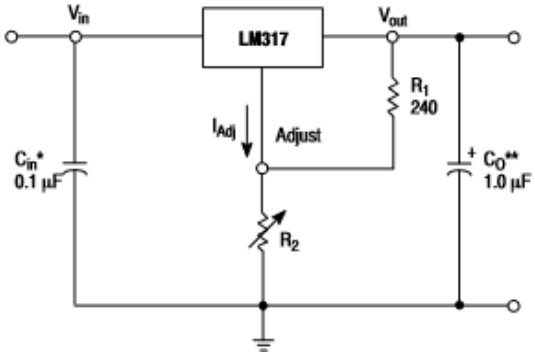


- Cin is required if regulator is located an appreciable distance from power supply filter.
- CO is not needed for stability; however, it does improve transient response.
- Since IAdj is controlled to less than 100 microA, the error associated with this term is negligible in most applications.

Pin Configuration

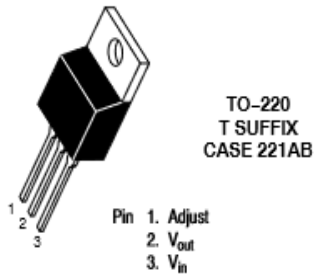

## Appendix C

## FRDM KL-25Z

The Freescale Freedom development platform is a set of software and hardware tools for evaluation and development. It is ideal for rapid prototyping of microcontroller-based applications. The Freescale Freedom KL25Z hardware, FRDM-KL25Z, is a capable and cost-effective design featuring a Kinetis L series microcontroller, the industry's first microcontroller built on the ARM® Cortex™-M0+ core.

FRDM-KL25Z can be used to evaluate the KL14, KL15, KL24 & KL25 Kinetis L series devices. It features a KL25Z128VLK, a device boasting a max operating frequency of 48MHz, 128KB of flash, a full-speed USB controller, and loads of analog and digital peripherals. The FRDM-KL25Z hardware is form-factor compatible with the Arduino™ R3 pin layout, providing a broad range of expansion board options. The on-board interfaces include an RGB LED, a 3-axis digital accelerometer, and a capacitive touch slider. The FRDM-KL25Z is the first hardware platform to feature the Freescale open standard embedded serial and debug adapter known as OpenSDA. This circuit offers several options for serial communications, flash programming and run-control debugging. The features of the FRDM-KL25Z include:

• MKL25Z128VLK4 in an 80 LQFP package

• Capacitive touch slider

• MMA8451Q accelerometer

• Tri-color (RGB) LED

• Flexible power supply options – USB, coin cell battery, external source

• Battery-ready, power-measurement access points • Easy access to MCU I/O via Arduino ™ R3 compatible I/O connectors

• Programmable OpenSDA debug interface with multiple applications available including: Mass storage device flash programming interface P&E Debug interface provides run-control debugging and compatibility with IDE tools CMSIS-DAP interface: new ARM standard for embedded debug interface Data logging application

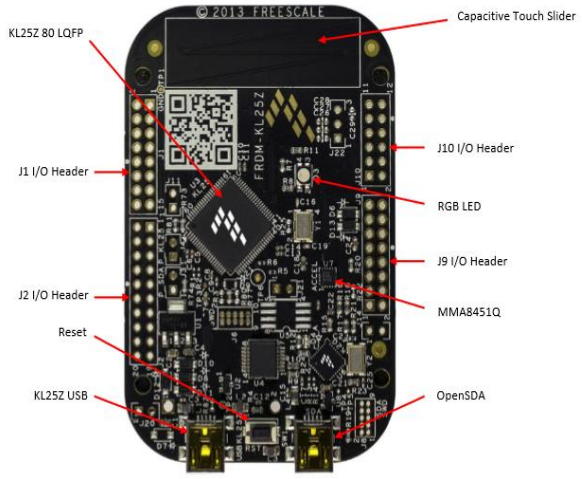


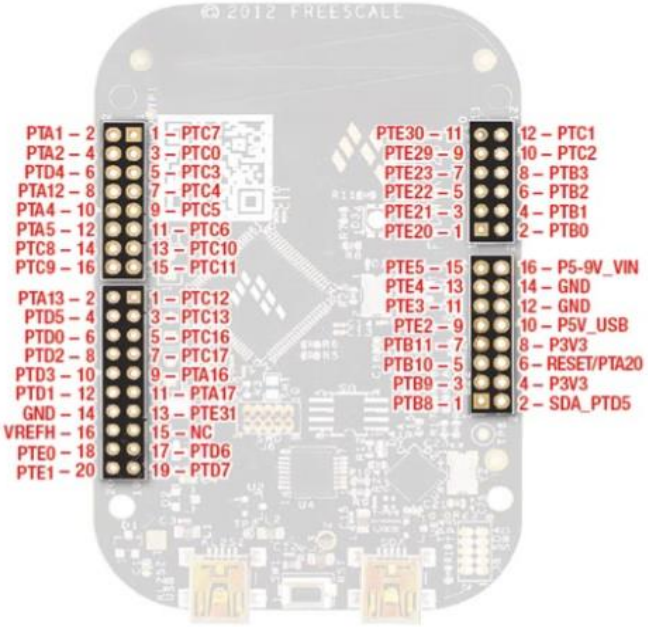


**KL25Z Microcontroller**

The target microcontroller of the FRDM-KL25Z is the KL25Z128VLK4, a Kinetis L series device in an 80 LQFP package. The KL25Z MCU features include:

• 32-bit ARM Cortex-M0+ core up to 48 MHz operation Single-cycle fast I/O access port • Memories 128 KB flash 16 KB SRAM

• System integration Power management and mode controllers Low-leakage wakeup unit Bit manipulation engine for read-modify-write peripheral operations Direct memory access (DMA) controller Computer operating properly (COP) Watchdog timer

• Clocks Clock generation module with FLL and PLL for system and CPU clock generation 4 MHz and 32 kHz internal reference clock System oscillator supporting external crystal or resonator Low-power 1kHz RC oscillator for RTC and COP watchdog

• Analog peripherals 16-bit SAR ADC w/ DMA support 12-bit DAC w/ DMA support High speed comparator

• Communication peripherals Two 8-bit Serial Peripheral Interfaces (SPI) USB dual-role controller with built-in FS/LS transceiver USB voltage regulator Two I2C modules One low-power UART and two standard UART modules

• Timers One 6-channel Timer/PWM module Two 2-channel Timer/PWM modules 2-channel Periodic Interrupt Timer (PIT) Real time clock (RTC) Low-power Timer (LPTMR) System tick timer

• Human-Machine Interfaces (HMI) General purpose input/output controller Capacitive touch sense input interface hardware module.

## References

[1] 802.15.7. IEEE Standard for Local and Metropolitan Area Networks. Part 15.7: Short-range Wireless Optical Communication Using Visible Light, *IEEE Standard* 802.15.7., Sept. 2011.

[2] B. Xu, X. Zhu, T. Song, Y. Ou, "Protocol design and capacity analysis in hybrid network of visible light communication and OFDMA systems,"

[3] A. Mostafa and L. Lampe, "Physical-layer security for indoor visible light communications," in *Proc. of Communications (ICC), IEEE*, June 2014, pp. 3342–3347.

[4] VLCC, "Visible Light Communications Consortium." [Online]. Available: http://www.vlcc.net.

[5] BBC News," Intelligent Machines: The jobs robots will steal first, http://www.bbc.com/news/technology-33327659, 14 September 2015.

[6] G. Zhou, Y. Chen," The research of carbon dioxide gas monitoring platform based on the wireless sensor networks," in Artificial Intelligence, Management Science and Electronic Commerce (AIMSEC), 2011 2nd International Conference
on, pp.7402-7405, 8-10 Aug. 2011.

[7] R. C. Chen, H. -Y. Guo, M. -P. Lin, H. S. Lin," The carbon dioxide concentration detection using mobile phones combine bluetooth and QR code," in Awareness Science and Technology (iCAST), 2014 IEEE 6th International Conference on pp.1-6, 29-31 Oct. 2014.

[8] R. Li, X. Sha, K. Lin," Smart greenhouse: A real-time mobile intelligent monitoring system based on WSN," in Wireless Communications and Mobile Computing Conference (IWCMC), 2014 International, pp.1152-1156, 4-8 Aug. 2014.

[9] A. Ahlbom, A. Green, L. Kheifets, D. Savitz, A. Swerdlow," Epidemiology of Health Effects of Radiofrequency Exposure", in International Commission for Non-Ionizing Radiation Protection Standing Committee on Epidemiology,2004

December; 112(17): 17411754. Published online 2004 September 23. doi: 10.1289/ehp.7306.

[10] C. Ott, O. Eiberger, W. Friedl, B. Bauml, U. Hillenbrand, C. Borst, A. Albu-Schaffer, B. Brunner, H. Hischmuller,S. Kielhofer, R. Konietschke, M. Suppa, T. Wimbock, F. Zacharias, and G. Hirzinger, "A humanoid two-arm system for dexterous manipulation," in Proceedings of the 2006 IEEE-RAS International Conference on Humanoid Robotics, 2006, pp. 276–283.

[11] K. S. Tan, I. Hinberg and J. Wadhwani, Electromagnetic interference in medical devices: Health Canadas past current perspectives and activities, IEEE International Symposium on Electromagnetic Compatibility, 2001, 12831284.

[12] Y. K.Cheong, X. W . Ng, W. Y. Chung," Hazardless Biomedical Sensing Data Transmission Using VLC," in Sensors Journal, IEEE, vol.13, no.9, pp.3347-3348, Sept. 2013 doi: 10.1109/JSEN.2013.2274329.

[13] Y. Y. Tan, W. Y. Chung,"Mobile health monitoring system through visible light communication", Bio-Medical Materials and Engineering, Vol. 24, No. 6, pp. 35293538, September 2014.

[14] M. K. Hasan, M. Shahjalal, M. Z. Chowdhury and Y. M. Jang, "Access Point Selection in Hybrid OCC/RF eHealth Architecture for Real-Time Remote Patient Monitoring," 2018 International Conference on Information and Communication Technology Convergence (ICTC), Jeju, 2018, pp. 716-719. doi: 10.1109/ICTC.2018.8539582.

[15] Roberts, R.D., "Space-time forward error correction for dimmable undersampled frequency shift ON-OFF keying camera communications (CamCom)," in Ubiquitous and Future Networks (ICUFN), 2013 Fifth International Conference on, vol., no., pp.459-464, 2-5 July 2013.

[16] T. L. Vu, T. Nguyen, C. S. Kim, E. B. Sin, J. Jeong and Y. M. Jang, "Survey of indoor optical camera communication (OCC) systems for the Internet of lights," 2017 International Conference on Information and Communication Technology Convergence (ICTC), Jeju, 2017, pp. 700-703.doi: 10.1109/ICTC.2017.8190758.

[17] Nezhad, M.H, Subari, K.S., Yahyavi, M, "Improvement of wireless transmission system performance for EEG signals based on the development of scalar quantization", Journal of Electrical Bioimpedance, vol. 4, pp. 62-72, Dec 2013.

[18] S. Chatterjee and A. Miller, 2010, "Biomedical Instrumentation Systems", Delmar CENGAGE learning.

[19] R.D.Bickford, Electroencephalography. In: Adelman G. ed. Encyclopedia of Neuroscience, Birkhauser, Cambridge (USA), 371-373.

[20] What to Know about EEG Tests [Online]. Available: https://www.medicalnewstoday.com/articles/325191.php

[21] V. Mihajlovic, B.Grundlehner, R. Vullers, and J. Penders, "1.4-Mb/s white organic LED transmission system using discrete multitone modulation," Wearable, Wireless EEEGsolutions in Daily Life Applications: What we are missing?" in IEEE Journal of Biomedical and Health Informatics, vol., no. 1., January 2015.

[22] D. R. Dhatchayeny, A. Sewaiwar, S. V. Tiwari, and Y. H. Chung, "Experimental Biomedical EEG Signal Transmission Using VLC," IEEE Sensors Journal, vol. 15, pp. 5386-5387, 2015.

[23] Z. Ghassemlooy, L. N. Alves, S. Zvanovec, and M. A. Khalighi, Visible light communications: Theory and applications. Boca Raton: CRC Press, 2017.

[24] D. Karunatilaka, F. Zafar, V. Kalavally, and R. Parthiban, "LED based indoor visible light communications: State of the art," IEEE Communications Surveys & Tutorials, vol. 17, no. 3, pp. 1649-1678, 2015.

[25] J. An and W. Chung, "A novel indoor healthcare with time hopping-based visible light communication," 2016 IEEE 3rd World Forum on Internet of Things (WF-IoT), Reston, VA, 2016, pp. 19-23.

[26] W. A. Cahyadi, T. Jeong, Y. Kim, Y. Chung and T. Adiono, "Patient monitoring using Visible Light uplink data transmission," 2015 International Symposium on Intelligent Signal Processing and Communication Systems (ISPACS), Nusa Dua, 2015, pp. 431-434.

[27] J. An and W. Chung, "Wavelength-Division Multiplexing Optical Transmission for EMI-Free Indoor Fine Particulate Matter Monitoring," in IEEE Access, vol. 6, pp. 74885-74894, 2018.

[28] D. R. Dhatchayeny, A. Sewaiwar, S. V. Tiwari and Y. H. Chung, "Experimental Biomedical EEG Signal Transmission Using VLC," in IEEE Sensors Journal, vol. 15, no. 10, pp. 5386-5387, Oct. 2015.

[29] G. Aggarwal, X. Dai, R. Binns and R. Saatchi, "Experimental Demonstration of EEG Signal Transmission Using VLC Deploying LabView," 2018 3rd International Conference and Workshops on Recent Advances and Innovations in Engineering (ICRAIE), Jaipur, India, 2018, pp. 1-6.

[30] J. An and W. Chung, "A novel indoor healthcare with time hopping-based visible light communication," 2016 IEEE 3rd World Forum on Internet of Things (WF-IoT), Reston, VA, 2016, pp. 19-23.

[31] W. A. Cahyadi, T. Jeong, Y. Kim, Y. Chung and T. Adiono, "Patient monitoring using Visible Light uplink data transmission," 2015 International Symposium on Intelligent Signal Processing and Communication Systems (ISPACS), Nusa Dua, 2015, pp. 431-434.

[32] Xiao-weing & Chung, Wan-Young. (2012). VLC-based medical healthcare information system. Biomedical Engineering: Applications, Basis and Communications. 24. 10.4015/S1016237212500123.

[33] F. Dellaert, D. Fox, W. Burgard, and S. Thrun, "Monte Carlo localization for mobile robots," in Proc. of the IEEE Int. Conf. on Robotics & Automation (ICRA), 1998.

[34] R. Ueda, T. Arai, K. Asanuma, K. Umeda and H. Osumi, "Recovery Methods for Fatal Estimation Errors on Monte Carlo Localization, Journal of the Robotics Society of Japan, 23, 4, pp.466-473, 2005.

[35] R. Murai et al., "A novel visible light communication system for enhanced control of autonomous delivery robots in a hospital," 2012 IEEE/SICE International Symposium on System Integration (SII), Fukuoka, 2012, pp. 510-516.

[36] Impact of Visible Light Communication in healthcare. Available at: https://aabme.asme.org/posts/impact-of-visible-light-communication-technology-in-health-care

[37] Tong Zhou, Xingguang Lee, Lei Chen, Temperature Monitoring System Based on Hadoop and VLC, Procedia Computer Science, Volume 131, 2018, Pages 1346-1354, ISSN 1877-0509.

[38] Haigh, Paul & Bausi, Francesco & Le Minh, Hoa & Papakonstantinou, Ioannis & Popoola, Wasiu & Burton, Andrew & Cacialli, Franco. (2015). Wavelength-Multiplexed Polymer LEDs: Towards 55 Mb/s Organic Visible Light Communications. IEEE Journal on Selected Areas in Communications. 33. 1-1. 10.1109/JSAC.2015.2432491.

[39] P. A. Haigh, Z. Ghassemlooy, and I. Papakonstantinou, "1.4-Mb/s white organic LED transmission system using discrete multitone modulation," IEEE Photonics Technology Letters, vol. 25, no. 6, pp. 615–618, 2013.

[40] H. Aoyama and M. Oshima, "Visible light communication using a conventional image sensor," in Proc. IEEE 12th Annu. Consum. Commun. Netw. Conf. (CCNC), Nov. 2015, pp. 103–108.

[41] Roberts, R.D., "Space-time forward error correction for dimmable undersampled frequency shift ON-OFF keying camera communications (CamCom)," in Ubiquitous and Future Networks (ICUFN), 2013 Fifth International Conference on, vol., no., pp.459-464, 2-5 July 2013.

[42] A. Al-Fuqaha, M. Guizani, M. Mohammadi, M. Aledhari, and M. Ayyash, ''Internet of Things: A survey on enabling technologies, protocols, and applications,'' IEEE Commun. Surveys Tuts., vol. 17, no. 4, pp. 2347–2376, 4th Quart., 2015.

[43] Z. Ghassemlooy, W. Popoola, and S. Rajbhandari, Optical wireless communications: system and channel modelling with Matlab®. CRC Press, 2012.

[44] A. G. Bell, "On the production and reproduction of sound by light," American journal of science, no. 118, pp. 305-324, 1880.

[45] H. Haas, "High-speed wireless networking using visible light," SPIE Newsroom, vol. 1, pp. 1-3, 2013.

[46] T. M. Okon and J. R. Biard, "The first practical LED," Edison Tech Center, pp. 1-14, 2015.

[47] N. Holonyak Jr and S. Bevacqua, "Coherent (visible) light emission from Ga (As1− xPx) junctions," Applied Physics Letters, vol. 1, no. 4, pp. 82-83, 1962.

[48] S. P. Denbaars, "Gallium-Nitride-based materials for blue to ultraviolet optoelectronics devices," Proceedings of the IEEE, vol. 85, no. 11, pp. 1740-1749, 1997.

[49] S. Nakamura, T. Mukai, and M. Senoh, "Candela-class high-brightness InGaN/AlGaN double-heterostructure blue-light-emitting diodes," Applied Physics Letters, vol. 64, no. 13, pp. 1687-1689, 1994.

[50] P. Pirinen, ‘‘A brief overview of 5G research activities,’’ in Proc. Int. Conf. 5G Ubiquitous Connectivity (5GU), Nov. 2014, pp. 17–22.

[51] M. Shafi et al., ‘‘5G: A tutorial overview of standards, trials, challenges, deployment, and practice,’’ IEEE J. Sel. Areas Commun., vol. 35, no. 6, pp. 1201–1221, Jun. 2017.

[52] L. Hanzo, H. Haas, S. Imre, D. O’Brien, M. Rupp, and L. Gyongyosi, ‘‘Wireless myths, realities, and futures: From 3G/4G to optical and quantum wireless,’’ Proc. IEEE, vol. 100, pp. 1853–1888, May 2012.

[53] P. A. Haigh, "Using equalizers to increase data rates in organic photonic devices for visible light communications systems," Northumbria University, July 2014.

[54] A. C. Boucouvalas, P. Chatzimisios, Z. Ghassemlooy, M. Uysal, and K. Yiannopoulos, ‘‘Standards for indoor optical wireless communications,’’ IEEE Commun. Mag., vol. 53, no. 3, pp. 24–31, Mar. 2015.

[55] M. Uysal and H. Nouri, ‘‘Optical wireless communications—An emerging technology,’’ in Proc. Int. Conf. Transp. Opt. Netw., Jul. 2014, pp. 1–7.

[56] Z. Ghassemlooy, S. Arnon, M. Uysal, Z. Xu, and J. Cheng, ‘‘Emerging optical wireless communications-advances and challenges,’’ IEEE J. Sel. Areas Commun., vol. 33, no. 9, pp. 1738–1749, Sep. 2015.

[57] M. A. Khalighi and M. Uysal, ‘‘Survey on free-space optical communication: A communication theory perspective,’’ IEEE Commun. Surveys Tuts., vol. 16, no. 4, pp. 2231–2258, 4th Quart., 2014. [38] W.-S. Tsai et al., ‘‘A 20-m/40-Gb/s 1550-nm DFB LD-based FSO link,’’ IEEE Photon. J., vol. 7, no. 6, Dec. 2015, Art. no. 7905907.

[58] D. K. Borah, A. C. Boucouvalas, C. C. Davis, S. Hranilovic, and K. Yiannopoulos, ‘‘A review of communication-oriented optical wireless systems,’’ EURASIP J. Wireless Commun. Netw., vol. 2012, p. 91, Dec. 2012.

[59] G. Povey, “Top 10 Visible Light Communications Applications”, 2011, Available online: http://visiblelightcomm.com/top-10-visible-light-communications-application. Accessed: 10/11/2019.

[60] Y. He, L. Ding, Y. Gong, & Y. Wang, “Real-time audio & video transmission based on visible light communication,” Optics and Photonics Journal, Vol. 3, pp. 153-157, 2013.

[61] Doniec M, Detweiler C, Vasilescu I, Chitre M, Hoffmann-Kuhnt M, Rus DA. AquaOptical: lightweight device for high-rate long-range underwater point-to-point communication. Mar Technol Soc J. 2010;44(4):55-65. 62

[62] Wang C, Yu H-Y, Zhu Y-J. A long distance underwater visible light communication system with single photon avalanche diode. IEEE Photonics J. 2016;8(5):1-11.

[63] Cossu G, Corsini R, Khalid AM, Balestrino S, Coppelli A, Caiti A, Ciaramella E. Experimental demonstration of high speed underwater visible light communications. Paper presented at: 2013 2nd International Workshop on Optical Wireless Communications (IWOW); 2013; Newcastle upon Tyne, UK

[64] N.B. Hassan, Z. Ghassemlooy, S. Zvanovec, P. Luo, and H. Le-Minh, "Non-line-of-sight $2 \times N$ indoor optical camera communications," Appl. Opt. 57, B144-B149 (2018)

[65] E. Eso, A. Burton, N. B. Hassan, M. M. Abadi, Z. Ghassemlooy and S. Zvanovec, "Experimental Investigation of the Effects of Fog on Optical Camera-based VLC for a Vehicular Environment," *2019 15th International Conference on Telecommunications (ConTEL)*, Graz, Austria, 2019, pp. 1-5.

[66] E. Eso *et al*., "Experimental Demonstration of Vehicle to Road Side Infrastructure Visible Light Communications," *2019 2nd West Asian Colloquium on Optical Wireless Communications (WACOWC)*, Tehran, Iran, 2019, pp. 85-89.

[67] G. Cossu et al., "A visible light localization aided optical wireless system," in Proc. IEEE GC Wkshps, Houston, TX, USA, 2011, pp. 802–807.

[68] M. Yoshino, S. Haruyama, and M. Nakagawa, "High-accuracy positioning system using visible LED lights and image sensor," in Proc. IEEE Radio Wireless Symp., Orlando, FL, USA, 2008, pp. 439–442.

[69] Z. Zhou, M. Kavehrad, and P. Deng, “Indoor positioning algorithm using light-emitting diode visible light communications,” Opt. Eng., vol. 51, no. 8, Aug. 2012, Art. ID. 085009

[70] P. Lou, H. Zhang, X. Zhang, M. Yao, and Z. Xu, "Fundamental analysis for indoor visible light positioning system," in 2012 1st IEEE International Conference on Communications in China Workshops (ICCC), 2012, pp. 59-63.

[71] A. Al-Qahtani et al., "A non-invasive remote health monitoring system using visible light communication," 2015 2nd International Symposium on Future Information and Communication Technologies for Ubiquitous HealthCare (Ubi-HealthTech), Beijing, 2015, pp. 1-3.

[72] V. Jungnickel *et al*., "A European view on the next generation optical wireless communication standard," *2015 IEEE Conference on Standards for Communications and Networking (CSCN)*, Tokyo, 2015, pp. 106-111.

[73] G. Pang, T. Kwan, C.-H. Chan, and H. Liu, “Led traffic light as a communications device,” IEEE/IEEJ/JSAI International Conference on Intelligent Transportation Systems, Tokyo, Japan, pp. 788- 793, 1999.

[74] K. Kulhavy, “Home: RONJA,” RONJA, 2012. [Online]. Available: http://ronja.twibright.com/

[75] VLCC, “Visible Light Communications Consortium,” [Online]. Available: http://www.vlcc.net/ modules/xpage1/

[76] OMEGA project, “Home Gigabit Access project,” [Online]. Available: http://www.ict-omega.eu/

[77] IEEE 802.15 WPAN, Task Group 7 (TG7), Visible Light Communication. [Online]. Available: http://www.ieee802.org/15/pub/TG7.html

[78] Li-Fi Consortium. [Online]. Available: http://lificonsortium.org/index.html

[79] P. H. Pathak, X. Feng, P. Hu, and P. Mohapatra, ‘‘Visible light communication, networking, and sensing: A survey, potential and challenges,’’ IEEE Commun. Surveys Tuts., vol. 17, no. 4, pp. 2047–2077, 4th Quart., 2015.

[80] United States Department of Energy. (2014). Energy Savings Forecast of Solid-State Lighting in General Illumination Applications. [Online]. Available: http://apps1.eere.energy.gov/buildings/publications/pdfs/ssl/ energysavingsforecast14.pdf

[81] J. George, M. Mustafa, N. Osman, N. Ahmed, D. Hamed, “A Survey on Visible Light Communication,” International Journal of Engineering and Computer Science, Vol. 3, Issue 2, Feb., pp. 3805-3808, 2014.

[82] S. Wu, H. Wang, and C.-H. Youn, “Visible light communications for 5G wireless networking systems: from fixed to mobile communications," IEEE Network, Vol. 28, Issue 6, pp. 41-45, 2014

[83] D. Karunatilaka, F. Zafar, V. Kalavally and R. Parthiban, "LED Based Indoor Visible Light Communications: State of the Art," in IEEE Communications Surveys & Tutorials, vol. 17, no. 3, pp. 1649-1678, third quarter 2015.

[84 ] E. Schubert, *Light-Emitting Diodes*. Cambridge, U.K.: Cambridge Univ. Press, 2006.

[85] M. Zhang and Z. Zhang, “Fractionally spaced equalization in visible light communication,” in *Proc. IEEE WCNC*, Shanghai, China, 2013, pp. 4282–4287.

[86] C. W. Chow, C. H. Yeh, Y. F. Liu, and Y. Liu, “Improved modulation speed of LED visible light communication system integrated to main electricity network,” *Electron. Lett.*, vol. 47, no. 15, pp. 867–868, Jul. 2011.

[87] X. He, Z. Xiao, and S. He, “A design of LED adaptive dimming lighting system based on incremental pid controller,” in *Proc. SPIE, LED Display Technol.*, Beijing, China, 2010, vol. 7852, Art. ID. 78520W.

[88] J. Hecht, “Changing the lights: Are LEDs ready to become the market standard?” *Opt. Photon. News*, vol. 23, no. 3, pp. 44–50, 2012. [54] S. P. Ying, C.-W. Tang, and B.-J. Huang, “Charaterizing LEDs for mixture of colored LED light sources,” in *Proc. Int. Conf. EMAP*, Kowloon, China, 2006, pp. 1–5.

[89] L. Svilainis, “Comparison of the EMI performance of LED PWM dimming techniques for LED video display application,” *J. Display Technol.*, vol. 8, no. 3, pp. 162–165, Mar. 2012.

[90] D. Steigerwald *et al.*, “Illumination with solid state lighting technology,” *IEEE J. Sel. Topics Quantum Electron.*, vol. 8, no. 2, pp. 310 320, Mar./Apr. 2002.

[91] E. Schubert, Y.-H. Wang, A. Cho, L.-W. Tu, and G. Zydzik, “Resonant cavity light emitting diode,” *Appl. Phys. Lett.*, vol. 60, no. 8, pp. 921–923, Feb. 1992.

[92] C. Tsai, Y. Lu and S. Ko, "Resonant-Cavity Light-Emitting Diodes (RCLEDs) Made From a Simple Dielectric Coating of Transistor Outline (TO)-Can Packaged InGaN LEDs for Visible Light Communications," in *IEEE Transactions on Electron Devices*, vol. 63, no. 7, pp. 2802-2806, July 2016.

[93] M.Islim, *et al*., “Towards 10Gb/s OFDM-based visible light communication using a GaN violet-micro-LED., 2017.

[94] J. J. D. McKendry *et al.*, "High speed visible light communications using individual pixels in a micro light emitting diode array," *IEEE Photon. Technol. Lett.*, vol. 22, no. 18, pp. 1346–1348, Sep. 2010.

[95] J. J. D. McKendry *et al.*, "Visible-light communications using a CMOScontrolled micro-light-emitting-diode array," *J. Lightw. Technol.*, vol. 30, no. 1, pp. 61–67, Jan. 2012.

[96] S. Zhang *et al.*, "1.5 gbit/s multi-channel visible light communications using CMOS-controlled GaN-based LEDs," *J. Lightw. Technol.*, vol. 31, no. 8, pp. 1211–1216, Apr. 2013.

[97] M. Dawson, "Ultra parallel visible light communications (UPVLC)," University of Strathclyde, Glasgow, U.K., 2012. [Online]. Available: http://gow.epsrc.ac.uk/NGBOViewGrant.aspx?GrantRef= EP/K00042X/1

[98] H. Jiang and J. Y. Lin, "Nitride micro-leds and beyond—A decade progress review," *Opt. Exp.*, vol. 21, no. S3, pp. A475–A484, May 2013.

[99] OLED display and their applications. Available online at https://electronicsforu.com/resources/oled-displays-applications Accessed: 17/12/2019.

[100] P. A. Haigh, Z. Ghassemlooy, S. Rajbhandari, and I. Papakonstantinou, "Visible light communications using organic light emitting diodes," IEEE Communications Magazine, vol. 51, no. 8, pp. 148-154, 2013

[101] H. Chun, C.-J. Chiang, and D. C. O'Brien, "Visible light communication using OLEDs: Illumination and channel modeling," in *Proc. IWOW Commun.*, Pisa, Italy, 2012, pp. 1–3.

[102] "OLED lighting," Konica Minolta, Tokyo, Japan, 2014. [Online]. Available: http://www.konicaminolta.com/oled/products/index.html

[103] A. Kelly *et al.*, “High-speed GaN micro-LED arrays for data communications,” in *Proc. 14th ICTON*, Coventry, U.K., 2012, pp. 1–5.

[104] H. Le Minh, Z. Ghassemlooy, A. Burton, and P. A. Haigh, “Equalization for organic light-emitting diodes in visible light communications,” in *Proc. IEEE GC Wkshps*, Houston, TX, USA, 2011, pp. 828–832.

[105] Y. Li, Z. Ghassemlooy, X. Tang, B. Lin, and Y. Zhang, "A VLC smartphone camera based indoor positioning system," IEEE Photonics Technology Letters, vol. 30, no. 13, pp. 1171-1174, 2018.

[106] R. Boubezari, H. Le Minh, Z. Ghassemlooy, and A. Bouridane, "Smartphone camera based visible light communication," Journal of Lightwave Technology, vol. 34, no. 17, pp. 4121-4127, 2016.

[107] B. Lin, Z. Ghassemlooy, C. Lin, X. Tang, Y. Li, and S. Zhang, "An indoor visible light positioning system based on optical camera communications," IEEE Photonics Technology Letters, vol. 29, no. 7, pp. 579-582, 2017.

[108] Hamamatsu. Si PIN photodiode S9055-01. Available: https://www.hamamatsu.com/jp/en/product/type/S9055- 01/index.html

[109] P. P. Manousiadis, S. Rajbhandari, R. Mulyawan, D. A. Vithanage, H. Chun, G. Faulkner, et al., "Wide field-of-view fluorescent antenna for visible light communications beyond the étendue limit," Optica, vol. 3, pp. 702-706, 2016.

[110] Hamamatsu. High speed, compact Si APD for the 700 nm band featuring low-bias operation. Available: https://www.hamamatsu.com/eu/en/product/type/S14643-02/index.html

[111] D. Chitnis and S. Collins, "A SPAD-based photon detecting system for optical communications," Journal of Lightwave Technology, vol. 32, pp. 2028-2034, 2014

[112] R. J. Sczebra, 4 Ways Cameras Are changing Healthcare, 2015. Avaible online at https://www.forbes.com/sites/robertszczerba/2014/10/15/4-ways-cameras-are-changing-healthcare/#627295b96a2f Accessed: 07/11/2019.

[113] N. T. Le, M. A. Hossain, and Y. M. Jang, "A survey of design and implementation for optical camera communication," Signal Processing: Image Communication, vol. 53, pp. 95-109, 2017.

[114] H. C. Hyun, T. Nguyen, J. S. Bong, K. H. Soon, and J. Y. Min, "Far distance LED-to-Ship Communication employing Optical Camera Communication,", pp. 1089-1090, 2015.

[115] N. Iizuka, "Image sensor communication—Current status and future perspectives," IEICE Transactions on Communications, vol. 100, pp. 911-916, 2017.

[116] X. Liu and Z. Zhu, "Advances in Optical Communications Technologies," IEEE Communications Magazine, vol. 56, pp. 176- 176, 2018.

[117] N. Saha, M. S. Ifthekhar, N. T. Le, and Y. M. Jang, "Survey on optical camera communications: challenges and opportunities," Iet Optoelectronics, vol. 9, pp. 172-183, 2015.

[118] T. Nguyen, A. Islam, T. Hossan, and Y. M. Jang, "Current status and performance analysis of optical camera communication technologies for 5G networks," IEEE Access, vol. 5, pp. 4574-4594, 2017.

[119] Ashok, A.; Jain, S.; Gruteser, M.; Mandayam, N.; Yuan, W.; Dana, K. Capacity of pervasive camera based communication under perspective distortions. In Proceedings of the 2014 IEEE International Conference on Pervasive Computing and Communications (PerCom 2014), Budapest, Hungary, 24–28 March 2014; pp. 112–120.

[120] Takai, I.; Harada, T.; Andoh, M.; Yasutomi, K.; Kagawa, K.; Kawahito, S. Optical vehicle-to-vehicle communication system using LED transmitter and camera receiver. *IEEE Photonic J.* 2014, *6*, 1–14.

[121] Roberts, R.D., "A MIMO protocol for camera communications (CamCom) using undersampled frequency shift ON-OFF keying (UFSOOK)," in *Globecom Workshops (GC Wkshps), 2013 IEEE* , vol., no., pp.1052-1057, 9-13Dec.2013.

[122] Izuka, N. OCC Proposal of Scope of Standardization and Applications. IEEE 802.15 SG7a Standardization Documents; IEEE: Piscataway, NJ, USA, 2014.

[123] P. Chavez-Burbano, V. Guerra, J. Rabadan, C. Jurado-Verdu, and R. Perez-Jimenez, "Novel Indoor Localization System Using Optical Camera Communication," in 2018 11th International Symposium on Communication Systems, Networks & Digital Signal Processing (CSNDSP), 2018, pp. 1-5.

[124] R. D. Roberts, Undersampled frequency shift ON-OFF keying (UFSOOK) for camera communications (CamCom), in: Proc. 22nd Wireless and Optical Commun. Conf., (WOCC), 2013, pp. 645–648.

[125] R. D. Roberts, Space-time forward error correction for dimmable undersampled frequency shift ON-OFF keying camera communications (CamCom), in: Proc. 5th IEEE Int. Conf. on Ubiquitous and Future Networks (ICUFN), 2013, pp. 459–464.

[126] R. D. Roberts, A MIMO protocol for camera communications (CamCom) using undersampled frequency shift ON-OFF keying (UFSOOK), in: Proc. IEEE Global Commun. Conf. (GLOBECOM) Wkshps, 2013, pp. 1052–1057.

[127] T. Nguyen, A. Islam, Y. M. Jang, Region-of-interest signaling vehicular system using optical camera communications, IEEE Photonics Journal 9 (1) (2017) 1–20.

[128] H. Aoyama, M. Oshima, Visible light communication using a conventional

image sensor, in: 12th Annual IEEE Consumer Commun. and Networking Conf., (CCNC), 2015, pp. 103–108.

[129] H. Aoyama, M. Oshima, Line scan sampling for visible light communication: Theory and practice, in: IEEE Int. Conf. on Commun., (ICC), 2015, pp. 5060–5065.

[130] N. Rajagopal, P. Lazik, A. Rowe, Visual light landmarks for mobile devices, in: Proc. of Int. Conf. on Info. Processing in Sensor Networks, 2014, pp. 249–260.

[131] H.-Y. Lee, H.-M. Lin, Y.-L. Wei, H.-I. Wu, H.-M. Tsai, K. C.-J. Lin, Rollinglight: Enabling line-of-sight light-to-camera communications, in: Proc. of MobiSys, 2015, pp. 167–180.

[132] C. H. Hong, M. A. Hossain, T. Nguyen, Y. M. Jang, Hybrid modulation scheme for indoor image sensor communication system using smartphone and LEDs, in: Int. Conf. on Ubiquitous and Future Networks (ICUFN), 2016, pp. 471–474. 45

[133] V. Nguyen, Y. Tang, A. Ashok, M. Gruteser, K. Dana, W. Hu, E. Wengrowski, N. Mandayam, High-rate flicker-free screen-camera communication with spatially adaptive embedding, in: Proc. IEEE INFOCOM, IEEE, 2016, pp. 1–9.

[134] T. Nguyen, N. T. Le, Y. M. Jang, Asynchronous scheme for optical camera communication-based infrastructure-to-vehicle communication, Int. J. of Distributed Sensor Networks 11 (5) (2015) 1–15.

[135] T. Nguyen, A. Islam, T. Hossan, and Y. M. Jang, “Current status and performance analysis of optical cameracommunication technologies for 5G networks,” IEEE Access 5, 4574–4594 (2017).8.

[136] I. Takai, S. Ito, K. Yasutomi, K. Kagawa, M. Andoh, and S. Kawahito, “LED and CMOS image sensor based optical wireless communication system for automotive applications,” IEEE Photonics J.5, 6801418 (2013).9.

[137] A. Sewaiwar, S. V. Tiwari, Y.-H. Chung, Visible light communication based motion detection, Opt. Express 23 (14) (2015) 18769–18776.

[138] D. Ionescu, V. Suse, C. Gadea, B. Solomon, B. Ionescu, S. Islam, A new infrared 3D camera for gesture control, in: IEEE Int. Instrumentation and Measurement Techno. Conf., (I2MTC), 2013, pp. 629–634.

[139] S. V. Tiwari, A. Sewaiwar, Y.-H. Chung, Color coded multiple access scheme for bidirectional multiuser visible light communications in smart home technologies, Optics Commun. 353 (2015) 1–5.

[140] N. Lalithamani, Gesture control using single camera for PC, Procedia ComputerScience 78 (2016) 146 – 152, 1st Int. Conf. on Info. Security and Privacy.

[141] A. Seaman, J. McPhee, Comparison of optical and inertial tracking of full golf swings, Procedia Engineering 34 (1) (2012) 461–466.

[142] R. T. Solberg, A. R. Jensenius, Optical or inertial, evaluation of two motion capture systems for studies of dancing to electronic dance music, in: Proc. of SMC, 2016, pp. 469–474.

[143] J. Kim and H. Jun, “Vision-based location positioning using augmented reality for indoor navigation,” IEEE Transactions on Consumer Electronics, vol. 54, no. 3, pp. 954–962, 2008.

[144] M. S. Ifthekhar, N. Saha, and Y. M. Jang, “Neural network based indoor positioning technique in optical camera communication system,” in Proceedings of the 5th International Conference on Indoor Positioning and Indoor Navigation (IPIN '14), pp. 431–435, Busan, South Korea, October 2014.

[145] H. Hile and G. Borriello, “Positioning and orientation in indoor environments using camera phones,” IEEE Computer Graphics and Applications, vol. 28, no. 4, pp. 32–39, 2008.

[146] M. S. Ifthekhar, M. A. Hossain, C. H. Hong, and Y. M. Jang, “Radiometric and geometric camera model for optical camera communications,” in Proceedings of the 7th International Conference on Ubiquitous and Future Networks (ICUFN '15), pp. 53–57, Sapporo, Japan, July 2015.

[147] I. Takai, T. Harada, M. Andoh, K. Yasutomi, K. Kagawa and S. Kawahito, "Optical Vehicle-to-Vehicle Communication System Using LED Transmitter and Camera Receiver," in *IEEE Photonics Journal*, vol. 6, no. 5, pp. 1-14, Oct. 2014

[148] A. Cailean et al., “Visible light communications: Application to cooperation between vehicles and road infrastructures,” in Proc. IEEE Intell. Veh. Symp., Jun. 2012, pp. 1055–1059.

[149] S. Okada et al., “On-vehicle receiver for distant visible light road-to-vehicle communication,” in Proc. IEEE Intell. Veh. Symp., Jun. 2009, pp. 1033–1038.

[150] Z. Wang, Q. Wang, W. Huang, Z. Xu, Optical Camera Communication: Fundamentals, John Wiley & Sons, Ltd, 2017, Ch. 8, pp. 239–290.

[151] A. Ashok, M. Gruteser, N. Mandayam, J. Silva, M. Varga, K. Dana, Challenge: Mobile optical networks through visual MIMO, in: Proc. of MobiCom/MobiHoc, ACM, 2010, pp. 105–112.

[152] R. F. Karlicek, “Smart lighting - beyond simple illumination,” in 2012 IEEE Photonics Society Summer Topical Meeting Series, pp. 147–148, July 2012.

[153] J. Vucic and K. D. Langer, “High-speed visible light communications: State- of-the-art,” in OFC/NFOEC, pp. 1–3, March 2012.

[154] J. J. D. McKendry, R. P. Green, A. E. Kelly, Z. Gong, B. Guilhabert, D. Mas-soubre,E.Gu,andM.D.Dawson,“High-speedvisiblelightcommunications usingindividualpixelsinamicrolight-emittingdiodearray,”IEEEPhotonics Technology Letters, vol. 22, pp. 1346–1348, Sept 2010.

[155] K. Ebihara, K. Kamakura, and T. Yamazato, “Layered transmission of space-time coded signals for image-sensor-based visible light communications,” Journal of Lightwave Technology, vol. 33, pp. 4193–4206, Oct 2015.

[156] D. K. Misra, Filter Design, pp. 333–391. John Wiley & Sons, Inc., 2004.

[157] A.Dornan,TheEssentialGuidetoWirelessCommunicationsApplications,Second Edition: FromCellularSystemstoWi-Fi.UpperSaddleRiver,NJ,USA:Prentice- Hall, Inc., 2nd ed., 2002.

[158] L.Zhou, X. Xi, J. Liu, and N.Yu, “L f ground-wave propagation over irregular terrain,”IEEETransactionsonAntennasandPropagation,vol.59,pp.1254–1260, April 2011.

[159] The development of CMOS image sensors. Available online at: https://www.azom.com/article.aspx?ArticleID=16321 Accessed: 15/11/2019

[160] CCD and CMOS sensor technology. Available online at: https://www.axis.com/files/whitepaper/wp_ccd_cmos_40722_en_1010_lo.pdf

[161] How stuff Work, What is the difference between CCD and CMOS image sensors in a digital camera? Availabe online at: http://electronics.howstuffworks.com/cameras-photography/ digital/question362.htm/printable

[162] Rolling Shutter vs Global Shutter | How to Choose, Availabe online at: https://andor.oxinst.com/learning/view/article/rolling-and-global-shutter Accessed: 15/11/2019.

[163] Digital Image Processing with MATLAB. Available at: https://www.intechopen.com/books/applications-from-engineering-with-matlab-concepts/digital-image-processing-with-matlab. Accessed: 02 September 2019

[164] E. Wengrowski, W. Yuan, K. J. Dana, A. Ashok, M. Gruteser, N. Mandayam, Optimal radiometric calibration for camera-display communication, in: IEEE Winter Conf. on App. of Computer Vision, 2016, pp. 1–10.

[165] M. Sonka, V. Hlavac, and R. Boyle, Image Processing, Analysis, and Machine Vision. Thomson-Engineering, 2007.

[166] Seliski, Computer Vision: Algorithms and Applications, Springer, 2011.

[167]16 OpenCV Functions to Start your Computer Vision journey (with Python code)

[168] Open CV. Available at: https://opencv.org/about/ Accessed: 01 Sepetmber 2019

[169] What is Computer vision. Available at: https://hayo.io/computer-vision/

[170] Haigh, P.A.; Bausi, F.; Le Minh, H.; Papakonstantinou, I.; Popoola, W.; Burton, A.; Cacialli, F. Wavelength-multiplexed polymer LEDs: Towards 55 Mb/s organic visible light communications. *IEEE J. Sel. Areas Commun.* 2015, *33*, 1819–1828.

[171] Haigh, P.A.; Ghassemlooy, Z.; Papakonstantinou, I. 1.4-Mb/s white organic LED transmission system using discrete multitone modulation. *IEEE Photonic Technol. Lett.* 2013, *25*, 615–618.

[172] Rachim, V.P., Jiang, Y., Lee, H.S., Chung, W.Y.: Demonstration of long-distance hazard free wearable monitioring system using mobile phone visible light. Opt .Express 25, 713–719 (2017)

[173] Yu, Y. H., et al.:An inflatable and wearable wireless system for making 32-channel electroencephalogram measurements. IEEE Trans. Neural Syst. Rehabil. Eng. 24, 806–813 (2016)

[174] Etoolbox.: Bioelectromagnetism MATLAB Toolbox. http://eeg.sourceforge.net. Accessed 28 Mar 2017

[175]. DD-160128FC-1A DENSITRON, Graphic OLED, 160128, RGB, 2.8 V, Parallel, Serial, 35.8 mm 0.8 mm, −20 °C | Farnell UK

[176] Electroencephalography I Laboratory. Property of Cleveland Medical Devices. Copying and distribution prohibited. CleveLabs Laboratory Course System Version 6.0. 2006 Cleveland Medical Devices Inc., Cleveland, OH.

[177] B. Luan, W. Jia, P. D. Thirumala, J. Balzer, D. Gao and M. Sun, "A feasibility study on a single-unit wireless EEG sensor," *2014 12th International Conference on Signal Processing (ICSP)*, Hangzhou, 2014, pp. 2282-2285.

[178] Bayer filter, Available online at: https://theailearner.com/tag/color-image/. Accessed: 13/11/2019